ENERGY BANDS OF ACCEPTOR-TYPE GRAPHITE INTERCALATION COMPOUDS

By

HENRYK ZALESKI, M.Sc.

A Thesis

Submitted to the School of Graduate Studies

in Partial Fulfilment of the Requirements

for the Degree

Doctor of Philosophy

McMaster University

ENERGY BANDS OF GRAPHITE INTERCALATION COMPOUNDS

DOCTOR OF PHILOSOPHY (1985)
(Physics)

McMASTER UNIVERSITY
Hamilton, Ontario

TITLE: Energy Bands of Acceptor-Type Graphite Intercalation Compounds.

AUTHOR: Henryk Zaleski, M.Sc. (Technical University of Wroclaw, Poland)

SUPERVISOR: Professor W.R. Datars

NUMBER OF PAGES: x, 126

ABSTRACT

Reaction of graphite with liquid antimony pentachloride produced stage 1 and 2 intercalation compounds. A stage-1 SbF_6^- compound was prepared by reaction of graphite with nitryl hexafluoroantimonate in solution and by reaction with the solid salt. Reaction of solid nitryl tetrafluoroborate with graphite produced a stage-2 compound.

The de Haas-van Alphen spectrum of the stage-1 $SbCl_5$ compound had a dominant oscillation of 1212 T. The oscillation was identified with the basic graphitic band. The dHvA spectrum of the stage-2 $SbCl_5$ compound depended on the cooling rate between room temperature and 77 K. The spectra of slowly-cooled samples had two fundamental oscillations of frequencies of 422 and 1190 T which were identified with the basic graphitic bands. Beat patterns of the fundamental frequencies were explained by doubling of the c-axis lattice constant. From the beat frequencies values of the interaction between states localized on graphene layers separated by an intercalate layer were estimated to be 0.6 meV and 0.7 meV. From these values the anisotropy of the conductivity was calculated to be 9×10^4.

The dHvA spectra of stage-1 SbF_6^- compound depended on the method of preparation. With samples prepared by

reaction of solid NO_2SbF_6, a dominant frequency of 1627 T was observed. Two fundamental oscillations of frequencies of 523 and 1377 T were observed in the spectrum of stage-2 BF_4^- compound and were identified with the basic graphitic bands.

The predictions of the rigid band model of Holzwarth (1980) were in agreement with measured dHvA frequencies and cyclotron masses with the Fermi energy adjusted to the charge transfer in each compound. The fitted values are -1.12 eV for stage-1 $SbCl_5$ compound, -0.88 eV for stage-2 $SbCl_5$, -1.28 eV for stage-1 SbF_6^- and -0.96 eV for stage-2 BF_4^- compound. The simpler model of Blinowski et al. (1980) was found less accurate.

ACKNOWLEDGMENTS

I would like to thank my supervisor, Dr. W.R. Datars for suggesting the project and his guidance through all phases of this work. Thanks are also given to Dr. P.K. Ummat for teaching me the art of sample preparation. Technical assistance of Clarence Verge and helping hands of the members of the Fermi surface group are also appreciated.

I also wish to thank Dr. I.D. Brown for careful and critical reading of this thesis and Dr. T. Birchall for valuable suggestions.

TABLE OF CONTENTS

LIST OF TABLES

LIST OF FIGURES

CHAPTER I

INTRODUCTION

Graphite is an allotrope of carbon. The carbon atoms in graphite are arranged in layers with strong covalent bonding within layers. The bonding between layers is of the van-der-Waals type which is much weaker. Graphite can react with many chemical species. During many of these reactions interatomic bonds within layers are not broken, instead, the layers are split and a reacting substance forms a monolayer between two graphite layers. This particular form of structure is called a graphite intercalation compound (GIC).

The intercalation process is not unique to graphite. It has been observed in other anisotropic systems like transition metal dichalcogenides, some silicates and metal chlorides. However, a distinct property of graphite intercalation compounds is that there is a constant number of graphite layers between two intercalate layers. This regular ordering of intercalate is called staging and the number of graphite layers between two intercalate layers is called the stage index.

A large number of species can be intercalated into graphite. At present there are several hundred species known to react. This creates a large number of similar systems

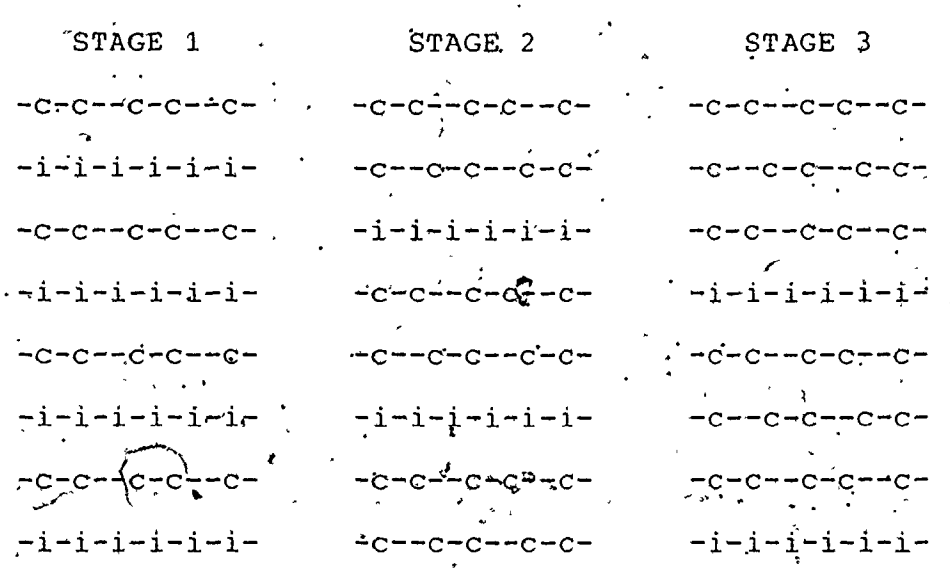

Figure I.1. Schematic diagram of the staging phenomenon for stages 1, 2, and 3. Carbon layers are indicated by (-c-) and intercalate layers by (-i-). The αβαβ stacking of graphene layers between intercalate layers is maintained for stages 2 and higher. The stacking of the graphene layers separated by intercalate layers varies from compound to compound.

whose properties can often be varied almost continuously by simply choosing appropriate intercalates. A large amount of work has been done studying chemistry, thermodynamic, structural and electronic properties of the compounds (see for example Dresselhaus and Dresselhaus 1980 and references therein). One of the most striking properties of GIC is a dramatic change of the basal plane electrical conductivity. Graphite is a semimetal and a moderate conductor. The conductivity is highly anisotropic with a high value in the graphite planes. The conductivity along the c-axis, that is

in the direction perpendicular to the graphite planes, is about 1000 times lower. Graphite has about 10^{-4} carriers per atom, half of them being electrons and half of them holes. On the other hand, in-plane mobilities are high because the carrier effective masses are low, less than 0.1 of the free electron mass.

The intercalation process is accompanied by a charge transfer between intercalate species and graphite. The direction of the transfer can be either way and the intercalates are classified as donors if electrons are transferred to graphite and as acceptors in the case of electron transfer from graphite to intercalate. The amount of charge transferred may be as high as one elementary charge per twenty carbon atoms. Since the charge on carbon layers is delocalized, one obtains up to two orders of magnitude increase of the carrier concentration and comparable increase of the basal-plane conductivity. In fact, basal plane conductivity values comparable to that of copper have been reported (Foley et al. 1977).

This qualitative explanation of the enhancement of the conductivity of graphite intercalation compounds by charge transfer has emerged from early systematic studies of their electronic properties. Quantitative models of the electronic structure of GIC were developed later based on the bands of graphite. These models have been used to

account for a variety of observed electronic properties of GIC. However, the success of the models in explaining quantum oscillatory phenomena has been rather limited. One of the reasons for this is the fact that there are many possible structures and compositions of nominally identical systems. In most cases, the measured electronic properties are averaged out over all carriers and are not sensitive to the details of structure and composition. This is not the case in measurements of quantum oscillatory phenomena where the measuring tools are the carriers of the crystal.

The conductivity along the c-axis also increases in donor compounds. In acceptor compounds it decreases even though the number of carriers increases. This results in a large anisotropy of conductivity, reaching the order of 10^5 in most acceptor compounds. This anisotropy still remains a puzzle. It was believed that intercalate layers are non-transparent for free carrier transport and attempts were made to explain c-axis conductivity by hopping models (Sugihara 1984) or by channeling carriers across intercalate layers through defects (Morelli and Uher 1983). At present, there are no measurements of band parameters relating to the c-axis carrier dispersion and c-axis conductivity models are necessarily speculative.

This work presents the results of the investigations of the electronic bands of several acceptor graphite

intercalation compounds by the de Haas-van Alphen effect. The compounds studied are antimony pentachloride graphite and ionic compounds SbF_6^- and BF_4^- graphite. The first reaction of antimony pentachloride with graphite was reported by Croft (1956). A compound containing 35 % of $SbCl_5$ was obtained. A systematic study of graphite-$SbCl_5$ system (Melin and Herold 1969) showed the existence of a series of distinct stoichiometric compositions which were identified with different stages. Stage 1 to 4 intercalation compound were obtained and their composition was described by a general formula $C_{12n}SbCl_5$ where n is the stage index. The stage 1 was found to quickly decompose when exposed to air. Higher stages were found more stable in an ambient atmosphere. In the work of Murthy et al. (1980) stages two and higher were synthesized by a two-zone method. Optical reflectance spectra of the compounds were found to remain unchanged after months of air exposure. Stage-1 compound was not obtained. The Mössbauer study of the antimony pentachloride compound (Boolchand et al. 1981) suggested that the intercalate undergoes a disproportionation reaction

$$3SbCl_5 + 2e^- \rightarrow SbCl_3 + 2SbCl_6^-$$

where two electrons are donated by the graphite host. Later studies by Friedt et al. (1984) questioned the identification of the $SbCl_6^-$ ion and the Raman studies (Jones et al. 1983) showed the presence of several intercalate

species including $SbCl_3$, $SbCl_5^{2-}$, $SbCl_6^-$ and $SbCl_6^{3-}$.

The first measurements of quantum oscillatory phenomena of the $SbCl_5$ compound were reported by Batallan et al. (1978). Stage 2 and 4 were investigated and the frequency of oscillations were found independent of stage. The de Haas-van Alphen work of Takahashi et al. (1981) showed stage dependence of the dHvA frequencies. The theoretical explanation of the observed oscillations in the stage-2 compound was done (Tanuma et al. 1981) using the rigid band model of Blinowski et al. (1980). Since the number of observed frequencies was larger than that expected from the model, in-plane zone folding technique (Harrison 1966) based on 7x7 intercalate superstructure was used. However, the value of charge transfer adjusted to fit the data was not in agreement with the one obtained from optical reflectance data of Blinowski et al. (1980) and Eklund et al. (1981).

The validity of the zone folding construction used by Tanuma et al. was put in doubt with the discovery of a commensurate-incommensurate phase transition at around 220 K from x-ray diffraction studies (Clarke et al. 1982). On the other hand, electron diffraction experiments (Timp et al. 1982) showed that the low temperature phase has a glassy structure. This apparent discrepancy was resolved recently by Roth et al. (1984) who showed that the transition to the

glassy phase is induced by the electron beam. No transition is observed in the stage-1 compound (Clarke et al. 1982).

The c-axis resistivity of stage 1 and 2 $SbCl_5$ graphite increases linearly with temperature (Morelli and Uher 1983). It was postulated that the transport of carriers along the c-axis is channeled through defects.

The action of nitryl salts (NO_2SbF_6, NO_2BF_4, NO_2PF_6) on graphite produces ionic intercalation compounds (Billaud et al. 1980a, Billaud et al. 1980b). The chemistry of the reaction is simple. The nitryl ion (NO_2^+) oxidizes graphite and the anion is inserted into the graphite lattice.

$$NO_2^+X^- + mC \rightarrow C_m^+X^- + NO_2$$

The reactions were carried out in the solution of nitryl salts in dry nitromethane and various stages were obtained depending on the concentration of the salt. With nitryl hexafluoroantimonate stages 1 to 9 were obtained. Reactions of nitryl tetrafluoroborate produced stage 2 and higher. Similar compounds can be obtained by an electrochemical reaction of lithium salts (Jobert et al. 1981). The compounds obtained in solution and by electrochemical method decompose when removed from the reaction vessels. They can only be studied by techniques that permit measurements in situ. These include x-ray characterization, basal-plane conductivity (Billaud et al. 1980a, Billaud et al. 1980b) and Mössbauer spectroscopy (Boolchand et al. 1983). Another

way of inserting fluoride anions was devised by Billaud and Chenite (1983). The starting materials were nitryl salts. They were thermally decomposed and the gaseous decomposition products reacted with graphite.

This work involves the preparation of compounds using known techniques and the development of new methods of preparation to obtain the pure homogeneous samples needed for the investigations. The energy bands are studied in graphite $SbCl_5$ stage 1 and 2, graphite SbF_6^- stage 1 and graphite BF_4^- stage 2 compounds. The experimental data relating to the in-plane carrier dispersion are compared to the rigid band models of the electronic structure of GIC. Furthermore, quantitative information about c-axis dispersion is obtained from the analysis of the dHvA data of stage 2 $SbCl_5$ compound. The anisotropy of the conductivity in that compound is explained by a band conduction mechanism.

CHAPTER II

THEORY

The constituents of graphite intercalation compounds are atomic and molecular monolayers rather than individual atoms. The layers have macroscopic size in two dimensions and the interactions between them are weak. Consequently, many basic properties of the compounds can be obtained by adding the contributions of individual layers.

The intraplanar bonding of carbon atoms is strong due to their covalent bonds and remains intact during the intercalation process. The spacing between carbon atoms within layers remains essentially unchanged (Nixon and Parry 1969), the frequency shift of graphitic Raman lines is less than 4 % (see data compiled by Dresselhaus and Dresselhaus 1980), and the in-plane mechanical strength of the intercalated compounds is similar to that of pristine graphite (Herinckx et al. 1972). The similarity between the pristine graphite and the intercalation compounds is also observed in electronic properties. An example is the high basal plane mobility of the carriers observed in both graphite and intercalation compounds. This similarity is a basis for the development of phenomenological models of the electronic structure of intercalation compounds based on the

band structure of graphite. Because the intralayer bonding of carbon atoms remains essentially unchanged during intercalation one expects that the electronic interactions are also preserved.

II.1. Electronic structure of graphite.

A carbon atom has four valence electrons which occupy 2s and 2p states. In graphite there is three-fold symmetry of the nearest neighbors and more appropriate basis states are $2p_z$ and three hybrid states made of 2s, $2p_x$ and $2p_y$ orbitals (sp^2 hybridization). Crystalline $2sp^2$ states give rise to bonding σ and antibonding σ^* bands which are separated by 6-12 eV. In between there are π and π^* bands made from $2p_z$ states. Three electrons of each atom completely fill σ bands, the remaining electrons go to the π bands. There is a small (~0.4 eV) overlap of the energy of π and π^* bands and, therefore, the top of the π bands is left unoccupied and a few electrons are in the bottom of the π^* bands. Thus, graphite is a compensated semimetal with the total carrier concentration of about 1 carrier per 10^4 atoms.

One of the first band structure calculations of graphite was done by Wallace (1947). A simple tight binding approximation was used but, nevertheless, it showed the characteristic features of the bands.

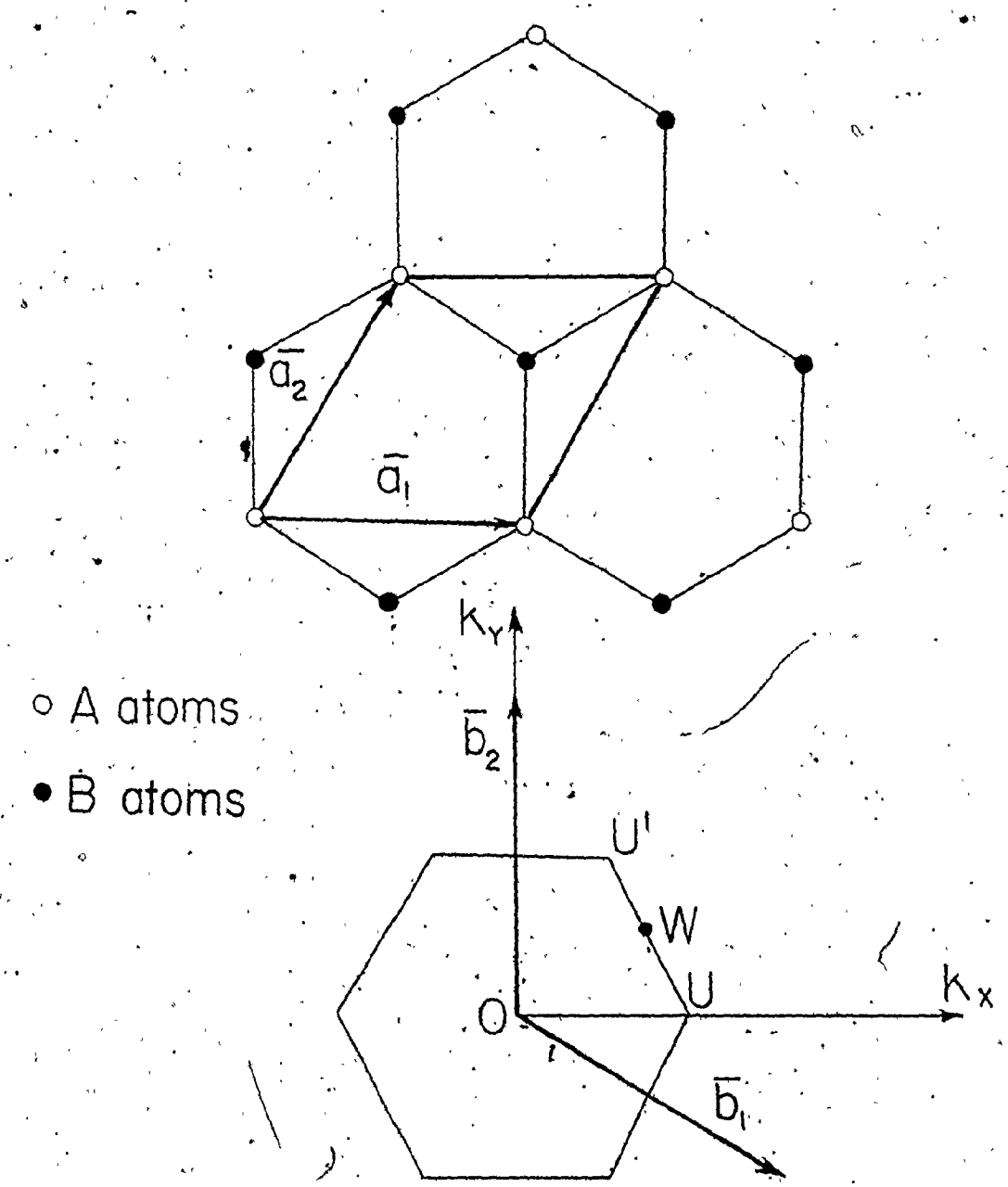

Figure II.1. Structure (top) and Brillouin zone (bottom) of a single graphite layer.

Wallace theory starts with a model of two-dimensional graphite consisting of a single graphite layer. The carbon atoms are arranged in a honeycomb array as shown in Figure II.1. The primitive lattice translation vectors are $\bar{a}_1$ and $\bar{a}_2$. There are two atoms per unit cell. The reciprocal lattice is hexagonal with vectors $\bar{b}_1$ and $\bar{b}_2$ of magnitude $4\pi/\sqrt{3}a$. The electron wave function is taken as

$$\psi = \phi_1 + \lambda\phi_2 \qquad (II.1)$$

where λ is a constant and ϕ_1 and ϕ_2 are Bloch combinations of $2p_z$ orbitals of atoms A and B, respectively.

$$\begin{aligned} \phi_1 &= \sum_A \exp(i\mathbf{k}\mathbf{r}_A)\, \chi(\mathbf{r}-\mathbf{r}_A) \\ \phi_2 &= \sum_B \exp(i\mathbf{k}\mathbf{r}_B)\, \chi(\mathbf{r}-\mathbf{r}_B) \end{aligned} \qquad (II.2)$$

Following a standard tight binding procedure one obtains a 2x2 Hamiltonian whose matrix elements are given by

$$H_{ij} = 1/N \int \phi^*_i \hat{H}\, \phi_j d^3r \qquad (II.3)$$

where N is the number of unit cells in the crystal. From symmetry $H_{11} = H_{22}$, furthermore $H_{12} = H^*_{21}$. The energy solution is then given by

$$E = H_{11} \pm |H_{12}| \qquad (II.4)$$

The elements H_{ij} are evaluated in an approximation that includes interaction between nearest and second nearest neighbors. Terms of the form $\int \chi^*(\mathbf{r}-\mathbf{r}_A)\hat{H}\,\chi(\mathbf{r}-\mathbf{r}_A)d^3r$ are constant and can be set to zero by choosing an appropriate energy scale. The element H_{11} is

$$H_{11} = \sum_{1} \exp[ik(r_A - r_{A1})] \int \chi^*(r-r_A)\hat{H}\,\chi(r-r_{A1})\,d^3r \qquad (II.5)$$

where the index 1 runs over six A atoms located at (a,0), (a/2,-a$\sqrt{3}$/2), (-a/2,a$\sqrt{3}$/2), (-a,0), (-a/2,-a$\sqrt{3}$/2) and (a/2, -a$\sqrt{3}$/2). $2p_z$ orbitals have circular symmetry in the xy plane and the integrals $\gamma_0' = \int \chi^*(r-r_A)\hat{H}\,\chi(r-r_{A1})d^3r$ depend only on $|r_A - r_{A1}|$ and are the same for all the atoms considered. Performing summation of exponentials one gets

$$H_{11} = -2\gamma_0'[\cos(k_x a) + 2\cos(k_y a\sqrt{3}/2)\cos(k_x a/2)] \qquad (II.6)$$

H_{12} denotes interaction between an atom A and its three B neighbors located at (a/2,-a/2$\sqrt{3}$), (0,a/$\sqrt{3}$) and (-a/2,-a/2$\sqrt{3}$). Denoting $\gamma_0 = \int \chi^*(r-r_A)\hat{H}\,\chi(r-r_B)d^3r$ (the resonance integral between atoms considered) one obtains

$$H_{12} = -\gamma_0[\exp(ik_y a/\sqrt{3}) + 2\exp(-ik_y a/2\sqrt{3})\cos(k_x a/2)] \qquad (II.7)$$

The resultant band structure is shown schematically in Figure II.2. There are two bands that meet at the point U of the Brillouin zone. The number of states in a band is equal to 2N, where N is the number of unit cells in the crystal. The number of electrons is also equal to 2N because there are two atoms per unit cell and each donates one electron. This results in a completely filled bottom band and an empty upper band. In effect, two-dimensional graphite is a zero gap semiconductor with no free carriers at T = 0.

At finite temperature there is a thermal generation of carriers, the electrons are excited into states at the

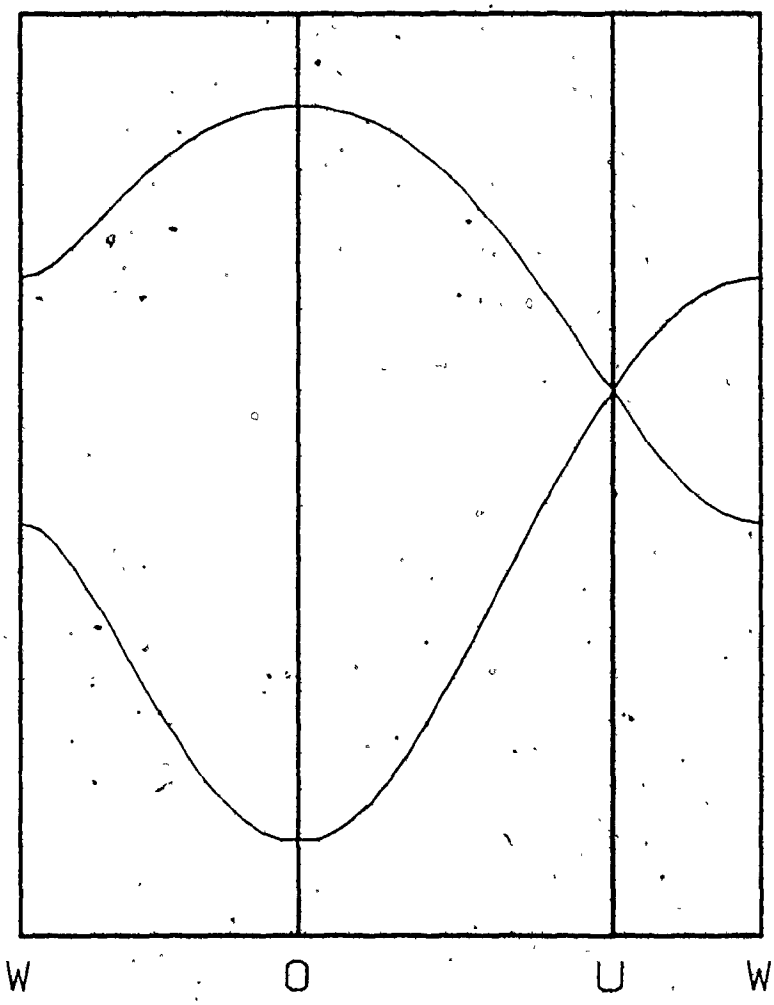

Figure II.2. Schematic energy bands of two-dimensional graphite.

bottom of the conduction band leaving free holes at the top of the valence band. The carriers occupy states in the region around the corner of the Brillouin zone. Expanding Hamiltonian elements around the point U one obtains

$$H_{11} = 3\gamma_0' + \frac{3}{4}\gamma_0' a^2 |\kappa|^2 + \ldots \qquad (II.8)$$

and

$$H_{12} = -\gamma_0 \frac{\sqrt{3}}{2}(\kappa_x + i\kappa_y) + \ldots \qquad (II.9)$$

where $\kappa = k - k_U$. In the lowest order, the energy is linear in κ, that is

$$E = 3\gamma_0' \pm \gamma_0 \frac{\sqrt{3}}{2} |\kappa| a \qquad (II.10)$$

The linear dispersion corresponds to a low carrier effective mass which is observed experimentally.

A three-dimensional crystal of graphite consists of layers spaced by $c_0 = 3.35$ A (Figure II.3). The layers are stacked in $\alpha\beta\alpha\beta$ order with every second layer rotated by 60 degrees around an A atom. This gives a c-axis lattice vector equal to $2c_0$ and leaves the in-plane lattice vectors the same as in two-dimensional graphite. There are four atoms per unit cell which we denote by A, B, A' and B'.

The electron wave function is taken as a combination of four Bloch sums of atomic $2p_z$ orbitals

$$\psi = \sum_m \lambda_m \{ \sum_l \exp(ikr_{l,m}) \; \chi \; (r - r_{l,m}) \} \qquad (II.11)$$

where index l numbers unit cell and m numbers base atoms. Interactions between atoms AA, AB, AA', BB' and equivalent pairs are included in the calculations. This leads to a 4x4

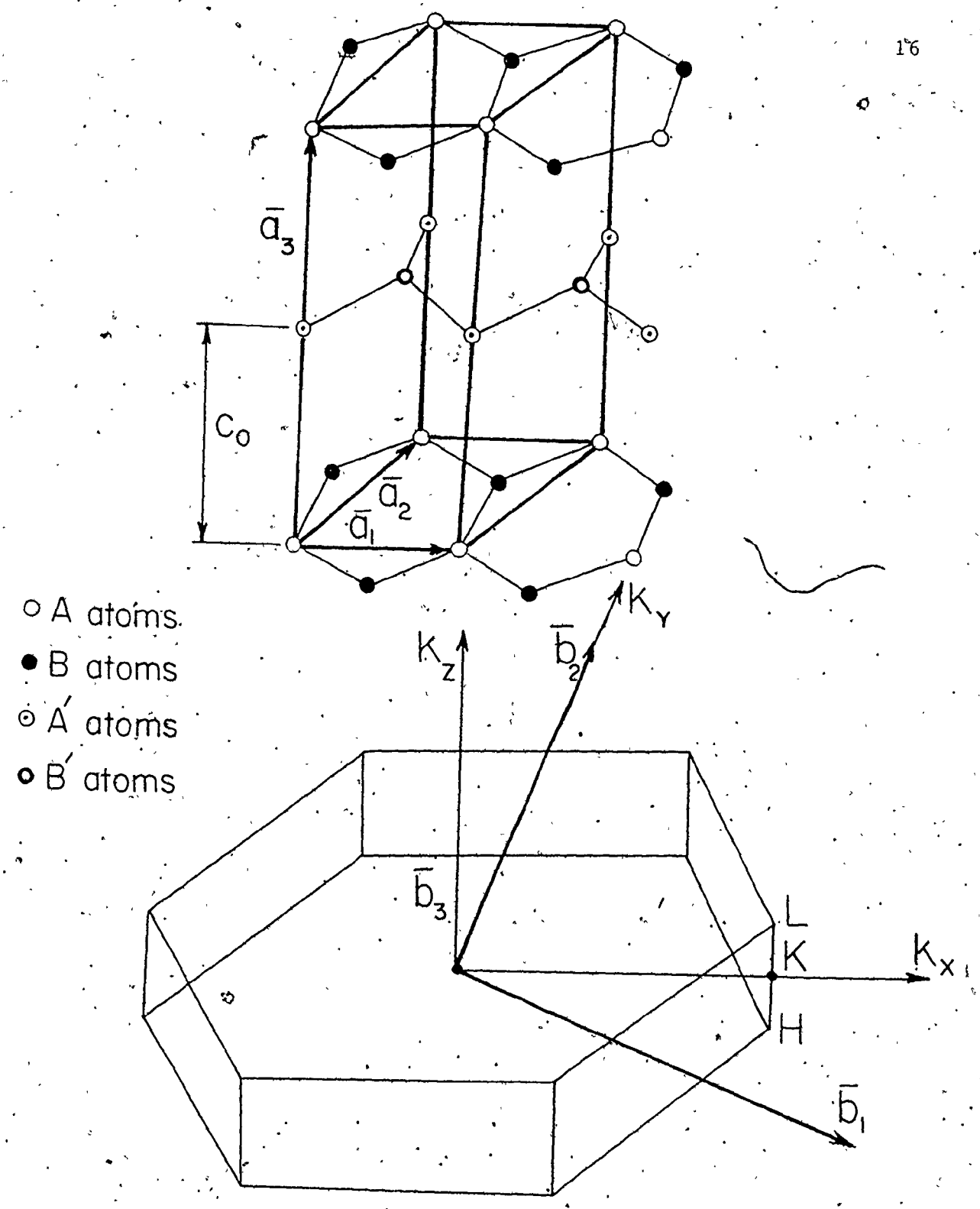

Figure II.3. Crystal structure and Brillouin zone of graphite.

Hamiltonian whose diagonal elements are the same as in the case of two-dimensional graphite

$$H_{11} = H_{22} = H_{33} = H_{44} = -2\gamma_0'[\cos(k_x a) + 2\cos(k_y a\sqrt{3}/2)\cos(k_y a/2)] \quad (II.12)$$

Similarly,

$$H_{12} = -\gamma_0[\exp(ik_y a/\sqrt{3}) + 2\exp(-ik_y a/2\sqrt{3})\cos(k_x a/2)] \quad (II.13)$$

H_{13} denotes interaction between A and A' atoms

$$H_{13} = 2\gamma_1\cos(k_z c_0) \quad (II.14)$$

where $\gamma_1 = \int \chi^*(\mathbf{r}-\mathbf{r}_A)\hat{H}\,\chi(\mathbf{r}-\mathbf{r}_{A'})d^3r$. The element H_{14} denotes interactions between atoms A and B'. Denoting γ_1' the appropriate resonance integral one gets

$$H_{14} = 2\gamma_1'\cos(k_z c_0)[\exp(-ik_y a/\sqrt{3}) + 2\exp(ik_y a/2\sqrt{3})\cos(k_x a/2)] \quad (II.15)$$

The remaining elements are obtained assuming that the resonance integrals are dependent only on the relative positions of atoms and using the symmetry of atomic positions

$$H_{23} = H_{14}$$
$$H_{24} = H_{23}^* \quad (II.16)$$
$$H_{34} = H_{12}^*$$

It is convenient to denote diagonal matrix elements by H_0 and parameterize $\Gamma = 2\cos(k_z c_0)$ and $S = \exp(ik_y a/\sqrt{3}) + 2\exp(-ik_y a/2\sqrt{3})\cos(k_x a/2)$.

The secular equation in this notation has the following form

$$\det \begin{vmatrix} H_0-E & -\gamma_0 S & \gamma_1 \Gamma & \gamma_1' \Gamma S^* \\ -\gamma_0 S^* & H_0-E & \gamma_1' \Gamma S^* & \gamma_1' \Gamma S \\ \gamma_1 \Gamma & \gamma_1' \Gamma S & H_0-E & -\gamma_0 S^* \\ \gamma_1' \Gamma S & \gamma_1' \Gamma S^* & -\gamma_0 S & H_0-E \end{vmatrix} = 0 \qquad (II.17)$$

which is a fourth degree equation with no general analytic solution. One can neglect γ_1' in the lowest approximation and then the approximate solutions become

$$E = H_0 \pm \tfrac{1}{2}\gamma_1 \Gamma \pm [\tfrac{1}{4}\gamma_1^2 \Gamma^2 + \gamma_0^2 |S|^2]^{\frac{1}{2}} \qquad (II.18)$$

S vanishes along the zone edge HKH and one obtains two degenerate bands of $E_2 = E_3 = H_0$. The energies of the two remaining bands are $E_1 = H_0 - \gamma_1 \Gamma$ and $E_4 = H_0 + \gamma_1 \Gamma$. Away from the edge the lowest term is quadratic in the in-plane vector $\kappa = k - k_K$ (Figure II.4.). Elements containing γ_1' are multiplied by S and are zero at the zone edge. For small values of κ they can be neglected because their lowest order contribution to energy is proportional to $(a\kappa)^4$. There is no overlap between valence and conduction bands and within this approximation graphite remains a zero-gap semiconductor.

The model of Wallace failed to predict the semimetallic properties of graphite. Nevertheless, it showed that the carriers are located in the region around the edge of the Brillouin zone. This was the basis for the development of the model by Slonczewski and Weiss (1958) and McClure (1957) (SWMcC) that is widely used for the description of the electronic properties of graphite.

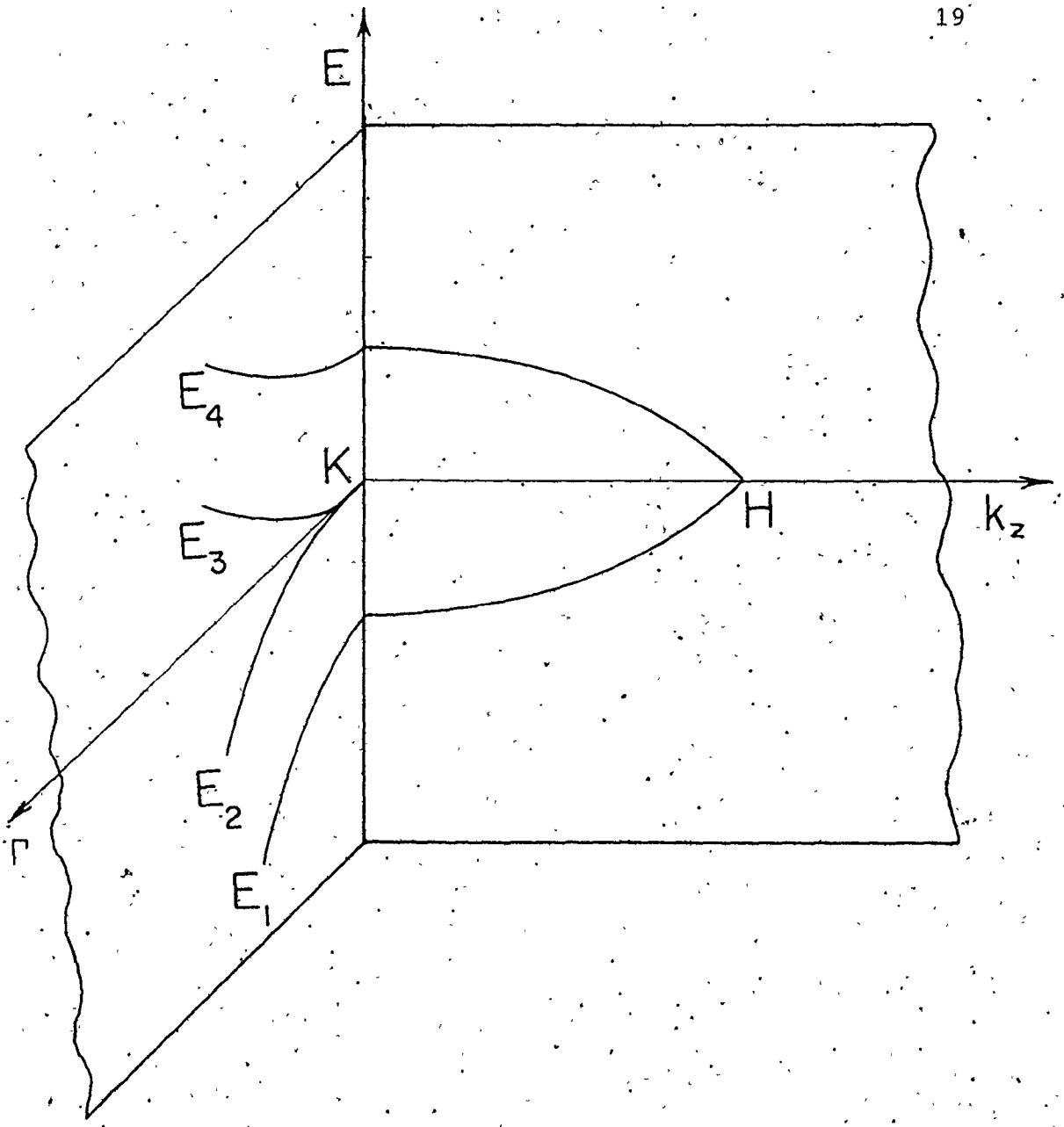

Figure II.4. Schematic energy bands near HKH zone edge of graphite obtained from the three-dimensional model of Wallace.

The basic idea of the model is to use the fact that the region occupied by carriers is small compared with the in-plane reciprocal lattice vector and make a Taylor expansion of the Hamiltonian in the k_{xy} plane and a Fourier expansion in the k_z direction. The in-plane expansion uses k·p formalism which is based on the following.

Suppose for a given value of k_0 a Bloch wave function $\psi(k_0,r)$ satisfies the Schrodinger equation

$$\hat{H}\,\psi(k_0,r) = E_0\,\psi(k_0,r) \qquad (II.19)$$

For the value of $k = k_0+\kappa$, one looks for a solution of the form

$$\psi(\kappa,r) = e^{i\kappa r}\,\psi(k_0,r) \qquad (II.20)$$

substituting the wave function into the Hamiltonian one gets

$$\hat{H}\,\psi(\kappa,r) = [\frac{\hat{p}^2}{2m} + V(r)]e^{i\kappa r}\,\psi(k_0,r) =$$

$$= e^{i\kappa r}\{\frac{\hbar^2\kappa^2}{2m} + \frac{\hbar}{m}\kappa\hat{p} + \frac{\hat{p}^2}{2m} + V(r)\}\,\psi(k_0,r) \qquad (II.21)$$

The last two terms give E_0 because

$$\{\frac{\hat{p}^2}{2m} + V(r)\}\,\psi(k_0,r) = \hat{H}\,\psi(k_0,r) = E_0\,\psi(k_0,r) \qquad (II.22)$$

Therefore, one obtains a new equation

$$\hat{H}'\,\psi(k_0,r) = E(\kappa) \qquad (II.23)$$

where $\hat{H}' = \{\frac{\hbar^2\kappa^2}{2m} + \frac{\hbar}{m}\kappa\hat{p}\}$ and $E(\kappa) = E(k)-E_0$.

Thus, the problem is reduced to finding the energy change induced by the perturbation $\hat{H}'$ which is described by the momentum operator $\hat{p}$ acting on states $\psi(k_0,r)$.

The values of the $\hat{p}$ matrix can be evaluated knowing the exact solution to the Hamiltonian for the value of k_0.

In practice, group theory considerations are used to derive the form of the matrix and the values of elements are obtained experimentally.

In two-dimensional graphite the carrier properties are determined by the band structure in the vicinity of the corner U of the Brillouin zone. A $\mathbf{k}\cdot\mathbf{p}$ expansion of the bands gives the electron energy as

$$E = E_0 \pm \frac{\hbar}{m} p_0 |K| \qquad \text{(II.24)}$$

which is identical to the result obtained by Wallace from the tight binding calculations with $\gamma_0 \frac{\sqrt{3}}{2} a = \frac{\hbar}{m} p_0$.

In the case of three-dimensional graphite, four bands are included. They are Bloch states of atoms B, B' and Bloch states made of symmetrical and antisymmetrical combinations of the states of atoms A and A'. A Fourier expansion is used for the k_z dispersion and a $k\cdot p$ expansion is used for the dispersion in the k_{xy} plane. The Hamiltonian is commonly written in the form

$$H = \begin{pmatrix} E_1 & 0 & H_{13} & H_{13}^* \\ 0 & E_2 & H_{23} & -H_{23}^* \\ H^*_{13} & H^*_{23} & E_3 & H_{33} \\ H_{13} & -H_{23} & H_{33}^* & E_3 \end{pmatrix}, \qquad \text{(II.25)}$$

For an accurate description of the Fermi surface properties, seven expansion parameters are satisfactory $\gamma_0 \ldots \gamma_5$ and Δ. In terms of these parameters, the matrix

elements are

$$E_1 = \Delta + \gamma_1\Gamma + \tfrac{1}{2}\gamma_5\Gamma^2$$
$$E_2 = \Delta - \gamma_1\Gamma + \tfrac{1}{2}\gamma_5\Gamma^2$$
$$E_3 = \tfrac{1}{2}\gamma_2\Gamma^2 \qquad \text{(II.26)}$$
$$H_{13} = \tfrac{1}{\sqrt{2}}(-\gamma_0 + \gamma_4\Gamma)\sigma\exp(i\alpha)$$
$$H_{23} = \tfrac{1}{\sqrt{2}}(\gamma_0 + \gamma_4\Gamma)\sigma\exp(i\alpha)$$
$$H_{33} = \gamma_3\Gamma\sigma\exp(i\alpha)$$

where $\Gamma = 2\cos(k_z c_0)$, $\sigma = \frac{\sqrt{3}}{2}a|\kappa|$ and κ is the in-plane wave vector and α is the angle between κ and the $K\Gamma$ direction. The values of expansion parameters and their physical meaning are given in Table II.1.

The Fermi surface of graphite is shown in Figure II.5. It consists of three elongated trigonally warped hole and electron pockets. The Fermi surface has three-fold symmetry with respect to HKH edge of the Brillouin zone. The Fermi surface is highly anisotropic, the length along the c-axis is about 13 times the width perpendicular to that direction. The center pocket contains electrons and the outer pockets contain holes. The zone boundary cuts hole pockets into two pieces which are referred to as majority and minority holes. It is interesting to note that the band overlap and, consequently, the number of carriers depends on the width of E_3 bands along the HKH edge determined by γ_2, the parameter describing interaction between the second nearest neighbor in the c direction.

Table II.1. Slonczewski-Weiss-McClure band parameters for graphite (from Dresselhaus and Dresselhaus 1980)

Band Parameter	Order of Magnitude (eV)	Physical origin
γ_0	3.16 ± 0.05	Overlap of neighboring atoms in a single layer plane.
γ_1	0.39 ± 0.01	Overlap of orbitals associated with carbon atoms located one above the other in adjacent planes. Width of π bands at point K is $4\gamma_1$.
γ_2	-0.020 ± 0.002	Interaction between atoms in next nearest layers and from coupling between π and σ bands. Band overlap is $2\gamma_2$. Majority de Haas-van Alphen frequencies determined by γ_2.
γ_3	0.315 ± 0.015	Coupling of the two E_3 bands by a momentum matrix element. Trigonal warping of the Fermi surface determined by γ_3.
γ_4	0.044 ± 0.024	Coupling of E_3 bands to E_1 and E_2 bands by a momentum matrix element. Determines inequality of K-point effective masses in valence and conduction bands.
γ_5	-0.038 ± 0.005	Interaction between second nearest layer planes. Introduced in E_1 and E_2 to be consistent in the order of the Fourier expansion.
Δ	-0.008 ± 0.002	Difference in crystalline fields experienced by inequivalent carbon sites in layer planes. Volume of minority hole carrier pocket sensitive to Δ.

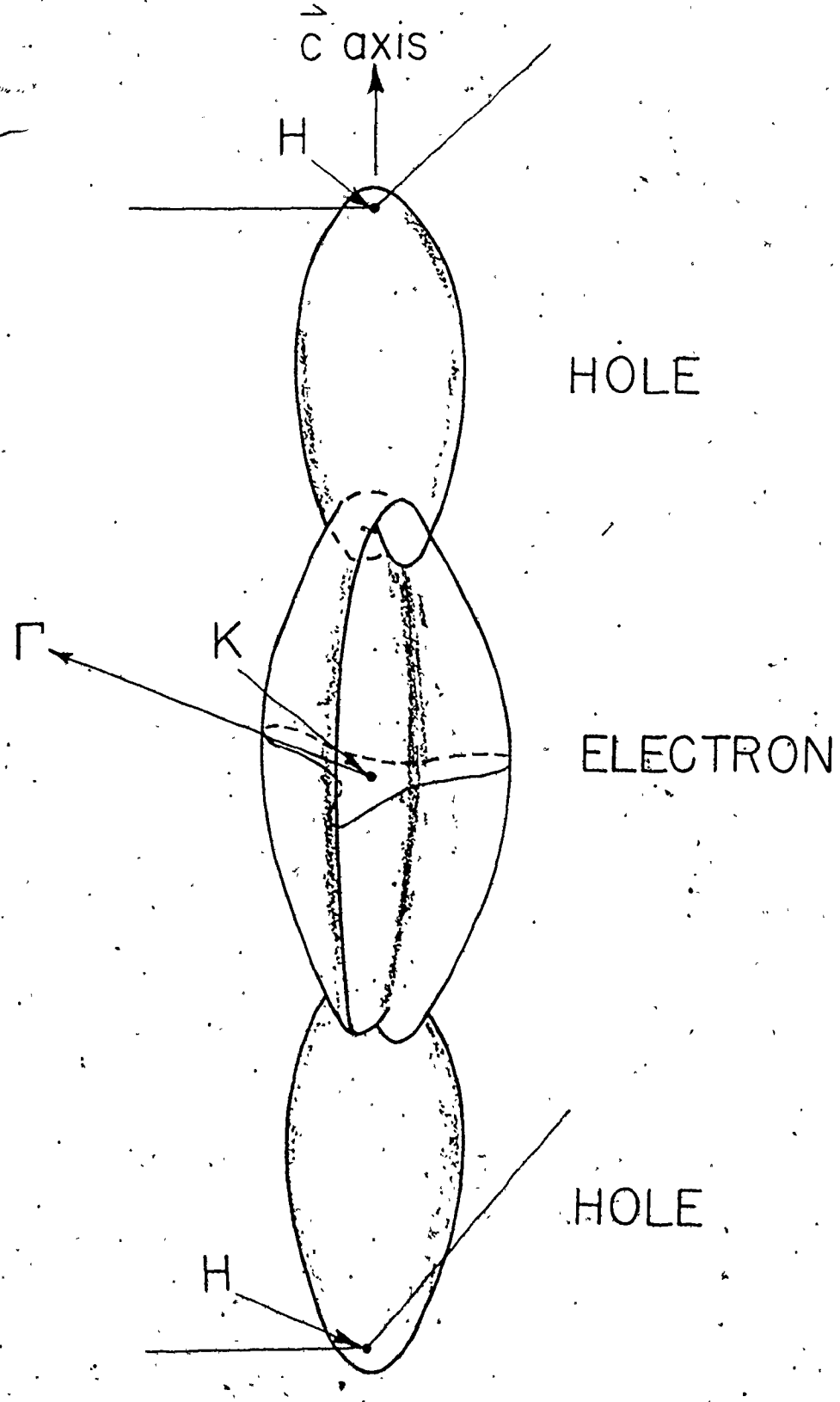

Figure II.5. Fermi surface of graphite.

The model of Slonczewski, Weiss and McClure is based on a first order expansion of the bands in the region of the Brillouin zone around the HKH edge. Therefore, it is not valid for the description of the electronic structure far away from the edge. A full band structure model was proposed by Johnson and Dresselhaus (1973) to account for the optical properties of graphite in the visible and ultraviolet range.

The model uses a Fourier expansion in which the Hamiltonian matrix elements describe interactions between orthogonalized atomic functions, e.g, Wannier functions. The matrix elements have the form

$$H_{ij} = \sum_{l} \exp(ikR_{ij}^{l})\gamma_{ij}^{l} \qquad (II.27)$$

where the indices i and j denote base atoms and γ_{ij}^{l} denote interactions between Wannier functions centered on atomic sites separated by a vector R_{ij}^{l}. The form of the Hamiltonian is similar to the one developed by Wallace (1947) for three-dimensional graphite. In the notation used by Johnson and Dresselhaus, the Hamiltonian matrix elements are written in the form

$$H_{ij} = \sum_{nml} M_{ij}^{nml} f_{nml}(k) \qquad (II.28)$$

where symmetrized Fourier function $f_{nml}(k)$ is, apart from an integer factor, a sum of exponential functions of equation (II.25) performed over all atomic sites separated by vectors whose magnitudes are equal to that of the vector $(na, ma/\sqrt{3}, lc_0)$ and Fourier coefficients M_{ij}^{nml} are equal to

Table II.2. Values of the Fourier-expansion parameters.

Parameter	Value (eV)
M_{AA}^{000}	0.0069
M_{BB}^{000}	0.0136
M_{AB}^{010}	-4.20
M_{AA}^{000}	0.0
M_{BB}^{000}	0.0
M_{AB}^{020}	-0.677
M_{AB}^{120}	-0.135
M_{AA}^{001}	0.267
M_{AB}^{011}	0.36
M_{BB}^{011}	0.60
M_{AA}^{002}	-0.0069
M_{BB}^{002}	-0.002

corresponding γ's times the integer factor where it is left out in calculations of the function $f_{nml}(k)$.

Ten interaction parameters are included in the model. The values of parameters are obtained by expanding the Hamiltonian in the lowest order around the edge of the Brillouin zone and comparing the coefficient of expansion to the SWMcC band parameters. Additional parameters are derived from optical data. The values of Fourier expansion coefficients are given in Table II.2. The parameters M_{AA}^{100} and M_{BB}^{100} were set to zero because they do not contribute to the frequency-dependent dielectric constant.

II.2 Development of the rigid band model of GIC.

Graphite is a compensated semimetal with a total carrier concentration of about 1 carrier per 10^4 atoms. The small number of carriers results from the fact that the valence band is almost full and the conduction band almost empty. The intercalated species are either fully or partially ionized. A charge of equal magnitude and opposite sign on carbon atoms maintains the neutrality of the compound. This charge is obtained by either removing electrons from the top of the valence bands or by filling the bottom of the conduction bands. In either case, a large increase of free carrier concentration results (Figure II.5). This mechanism of charge transfer between rigid graphite

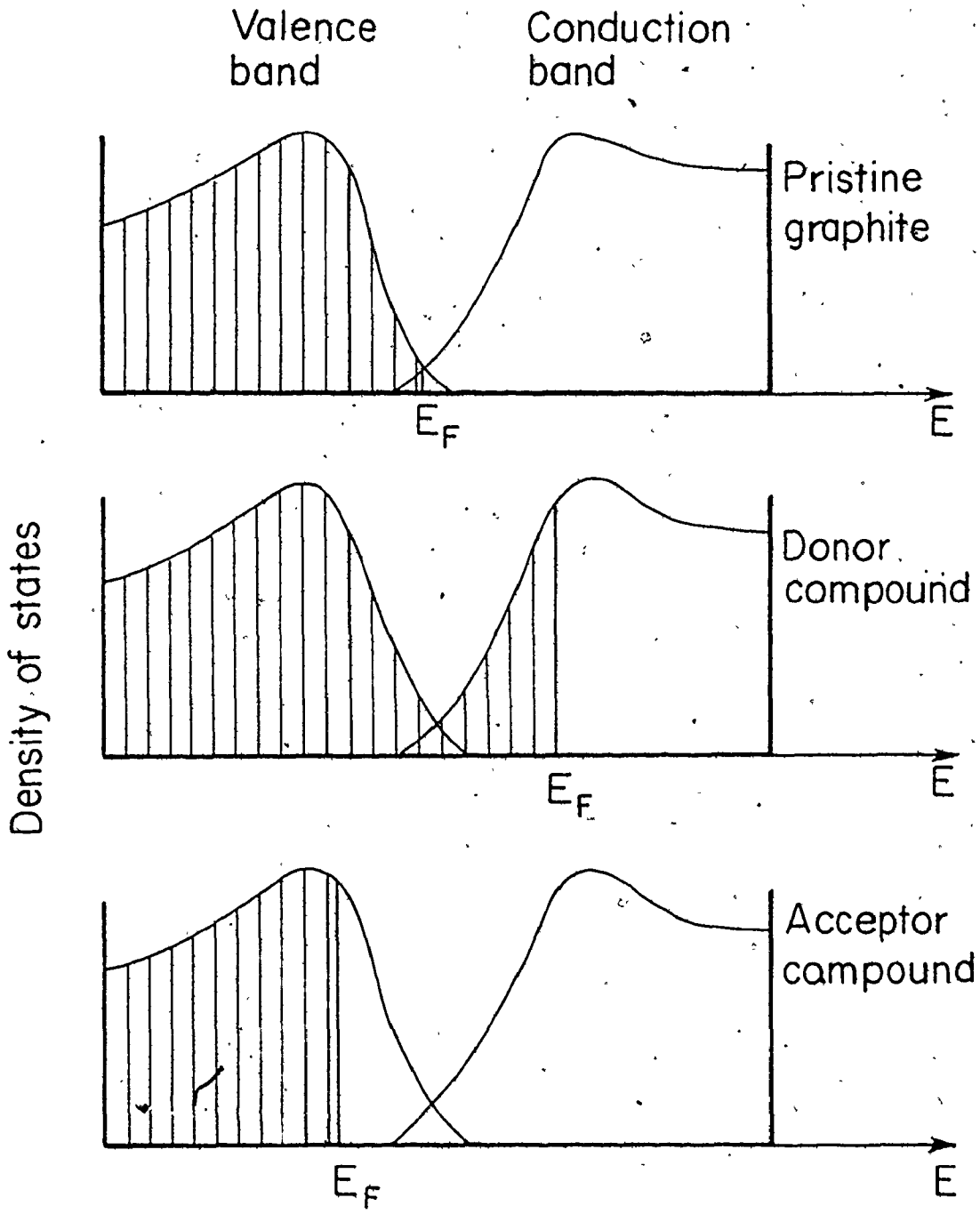

Figure II.6. Charge transfer in graphite intercalation compounds. The hatched areas correspond to filled states.

bands and intercalated potassium and bromine was proposed by McDonnell et al. (1951) to qualitatively explain a large increase of electric conductivity of the respective compounds. The idea of a rigid band model was then explored to describe the electronic properties of higher stage intercalation compounds (Dresselhaus et al. 1977). The band structure of GIC was assumed to be described by the SWMcC model. The effect of intercalant was primarily to increase the number of carriers by moving the Fermi energy.

Following these simple models, strictly quantitative models of the electronic structure of graphite intercalation compounds were developed that accounted for several major modifications of the structure of the graphitic π bands in intercalation compounds. The modifications result from:

i The staging, that is the presence of a regular intercalate stacking every n graphene layers for a stage n compound. This is a long range ordering that changes the c-axis spacing which results in changes in the number of atoms per unit cell and the number of bands. Furthermore, interactions between graphene and intercalate layers change c-axis band parameters.

ii Charge distribution between graphene layers. This charge distribution depends on the spatial distribution of the electronic wave functions which, in turn, depends on the atomic electrostatic potential which depends on the

charge distribution. The solution has to be self-consistent.

iii Change of interaction parameters due to charging of the bands.

iv Possible interaction between carbon and intercalate orbitals

v In-plane intercalate structure which defines a new in-plane lattice spacing.

In general, all the factors listed above introduce their own parameters which should be included in the band structure calculations. These parameters are not known a priori and have to be determined experimentally. One is then forced to consider special cases in which not all of the modifications are necessary.

Firstly, in the lowest stage compounds (1 and 2) the problem of charge distribution is eliminated because all the carbon atoms are adjacent to intercalate. Furthermore, there are only one or two basic bands which can be easily identified if detected.

Secondly, among the large number of species that can be intercalated there are a few whose in-plane structure does not affect the Fermi surface.

Thirdly, one can assume in the first approximation that the interaction between carbon atoms and intercalate and between carbon atoms separated by intercalate layer is

zero while the remaining interactions between carbon atoms are the same as in the pristine graphite. This gives a system consisting of two-dimensional mutually decoupled conductors made of n graphene layer for a stage n compound.

The last assumption is applicable in the case of acceptor compounds because the large anisotropy (10^5) of conductivity suggests that the c-axis electron dispersion is small. This results from small interactions along the c-axis which can be assumed to be zero or included as a small perturbation. In donor compounds, the distance between carbon and intercalate atoms is smaller than the sum of ionic radii which implies the hybridization of graphite and intercalate bands. In this case the rigid band model based on the π bands of graphite is not expected to be valid (Fischer 1977).

II.3 Rigid band models of GIC.

The band structure models of graphite intercalation compounds are based on the following assumptions:

i The bands are made from carbon $2p_z$ orbitals.

ii The band structure of stage 1 and 2 compounds is the same as a structure of a single and double graphene layer, respectively.

iii The interactions between carbon orbitals are the same as in pristine graphite.

iv All interactions with an intercalate are ignored

v The in-plane lattice vectors are the same as those in pristine graphite

vi The Fermi energy is adjusted to accommodate all carriers coming from the intercalate.

There are several qualitative conclusions that follow directly from these assumptions. The electronic structure is two-dimensional and the energy depends on the in-plane component of the electron momentum. There are 2n atoms per unit cell that gives 2n base states and 2n bands. Because the interplanar interactions are an order of magnitude weaker than the in-plane interactions, one expects that there will be n valence and n conduction bands with little overlap between them and either the valence or conduction bands will be partially occupied. Finally, the Fermi surface size is about 1/100 of the in-plane Brillouin zone size and is located near the corner of the zone.

It has to be emphasized that the models describe the electronic structure of intercalation compounds rather than that of graphite. The interactions between carbon atoms in GIC are assumed to have the same values as those in pristine graphite. However, the number of atoms per unit cell varies from stage to stage and, in fact, for various stages different band structures are obtained.

The simplest model of the electronic structure has

been proposed by Blinowski et al. (1980). The model is based on the tight binding approximation and includes nearest neighbor interactions.

For a stage-1 intercalation compound there are two atoms per unit cell denoted by A and B and only the interactions between the nearest neighbor A and B atoms are included. This gives the Hamiltonian matrix element H_{11} = constant which can be set to zero by choosing an appropriate energy scale. The element H_{12} is equal to

$$H_{12} = -\gamma_0[\exp(ik_y a/\sqrt{3}) + 2\exp(-ik_y a/2\sqrt{3})\cos(k_x a/2)] \quad (II.29)$$

The energy solutions are then

$$E = \pm |H_{12}| \quad (II.30)$$

This result can be obtained from the two-dimensional graphite model of Wallace (1947) by putting $\gamma_0' = 0$.

Since the Fermi surface is small compared to the in-plane Brillouin zone size, the energy is well approximated by the linear relation

$$E = \pm \frac{\sqrt{3}}{2}\gamma_0 a|K| \quad (II.31)$$

where $K = k - k_U$. The resultant dispersion in the vicinity of the point U is shown schematically in Figure II.7.

In a stage-2 compound there are two graphene layers and one has to include interplanar interactions in addition to the in-plane interaction. In the model of Blinowski et al., only γ_1 is included. The Hamiltonian has the form

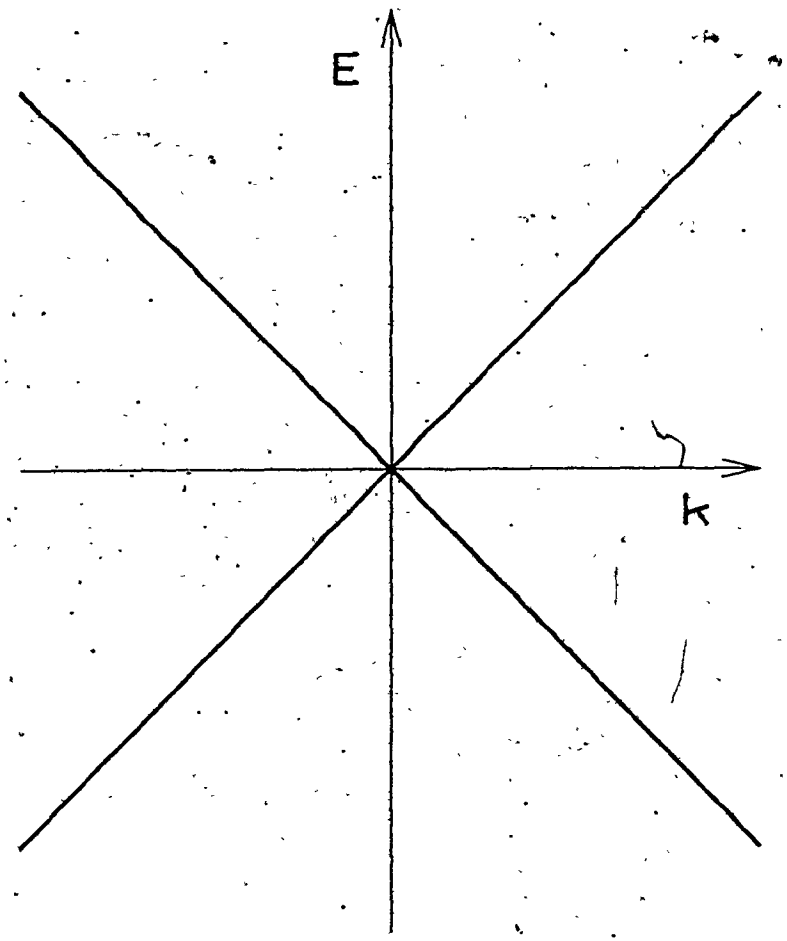

STAGE 1

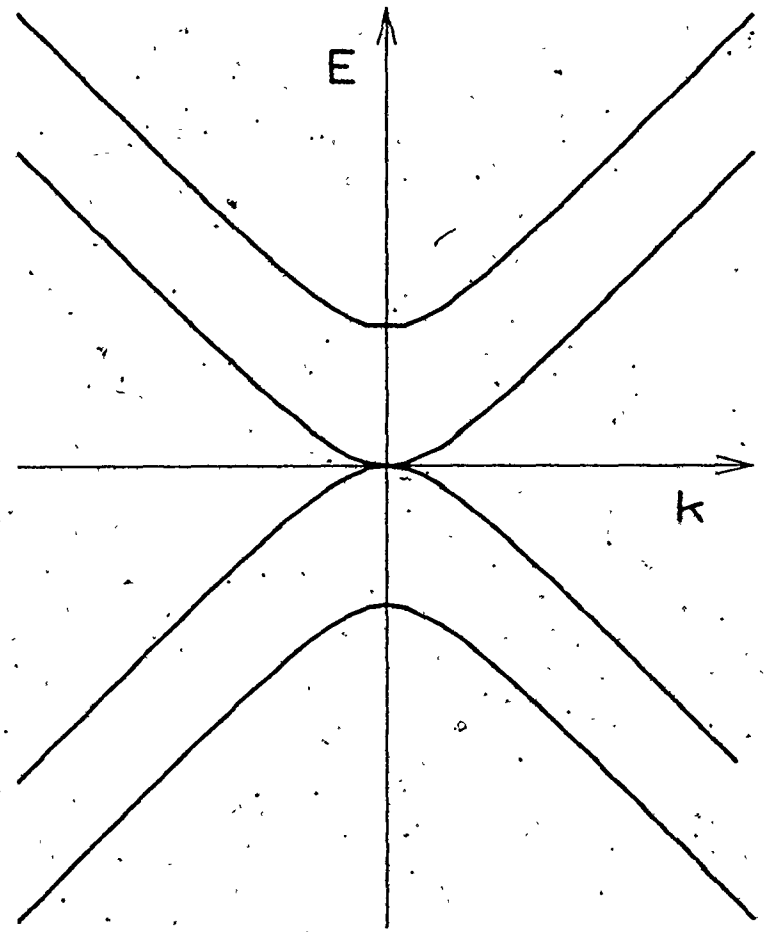

STAGE 2

Figure I.1.7, Schematic energy bands of stage-1 and stage-2 intercalation compounds near the point U according to the model of Blinowski et al.

$$\hat{H} = \begin{pmatrix} 0 & H_{12} & H_{13} & 0 \\ H_{12}^{*} & 0 & 0 & 0 \\ H_{13}^{*} & 0 & 0 & H_{12}^{*} \\ 0 & 0 & H_{12} & 0 \end{pmatrix} \qquad \text{(II.32)}$$

where H_{12} is the same as in the 2-D case and $H_{13} = \gamma_1$. This result can be obtained from Wallace's model by neglecting all parameters except γ_0 and γ_1 and setting $\Gamma = 1$. Again, one assumes that the wave vector is small and the energy is given by (Figure II.7)

$$E = \pm \tfrac{1}{2}\{(\gamma_1^2 + 3\gamma_0^2 a^2 k^2)^{\frac{1}{2}} \pm \gamma_1\} \qquad \text{(II.33)}$$

In this case two valence and two conduction bands are obtained. The valence and conduction bands meet at the point U, but there is no overlap between them.

The model has also been extended to higher stages (Blinowski and Rigaux 1980) in which case the electrostatic effect due to charge distribution has also been included.

A more elaborate model of the band structure of GIC was proposed by Holzwarth (1980). The model uses a Fourier expansion formalism, the same one that was used by Johnson and Dresselhaus (1973) for calculation of the full zone band structure of graphite.

The basis states are Wannier functions, that is, orthogonalized $2p_z$-like functions centered on atomic sites. The interactions between states of atoms separated by a vector $(na, ma/\sqrt{3}, lc_0)$, where n,m,l are integers whose values

are restricted by atomic positions, are denoted by $M_{\alpha\beta}^{nml}$ where α and β denotes types of atoms (A or B). There are two atoms per layer that give a 2nx2n Hamiltonian size for an n-stage compound. All diagonal Hamiltonian matrix elements are real. Also, the A atom sublattice is invariant with respect to in-plane inversion and the Hamiltonian matrix elements between A atoms on different layers are real.

$$H_{\alpha\beta}^{ij}(k) = \sum_{nm}{}' \tfrac{1}{2}(1+\delta_{ij}) M_{\alpha\beta}^{nm(i-j)} \mathrm{Re}[f_{nm}(k)] \qquad (II.34)$$

The remaining elements are

$$H_{\alpha\beta}^{ij}(k) = \sum_{nm}{}' \tfrac{1}{2}(1+\delta_{ij}) M_{\alpha\beta}^{nm(i-j)} f_{nm}(k) \qquad (II.35)$$

where i and j denote layers. For stages 2 and higher the B atom sublattice is not invariant with respect to the in-plane inversion and the corresponding matrix elements do not have to be real as was suggested in the original work of Holzwarth (1980). The factor $\frac{1}{2}$ comes from the loss of periodicity along the c-axis. The function $f_{nm}(k)$ is

$$\begin{aligned} f_{nm}(k) = {} & \cos(nk_x a)\exp(imk_y a/\sqrt{3}) + \\ & + \cos[\tfrac{1}{2}(n+m)k_x a)]\exp[i\tfrac{1}{2}(3n-m)k_y a/\sqrt{3}] + \\ & + \cos[\tfrac{1}{2}(n-m)k_x a]\exp[-i\tfrac{1}{2}(3n+m)k_y a/\sqrt{3}] \end{aligned} \qquad (II.36)$$

The values of the matrix parameters $M_{\alpha\beta}^{nm(i-j)}$ are given in Table II.3. The intralayer elements were obtained by fitting the model to the first-principle band structure calculation of two-dimensional graphite (Painter and Ellis 1970) especially around the point U of the Brillouin zone. The interlayer elements were derived from SWMcC band parameters.

Table II.3. Values of interaction parameters for graphite π bands.

Parameter	Value (eV)
M_{AA}^{000}	0.0
M_{AA}^{100}	0.37
M_{AB}^{010}	-2.59
M_{AB}^{0-20}	0.05
M_{AB}^{1-20}	0.42
*M_{BB}^{000}	-0.02
M_{AA}^{001}	0.25
M_{AA}^{002}	0.01
M_{AB}^{0-11}	0.24
M_{BB}^{011}	0.58
M_{BB}^{002}	-0.01

* This parameter describes the difference in crystalline field resulting from different configurations of out-of-plane neighbors of A and B atoms. It is zero in stage 1 and -0.01 eV in stage 2.

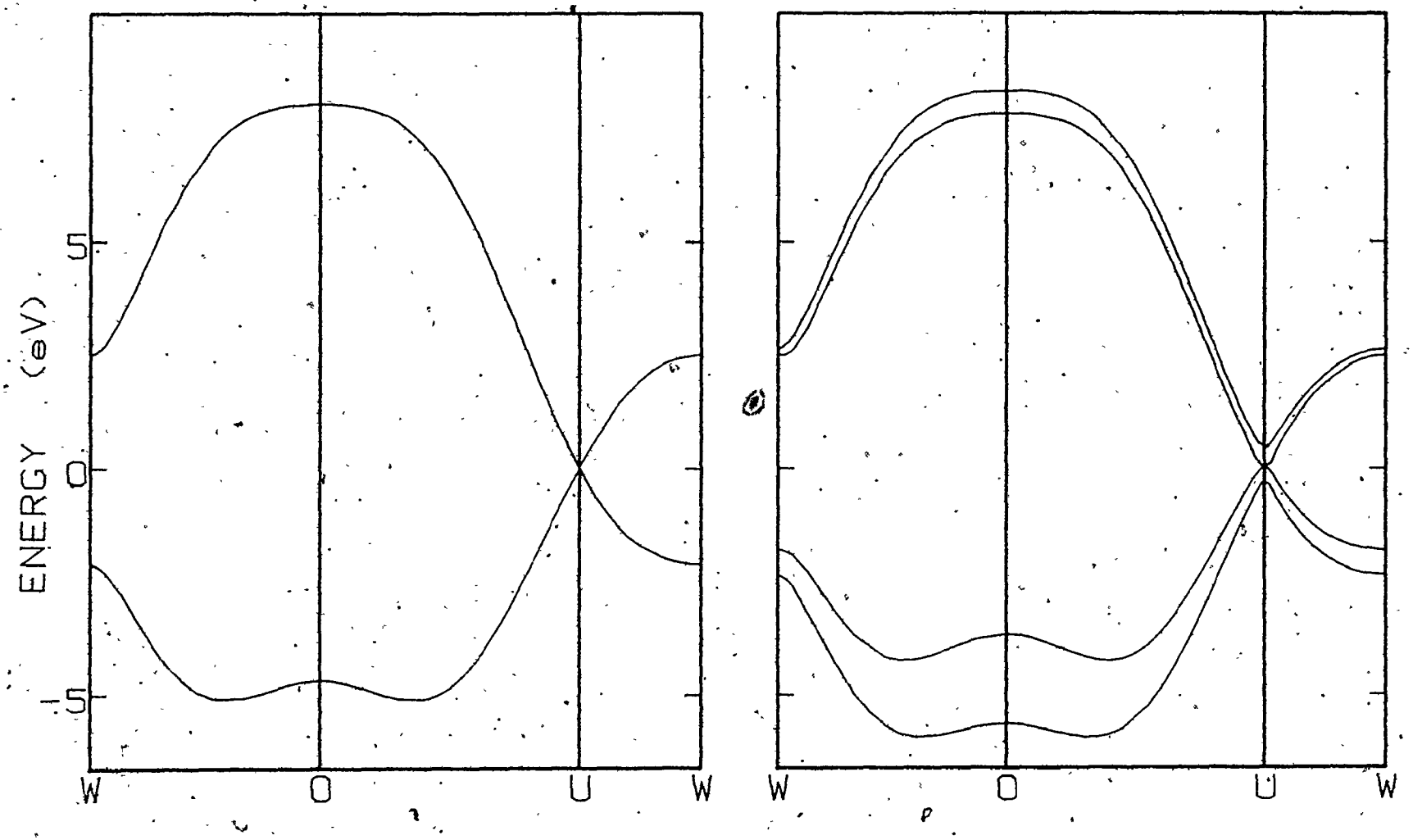

Figure II.8. Band structure of stage 1 (left) and 2 (right) graphite intercalation compounds calculated from the model of Holzwarth.

The band structures of stages 1 and 2 obtained from this model are shown in Figure II.8.

The band structure obtained from the Holzwarth model is qualitatively similar to that from Blinowski et al. that is, the number of bands and their essential features are the same. There are n valence and n conduction bands for a stage-n compound. The valence and conduction bands meet at the point U of the Brillouin zone. There is no overlap between valence and conduction bands in stage 1 and 2.

The addition of extra terms into the Hamiltonian of the Holzwarth model modifies the energy dependence on the electron momentum. The model is expected to be valid for a larger Fermi surface size than the simpler one proposed by Blinowski et al. This is an important factor since a typical Fermi surface size is about 10 % of the Brillouin zone size. The effective masses of valence and conduction bands are no longer the same and, furthermore, the bands are trigonally warped with three-fold symmetry around the point U.

CHAPTER III

EXPERIMENTAL TECHNIQUE AND APPARATUS

The major tool of study of the electronic properties of graphite intercalation compounds in this work is the de Haas-van Alphen effect. In this chapter the effect is described briefly. Following this, the details of the apparatus are presented.

III.1. De Haas-van Alphen effect.

The quantum mechanical solution to the problem of an electron in a crystal in the presence of a magnetic field can not, in general, be obtained. Instead, a semiclassical approximation and the Bohr-Sommerfeld quantization condition are used (Onsager 1952). The motion of an electron in the presence of a magnetic field is described by the Lorentz force equation

$$\hbar\dot{\mathbf{k}} = e(\mathbf{v} \times \mathbf{B}) \qquad \text{(III.1)}$$

where B is the magnetic field vector and v is the electron velocity. The constants of motions are energy and the component of momentum $k_{\parallel}$ parallel to the direction of the magnetic field. The electron orbit in reciprocal space is then an intersection of a constant-energy surface with a plane normal to the direction of the magnetic field. The

shape of the orbit depends on the particular band structure and need not be a closed curve. The real space orbit can be obtained by integrating (III.1)

$$\hbar(k - k_0) = e(r - r_0) \times B \qquad \text{(III.2)}$$

That is, the reciprocal space trajectory has the same shape as a projection of a real space trajectory on a plane normal to B except it is scaled by $\alpha = eB/\hbar$ and rotated by $\pi/2$. When the orbit is a closed curve, it becomes quantized. The allowed states are obtained using the Bohr-Sommerfeld quantization rule

$$\oint p\,dq = \oint (\hbar k - eA)\cdot dr = 2\pi\hbar(n + \gamma) \qquad \text{(III.3)}$$

where A is the vector potential, n an integer and γ is a phase factor ($\frac{1}{2}$ for free electrons). Substituting equation (III.2) and using Stokes' theorem one gets

$$\Phi = \frac{2\pi\hbar}{e}(n + \gamma) \qquad \text{(III.4)}$$

that is, the flux through allowed orbits is, apart from a phase factor, an integral multiple of the fundamental flux quantum $2\pi\hbar/e$. The reciprocal space areas of orbits are scaled by α^2 and are given by Onsager's condition

$$A_n = \frac{2\pi eB}{\hbar}(n + \gamma) \qquad \text{(III.5)}$$

That is, the area of allowed orbits in the plane normal to the magnetic field is quantized. The wavevector component parallel to the magnetic field $k_{\parallel}$, is not quantized and can assume the same values as in the absence of the field. The allowed states form tubes in reciprocal space whose axes are

parallel to the magnetic field direction and cross-sectional areas are given by (III.5). These states are called Landau levels.

The quantization of the allowed states leads to quantization of the energy spectrum and only energy values corresponding to orbits that satisfy Onsager's condition are allowed. The difference between areas of two subsequent Landau levels is $2\pi eB/\hbar$. The energy difference is

$$\Delta E = \left(\frac{\partial A}{\partial E}\right)^{-1} \Delta A = \hbar eB / \left(\frac{\hbar^2}{2\pi} \frac{\partial A}{\partial E}\right) \qquad \text{(III.6)}$$

The quantity $\left(\frac{\hbar^2}{2\pi} \frac{\partial A}{\partial E}\right)$ is called the cyclotron mass by analogy with the case of free electrons in a magnetic field whose energy levels are given by the formula

$$E_n = \frac{\hbar eB}{m} (n + \tfrac{1}{2}) \qquad \text{(III.7)}$$

The quantization of allowed states has a dramatic effect on the electron gas in a metal. At zero field, the number of states that electrons can occupy is equal to the number of atoms in a crystal that is about 10^{21}. In a magnetic field of about 1 Tesla, there are about 10000 Landau levels that can be occupied. This number has to be multiplied by the number of allowed $k_{\parallel}$ states, about 10^7. This gives a reduction of the number of allowed states by ten orders of magnitude. Each Landau level is highly degenerate to accommodate the electrons from all the states which are no lohger allowed.

The electronic properties of a metal depend on the

electrons at the Fermi energy which can be excited to empty states of higher energy states under a small perturbation. In the presence of a magnetic field, there is a large number of those electrons when a Landau level is tangent to the Fermi surface. When the magnetic field is increased, the level moves away from the Fermi surface and becomes empty. The number of "active" electrons decreases. Further increase of the magnetic field brings the next level tangent to the Fermi surface and the number of electrons at the Fermi energy becomes large again. This periodic variation of the number of electrons at the Fermi energy is observed in effects called quantum oscillatory phenomena. The best known are oscillations of electrical conductivity (Shubnikov-de Haas effect), magnetic susceptibility (de Haas-van Alphen effect), and magnetothermal oscillations (MTO). The period of oscillation is determined by the condition that a Landau level is tangent to the Fermi surface which occurs whenever the area of an orbit is equal to the extremal Fermi cross-section area.

$$A_n = \frac{2\pi eB}{\hbar} (n + \gamma) = A_F \qquad \text{(III.8)}$$

which is periodic in 1/B and the period is inversely proportional to the Fermi cross-sectional area

$$\Delta(1/B) = \frac{2\pi e}{\hbar} \frac{1}{A_F} \qquad \text{(III.9)}$$

In practice, the frequency of oscillation is measured and the cross-sectional area is calculated from

$$A_F = \frac{2\pi e}{\hbar} f \qquad \text{(III.10)}$$

where f is the dHvA frequency.

The quantum oscillatory phenomena, especially the de Haas-van Alphen effect, are very precise tools that are widely used to measure the size of a Fermi surface. They also give other information about the Fermi surface. The amplitude of the dHvA oscillations depends on the curvature of the Fermi surface along k_H. Other factors that affect the dHvA amplitude are scattering time and temperature. The scattering of carriers increases the width of Landau levels and reduces the dHvA amplitude. Temperature further reduces the amplitude of the oscillations of magnetization because thermal excitation of carriers decreases the sharp change of population of levels when they cross the Fermi energy. The effect of temperature is expected to depend on the ratio of temperature to the energy difference between Landau levels described by a dimensionless parameter $X = k_B T/\Delta E$. The theory of Lifshitz and Kosevich (1956) shows that the dHvA amplitude is proportional to $X/\sinh(2\pi^2 X)$. The difference of energy of Landau levels is dependent on the magnetic field and the cyclotron mass of carriers. The dHvA measurements are done at very low temperatures at which the phonon scattering is negligible. The scattering time is then independent of the temperature. Thus, cyclotron mass can be determined by fitting the temperature dependence of the dHvA

amplitude to the formula

$$A \propto T / \sinh(bm_c T/Bm_0) \qquad \text{(III.11)}$$

where T is the temperature, m_c is the cyclotron mass, B is the magnetic field, m_0 is the free electron mass and b is a constant equal to

$$b = 2\pi^2 k_B m_0/\hbar e = 14.693\ TK^{-1} \qquad \text{(III.12)}$$

III.2. Apparatus.

The de Haas-van Alphen measurements were performed with a standard low-frequency modulation technique. In this method, a sample is placed inside a set of coils. An alternating current of audio frequency (47-517 Hz range of frequency was used in the experiments) is fed to one coil which produces modulation of the magnetic field. The signal which is proportional to the rate of change of the sample magnetization is detected by another coil placed around a sample. A second coil is connected antiparallel to the pick-up coil to offset a steady component of the induced voltage.

The coil assembly was placed inside a 5.5 Tesla superconducting solenoid. All the measurements were done with the c-axes of the samples parallel to the direction of the magnetic field. In order to facilitate reproducible positioning of samples and also insulate them from the ambient atmosphere, a special coil assembly was made (Figure III.1). The inner part could be removed easily and put into

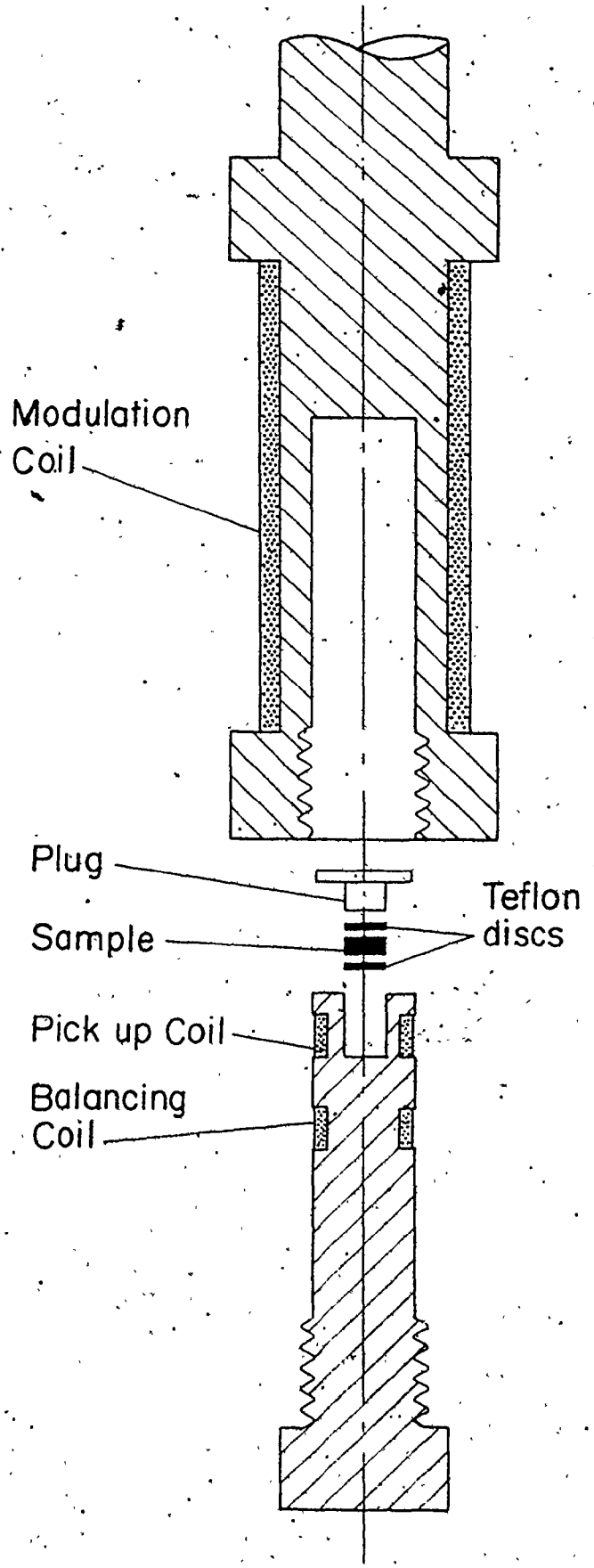

Figure 1. [illegible] holder and

a dry box. Samples were laid against a smooth surface inside the pick-up coil and sealed with a tight-fitting plug. This reliability of sample positioning was checked by measuring the dHvA effect of antimony with samples of similar shape and size. The antimony samples had their trigonal axis perpendicular to the flat faces of samples. From the analysis of the dHvA signal of antimony it was found that the reproducibility of orientation was within 2°.

Figure III.2 shows a block diagram of the detection system. Modulation current was supplied by a low distortion amplifier driven by a precision sine wave oscillator. A large resistor (250 Ω) was connected between the output of the amplifier and the modulation coil to stabilize the modulation current. The signal from the pick-up coil was fed into a lock-in amplifier set to operate at the second harmonic of the modulation frequency. The output of the amplifier was recorded on a chart. Digital processing was facilitated by sampling and recording the data. The dHvA signal was measured at the output of the lock-in amplifier. The value of the magnetic field was obtained by measuring the current of the supe,conducting magnet. Initially, the recording system consisted of a multiplexer that fed alternately signal and field values to a digital voltmeter. The output from the voltmeter was recorded on magnetic tape. The tape was then read and data analyzed by a CDC 6400

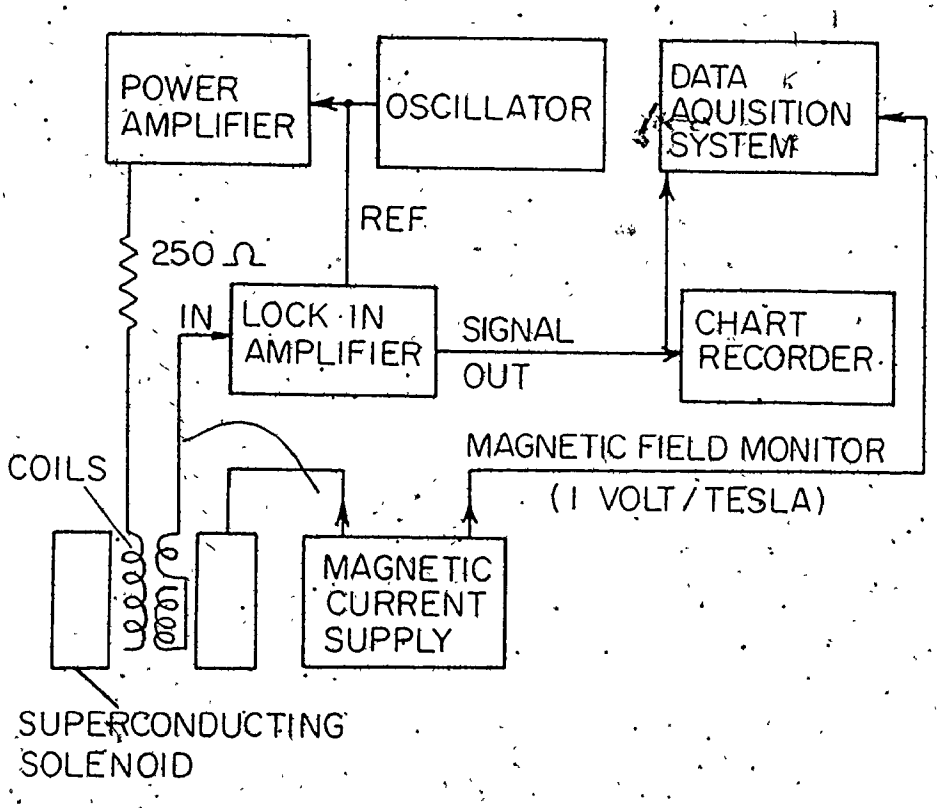

Figure III.2. Block diagram of the dHvA detection system.

computer. This system had two disadvantages. Firstly, the data were stored on the tape as a continuous stream of bits and had to be decoded. A single error could make the whole record unreadable. Secondly, the multiplexer and the voltmeter were triggered by a timer. The signal was sampled in regular time intervals that did not correspond to regular inverse magnetic field intervals required by the Fast Fourier Transform routine. The values required had to be interpolated from the recorded data. The interpolation calculations were time-consuming, introduced "ghost" frequencies and broadened the spectra. Later, to improve reliability of recording, an aquisition system controlled by a microcomputer was built.

The system consisted of two 16-bit analog-to-digital converters directly interfaced to a Pied Piper computer. In this system the signal and field values were simultaneously read every 0.2 s and only the signal values corresponding to the equally spaced intervals of the inverse magnetic field were stored for analysis. In practice, two refinements were found necessary to obtain good data. Firstly, the field readings were digitally filtered to reduce noise. Secondly, since the signal was usually sampled for the magnetic field values slightly different from the required ones, the value of the signal at the correct field was interpolated from the data. However, because the readings were taken very

frequently, a linear interpolation between two points was found sufficient. These calculations, field filtering and interpolation, were simple and were performed by the computer during data aquisition. The Fourier transform of the data obtained by this technique was free of "ghost" frequencies. The spectrum peaks were about 70 % sharper than those obtained from the old system for the same number of data points.

The cyclotron mass values were determined from the temperature dependence of the dHvA amplitudes between 1.3 and 4.2 K (typical). Various methods of measuring amplitudes were used in the present work. In the case where one dominant oscillation was observed the amplitudes were read off the recording chart. The second method used was to fit amplitudes of oscillations to a small magnetic field range of the recorded data. Sometimes a Fourier spectrum of the signal was truncated to contain only the contribution of the frequency of interest and then the spectrum was transformed back into inverse field domain and plotted. The results of all methods were consistent within the limits of error.

CHAPTER IV

SAMPLE PREPARATION

During this study a substantial amount of work was done on the preparation of intercalation compounds of graphite. This work involved improving existing methods of preparation and developing new ways of carrying out reactions.

The high reactivity of materials used for intercalation required handling in an atmosphere free of water vapor and oxygen. Most of the handling was then done in a glove box filled with dry nitrogen. The content of water vapor inside the dry box was less than 1 ppm.

The starting material for most of the work presented here was highly oriented pyrolitic graphite (HOPG) supplied by Dr Moore of Union Carbide. The slabs of HOPG were cut into pieces of about 3 x 3 mm . The pieces were cleaved to about 0.5 mm thickness. The outer layers were removed by peeling. The pieces were then washed in acetone in an ultrasonic cleaner. Single crystal natural graphite was also used and was obtained from a quarry near Harrisville N.Y.. The flakes of graphite were embedded in a marble-like mineral. They were removed by crushing the stones and then washing the pieces in boiling distilled water. Clean single

crystal and HOPG pieces were put into a glass container and dried under vacuum at an elevated temperature.

IV.1. X-ray characterization.

The stages of samples were determined with x-ray diffraction measurements using a powder diffractometer and Cu K_α radiation. Both single crystal and pyrolitic graphite samples were flat plates with the c-axis perpendicular to the plane of the samples. The samples were mounted in the diffractometer in the manner shown in Figure IV.1.

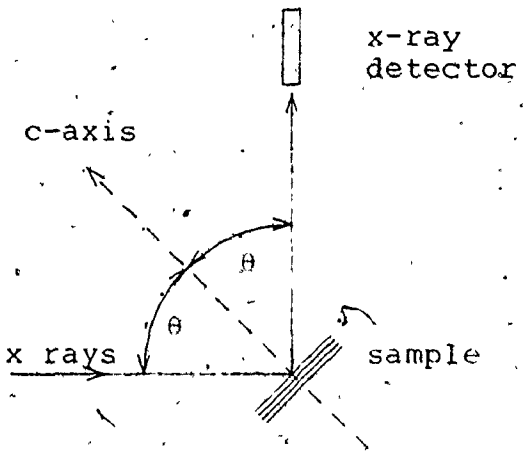

Figure IV.1. Geometry for measurement of x-ray (001) reflections.

The incident x rays were at the angle θ to the c-axis of the samples and detected at the angle of 2θ to the direction of incidence. The intensity of reflected radiation was recorded as a function of the angle 2θ (Figure IV.2). The positions

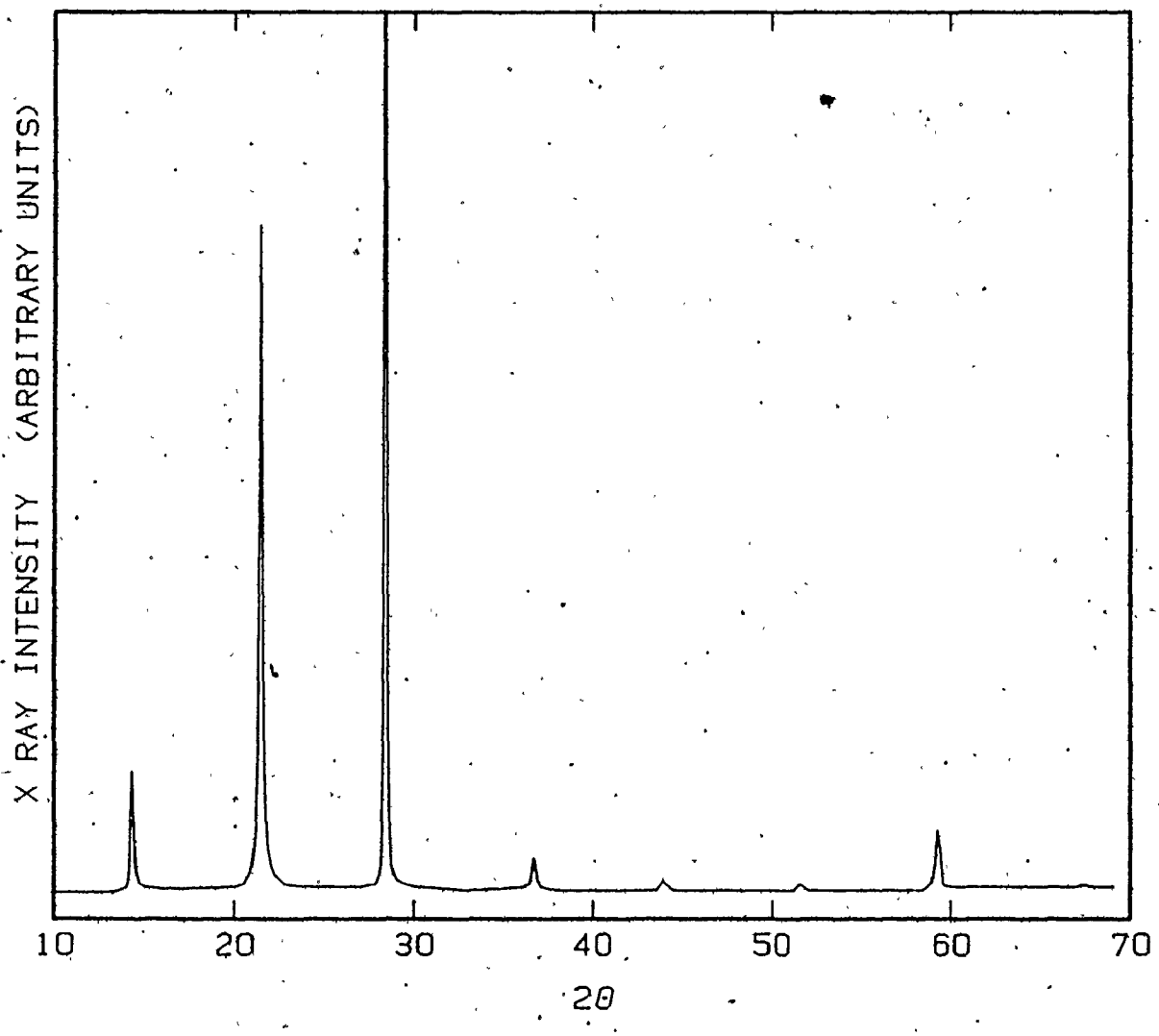

Figure IV.2. A typical (001) x-ray diffractogram of a stage-2 $SbCl_5$ intercalation compound.

of the (001) reflection peaks θ_1, were read off the recorder chart and values of $d_1 = I_c/l$, where I_c is the identity period along the c-axis, were calculated from the Bragg formula

$$d_1 = \lambda/2\sin(\theta_1) \qquad \text{(IV.1)}$$

A straight line was fitted to the order of reflection l versus $1/d_1$ and the value of I_c was calculated from the slope of the line. For samples that would decompose in air a holder was made (Figure IV.3) which permitted the isolation of samples from the atmosphere by two polyethylene discs.

IV.2. Preparation of antimony pentachloride graphite.

Antimony pentachloride was purified by three successive trap-to-trap vacuum distillations. Pure $SbCl_5$ was pale yellow in color and was stored in a pyrex tube that was kept in the dry box.

Stage 1 and 2 samples were obtained by the reaction of liquid $SbCl_5$ with graphite. Some stage-2 samples were also obtained by a two-zone method. The two-zone method of preparation of the stage-2 compound followed the preparation of Takahashi et al (1981). Most of the samples were obtained by reactions in liquid.

Reactions in liquid were performed in pyrex tubes (Figure IV.4). A piece of graphite was put into a tube and then a constriction was made in the middle of it. The tube

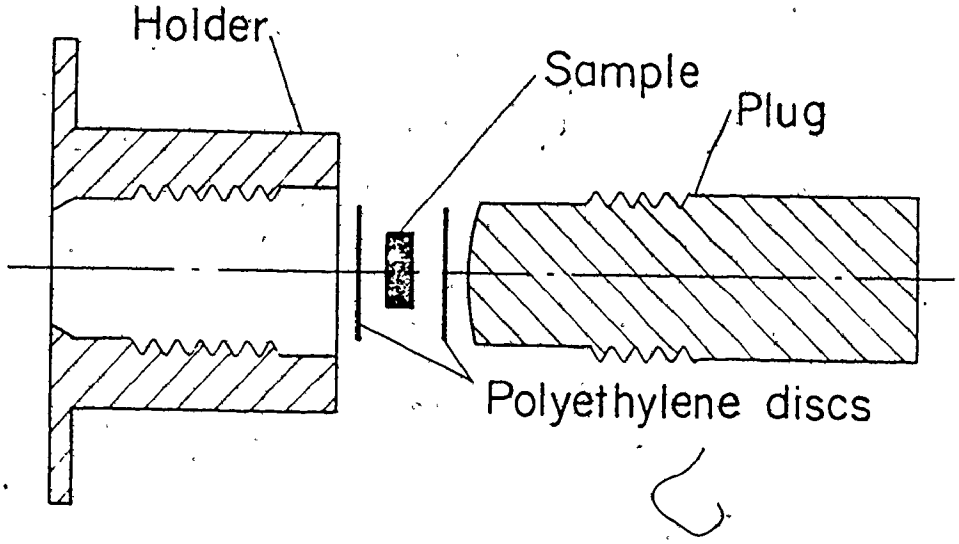

Figure IV.3. X-ray holder used for samples decomposing in air.

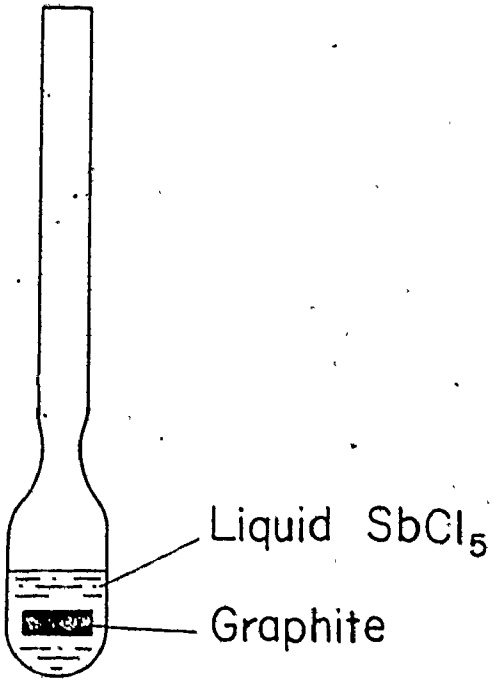

Figure IV.4. Reaction vessel used for preparation of $SbCl_5$ compounds.

was then connected to a vacuum line and evacuated for a few hours at an elevated temperature. After that, it was transferred into a dry box where antimony pentachloride was added to graphite. Nitrogen dissolved in antimony pentachloride was removed by pumping and periodically freezing $SbCl_5$ in the tube in liquid nitrogen. Then, the tube was sealed and put into an oven. After the reaction was completed the tube was inverted and the lower end was put into liquid nitrogen. When all unreacted $SbCl_5$ condensed in that end, the sample was sealed off.

Both stage 1 and 2 compounds were obtained by this method. Stage-1 compound was obtained by carrying out the reaction at about 200°C for one week. Stage 2 was obtained with a reaction of four days at approximately 100°C. The c-axis repeat distances were I_c = 9.42 ± 0.02 Å and 12.72 ± 0.02 Å for stage 1 and 2, respectively.

Stage-1 samples obtained by this technique had greenish-blue color and were relatively stable in the ambient atmosphere. Although, after a long air exposure, the surface of the samples showed signs of deterioration, the bulk was found to remain in stage 1 for up to five months.

It should be mentioned that some reactions did not produce a stage-1 compound. Instead, a mixture of stages 1 and 2 was obtained with stage-1 material occupying the interior layers while outer layers were mostly stage 2. The

results of x-ray and dHvA measurements, performed with these samples with outer layers removed were the same as those with pure stage-1 samples. However, the samples that did not react completely decomposed in air in a few days. This indicated that the decomposition of stage-1 antimony pentachloride graphite is accelerated by the presence of inhomogeneities.

IV.3. Preparation of SbF_6^- stage-1 compound.

The SbF_6^- compound was obtained by the reaction of nitryl hexafluoroantimonate with graphite and three methods of preparations were used. In the first method nitromethane solution of NO_2SbF_6 was used. Liquid sulphur dioxide was used as a solvent in the second method. In the third method graphite was reacted directly with solid nitryl salt.

a) Reaction in nitromethane solution.

A small amount (~2 ml) of dry nitromethane was poured into a glass. NO_2SbF_6 salt was added until some of the salt was left undissolved in the glass. One or two pieces of HOPG were then put into the solution. All the handling and reactions were done in the dry box. Reactions were carried out at room temperature and at about 60°C. Room temperature reaction proceeded slowly. After about one hour samples turned bluish on the surface indicating formation of

a stage-1 compound. The samples were left in the solution for one day to make sure that the reaction was completed. Samples decayed into a mixture of stage 1 and 2 in about one day after they were removed from the solution.

The reaction at higher temperature was much faster. Samples turned bluish and exfoliated after a few minutes. After about one hour the reaction changed character: the samples started to loose their bluish colour and the presence of a brown gas (NO_2) was observed. This process had to be avoided and the subsequent reactions were terminated before it started. Samples prepared by this method were stable up to 3 days after they were removed from the solution. The colour (blue-black) was more intense than in samples prepared at room temperature.

A fresh solution had to be prepared for each reaction. Attempts to reuse a solution for subsequent reactions failed to produce a stage-1 compound. This might have resulted from the presence of reaction by-products which could have been dissolved in the solution and could have inhibited subsequent reactions.

b). Reaction in SO_2 solution.

The reaction was carried out in a glass vessel containing two parts separated by a filter (Figure IV.5). A small amount of NO_2SbF_6 salt was put into part A of the

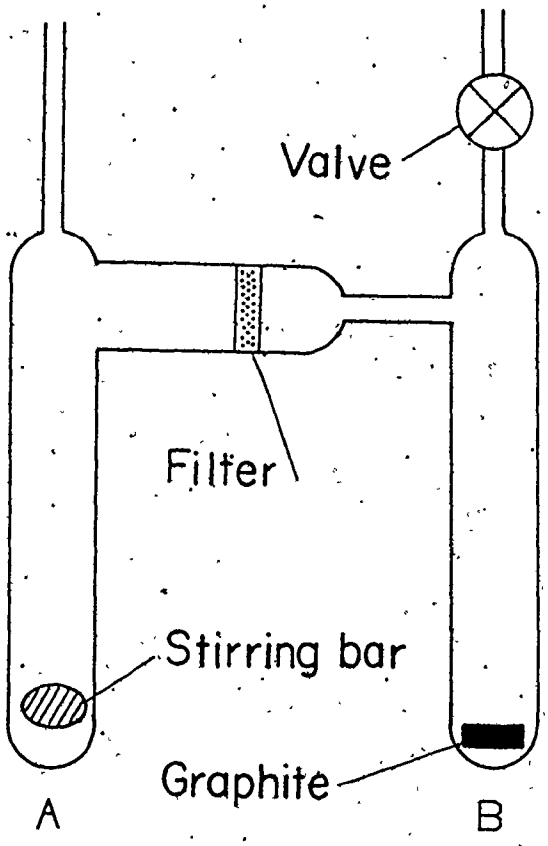

Figure IV.5. Reaction vessel used for preparation of SbF_6^- compound in liquid SO_2 solution.

vessel. The vessel was then evacuated and SO_2 was distilled into part B. Then the valve was closed and liquid SO_2 was poured into part A and mixed with the salt. Some undissolved salt was left indicating that the solution was saturated. Then pieces of HOPG were put into part B and the solution was poured onto it. After one day the solution was poured back into part A and excess SO_2 was gradually removed from part B by distillation with part A kept in cold water.

Samples appeared bluish-black and were unstable in a dry nitrogen atmosphere. Mass spectroscopy analysis of gases evolved during the decomposition of the samples showed that the decomposition was caused by evaporation of SO_2 which was trapped inside samples during the reaction. Freshly prepared samples were used for the dHvA study. X-ray characterization was done after the dHvA measurements.

Unlike nitromethane solution of NO_2SbF_6, the solution of the salt in liquid SO_2 could be used for subsequent reactions.

c) Reaction of HOPG with solid NO_2SbF_6.

During reaction of dissolved nitryl salts with graphite, solvent molecules are co-intercalated with anions (Billaud et al. 1980b). After samples are removed from the solution, the solvent molecules evaporate slowly from the samples causing decomposition. In search for more stable samples, the reaction was tried without using a solution.

Pieces of HOPG were put into 1/4" glass tube sealed at one end. Then a small amount of NO_2SbF_6 powder was placed in contact with the graphite. The tube was evacuated, sealed and put into an oven. Various temperatures were tried in the range of 40-180°C. In all cases, a blue-black compound was obtained indicative of a stage-1 sample. A high temperature reaction went fast (~15 minutes) but, unfortunately, the graphite exfoliated considerably and no dHvA oscillations were detected with those samples. Exfoliation was smaller when the reaction temperature was reduced. Good samples were prepared at temperatures in the range of 40 - 60°C. All samples were blue-black and stable in a dry nitrogen atmosphere and under vacuum.

The c-axis identity period of samples prepared in nitromethane solution was $I_c = 8.08 \pm 0.02$ Å and was independent of the reaction temperature. Samples prepared in SO_2 solution had $I_c = 8.24$ Å and those prepared without solution had $I_c = 8.19$ Å. The diffraction peaks were sharp and no traces of higher stages were observed in any of the samples prepared.

IV.4. Preparation of BF_4^- intercalation compound.

The BF_4^- compound was obtained by the reaction of graphite with solid nitryl tetrafluoroborate. Pieces of pyrolitic graphite (HOPG) were put into a glass tube in

contact with solid NO_2BF_4 salt. The tube was evacuated, sealed and put into an oven at 85 °C for one day. A black compound with greenish shade was obtained. The (001) x-ray diffraction pattern showed that a pure stage-2 compound was obtained. The c-axis identity period was $I_c = 11.13 \pm 0.02$ Å. The weight uptake during the reaction was also measured. The initial wight of one graphite piece was 5.6 ± 0.1 mg and increased to 9.4 ± 0.1 mg after the reaction. This gives the weight uptake of 68 ± 3 %. The samples were stable in a dry atmosphere and under vacuum.

CHAPTER V

EXPERIMENTAL RESULTS AND ANALYSIS

This work concentrated on the study of electronic properties of stage 1 and 2 acceptor-type graphite intercalation compounds. It was shown in Chapter II that a stage-1 compound has one graphitic band and a single de Haas-van Alphen oscillation should be observed. In a stage-2 compound, there are two valence bands and two dHvA oscillations are expected. However, in most compounds that have been studied previously, there were more dHvA oscillations than the number of basic graphitic bands. The large number of dHvA oscillations could have been caused by several phenomena. The most important is the presence of an intercalate superlattice. The extra periodicity created by an intercalate superlattice redefines the basic unit cell and may lead to splitting of the Fermi surface into smaller pieces. Additional problems are created by the presence of inhomegeneities. The inhomogeneous regions of macroscopic size give their own dHvA oscillations that make the dHvA spectra more complex. The correct identification of the observed dHvA frequencies is thus a key factor in the study of the compounds.

A proof of the correct identification of the oscillations can be obtained by comparing the observed frequencies with the amount of charge transfer for a particular compound. The charge transfer is obtained from dHvA data in the following way. The number of carriers per unit cell is equal to $2V_F/V_B$ where V_F is the total reciprocal space volume enclosed by the Fermi surface and V_B is the reciprocal space volume of the Brillouin zone. The factor of 2 comes from spin degeneracy. The volume of the Brillouin zone of a graphite intercalation compound is

$$V_B = (2\pi)^3/(\tfrac{3}{2}\, a^2 I_c) \qquad (V.1)$$

In the case of an acceptor compound the energy dependence on k_z is negligible and the volume enclosed by one piece of the Fermi surface is

$$V_{Fi} = 2\pi A_{Fi}/I_c \qquad (V.2)$$

where A_{Fi} is the Fermi surface cross-sectional area perpendicular to the k_z direction. The total volume is a sum of the volumes enclosed by all pieces of the Fermi surface multiplied by two. The factor of two comes from the fact that each band is doubly degenerate with two symmetry-related pockets of carriers around points U and U' of the Brillouin zone. The total volume is

$$V_F = \frac{4\pi}{I_c} \sum_i A_{Fi} \qquad (V.3)$$

The total charge per carbon atom x, is equal to the ratio of $2V_F/V_B$ (equations V.3 and V.1) divided by the 2n atoms in

the unit cell of an n-stage compound

$$x = \frac{a^2\sqrt{3}}{4\pi^2 n} \sum_i A_{Fi} \qquad (V.4)$$

The areas A_i are directly proportional to dHvA frequencies f_i, by

$$f_i = \frac{2\pi e}{\hbar} A_{Fi} \qquad (V.5)$$

Thus, the dHvA effect measures the charge transfer directly. Equation (V.4) was derived for basic graphitic bands. In the case of Fermi surface splitting due to an intercalate superlattice, one has to use the appropriate Brillouin zone size, the number of carbon atoms per unit cell and add all Fermi surface areas with opposite signs for electrons and holes including the appropriate multiplicities. This information cannot be obtained from the dHvA effect alone. Therefore, one can determine the charge transfer only from dHvA oscillations of the basic graphitic bands.

Unfortunately, the amount of charge transfer in most compounds is not known. Therefore, the agreement of the measured band parameters with theory was used to verify the identification of the dHvA frequencies. The use of theory as an aid in data interpretation seems inappropriate in the work which is aimed to check its validity. Nevertheless, there is a methodological justification for this procedure. The basic assumption is that the theoretical model is at least approximately correct. Then, the observed data have to

agree approximately with the theoretical predictions. If the discrepancy between theory and experiment is small, one can refine the theory using the experimental data. If, however, the model is not correct, there will be substantial disagreement in most compounds. In other words, the verification of theory is done on the basis of self-consistency.

The rigid band model of Holzwarth (1980) is used throughout this chapter. The model is the most elaborate and should be valid for any size of Fermi surface. The model of Blinowski et al. (1980) can be obtained as an approximation by neglecting terms other than the nearest neighbor interactions. In this chapter the comparison with theory is used to check the identification of the dHvA oscillations. The detailed discussion of the validity of the theoretical models is presented in the next chapter.

V.1. Antimony pentachloride graphite stage 1.

Stage-1 antimony pentachloride samples were handled in air. They were put into the dHvA holder and cooled slowly between room temperature and liquid nitrogen temperature. A typical recorder trace of the dHvA oscillations of a stage-1 sample is shown in Figure V.1. There is essentially a single oscillation. However, the envelope of the oscillation is slightly modulated and that indicates the presence of other

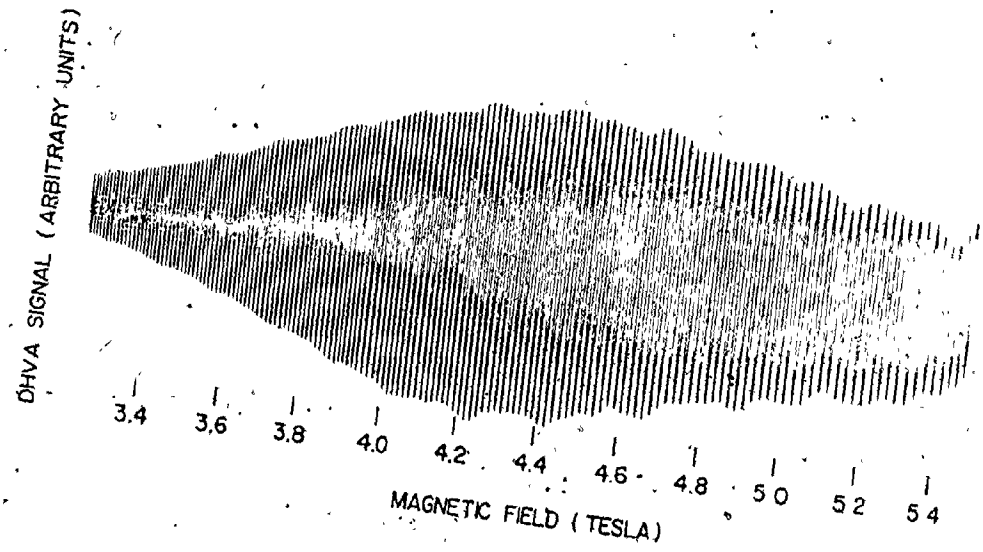

Figure V.1. De Haas-van Alphen oscillations of stage-1 $SbCl_5$ graphite intercalation compound.

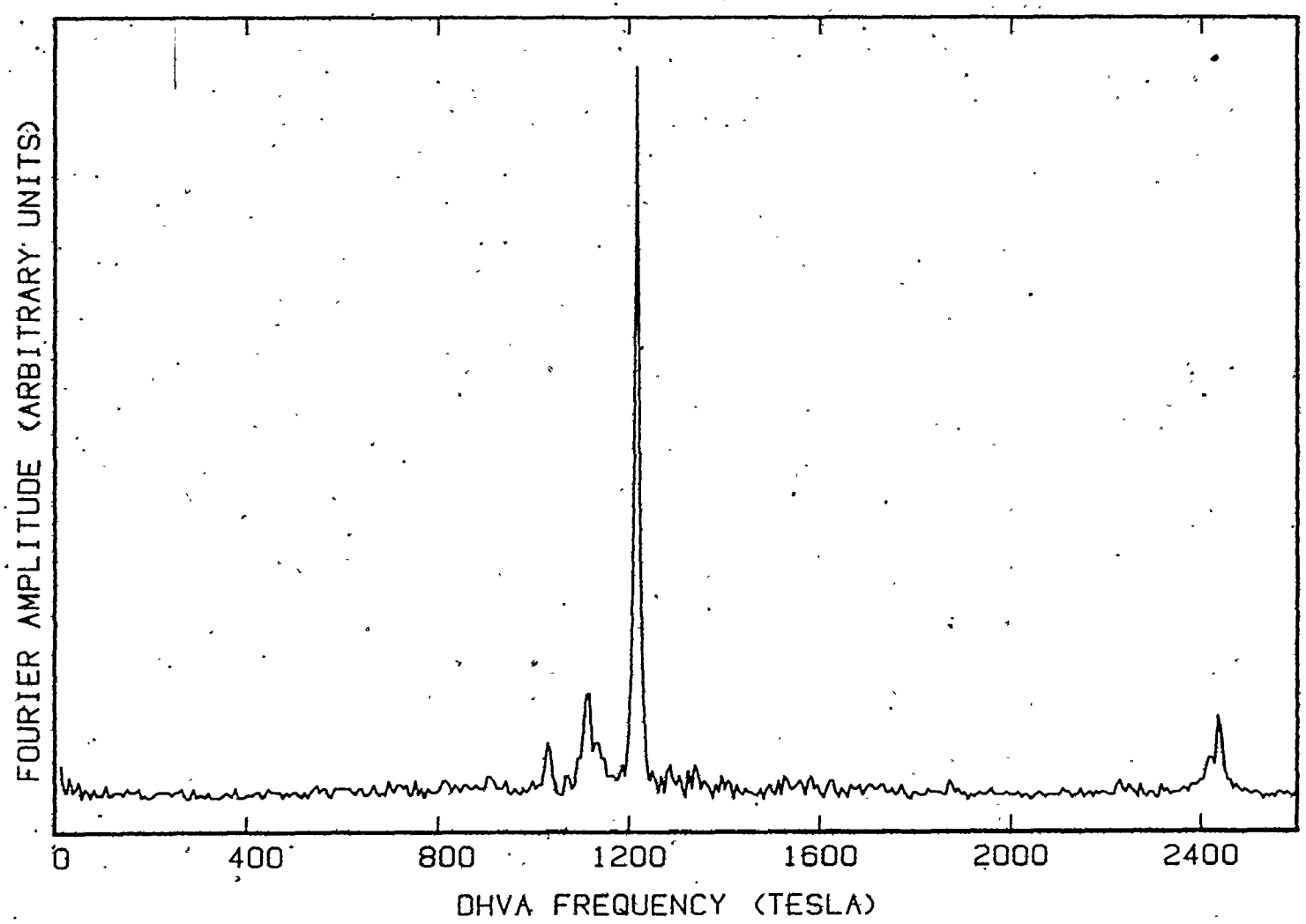

Figure.V.2. Fourier transform of the dHvA signal of stage-1 $SbCl_5$ compound.

dHvA oscillations. The Fourier transform of the data (Figure V.2) shows that there are two weaker oscillations of frequencies lower then that of the dominant one. The frequency of the dominant oscillation is $f_1 = 1212 \pm 2$ Tesla and the frequencies of the weaker oscillations are $f_2 = 1110 \pm 5$ T and $f_3 = 1026 \pm 5$ T. The relative amplitudes of f_2 and f_3 varied from sample to sample. This variation was found to be correlated with the time the samples were exposed to air prior to an experiment. For instance, the amplitudes of f_2 and f_3 relative to that of f_1 were 0.16 and 0.07, respectively, for a sample exposed to air for several minutes and increased to 0.25 and 0.1, respectively, for a sample kept in air for 10 days. After 2.5 months of air exposure, the amplitudes reached 0.9 and 0.16, respectively. In all cases (001) x-ray traces showed no deviation from a typical stage-1 (001) pattern. The values of the frequencies of the oscillations were reproducible from sample to sample and did not depend on air exposure.

The carrier effective mass corresponding to f_1 was obtained from the temperature dependence of the dHvA amplitude between 1.3 and 4.2 K (Figure V.3). The value of $0.271 \pm 0.001\ m_0$, where m_0 is the free electron mass, was reproduced with different samples within the limits of error. The effective masses of f_2 and f_3 could not be determined accurately. In samples with limited exposure to

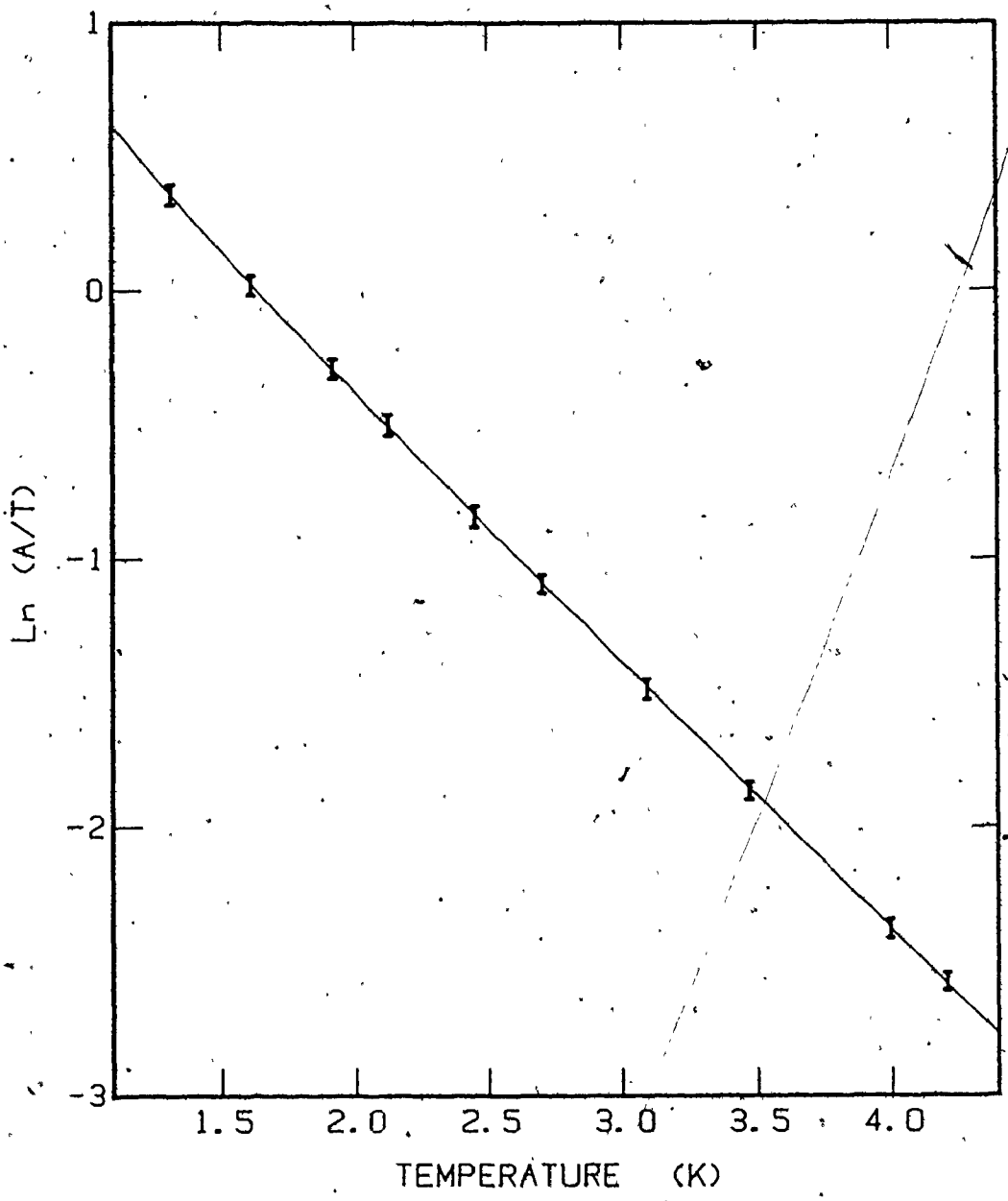

Figure V.3. Temperature dependence of the amplitude of the 1212 T oscillation. The data were fitted to the formula $A \propto T/\sinh(bm_c T/Bm_0)$ (solid line). The fitted mass is 0.271 m_0 with statistical uncertainty of 0.001 m_0.

air the presence of the strong f_1 oscillation of similar frequency introduced large errors in amplitude determination of f_2 and f_3 and in samples with long air exposure, the dHvA effect was detected only at the lowest possible temperature. However, the modulation of the dominant oscillation amplitude observed on the recorder trace was not found to depend on temperature and this suggests that the masses corresponding to f_2 and f_3 are similar to that of f_1. The spectra obtained with fresh samples that had not reacted completely and had stage-2 layers removed were the same as those with pure samples.

The variation of the amplitudes of f_2 and f_3 oscillations from sample to sample indicates the presence of macroscopic regions of different, although well defined, electronic structure within the samples. The presence of those regions is likely caused by some environmental-related aging processes.

The dominant frequency is interpreted to be intrinsic to pure and homogeneous stage-1 antimony pentachloride intercalated graphite and identified with the basic graphitic band. From equation V.5 the Fermi surface area corresponding to the frequency f_1 is 0.116 $Å^{-2}$. Using the band structure model of Holzwarth and the experimental value of the Fermi surface area, a value of the Fermi energy of -1.12 eV and the cyclotron mass of 0.274 m_0 were

calculated. This theoretical cyclotron mass is in good agreement with the measured value of 0.271 ± 0.001 m_0.

The fitted value of the Fermi energy also agrees with that of -1.1 to -1.2 eV determined from optical data (Heinz et al. 1983). The good agreement between theoretical predictions and experimental band parameters confirms the identification of the observed oscillation with the basic graphitic band.

Having identified the basic graphitic band one can determine the amount of charge transfer in the compound. Substituting the experimental value of the Fermi area into equation V.4 one obtains the value of 0.0307 elementary charge per carbon atom.

V.2. Stage-2 antimony pentachloride graphite.

The dHvA spectra of stage-2 samples do not change with air exposure nor do they depend on the method of preparation (reaction in liquid or in vapor phase). On the other hand, the spectra were found to depend on cooling rate between room temperature and 77 K. The frequencies and relative amplitudes of oscillations observed with samples cooled at various rates are presented in Table V.1. The experimental conditions were chosen to maximize the amplitudes of medium frequency oscillations (200-400 Tesla). The amplitudes of frequencies lower and higher than that

Table V.1. The dHvA oscillations and their Fourier amplitudes of stage-2 $SbCl_5$ samples cooled with different rates. The ranges of magnetic field analysed were similar for each sample (2-5 Tesla). The frequencies of oscillations are in Tesla and the numbers in brackets are Fourier amplitudes relative to the amplitude of the strongest oscillation in each sample. The sample 4B was cooled down in about 1 hour. The sample D21 was cooled down in 24 hours. The sample J10 was cooled to 240 K within about 1 hour and then overnight to 77 K. The sample number 30 was cooled slowly first, warmed to room temperature and quenched to 4.2 K within minutes.

4B	J10	D21	30
	13 (*)	13 (*)	
58 (30)			
			85 (21)
94 (57)	94 (4)		
110 (14)	114 (2)		
123 (27)			
136 (29)	136 (6)	137 (2)	
148 (14)			
158 (14)			
242 (36)	244 (3)	254 (1)	256 (43)
300 (67)	302 (6)		
352 (67)	354 (19)	350 (2)	355 (100)
363 (100)	364 (16)		366 (58)
	387 (41)	387 (8)	382 (67)
	398 (40)	400 (6)	
	420 (100)	422 (100)	421 (57)
	582 (5)		512 (19)
626 (10)	627 (4)		633 (2)
648 (16)	647 (8)	650 (2)	
	842 (4)	847 (4)	
	1126 (3)		
	1185 (8)	1189 (9)	

* This frequency was not seen in Fourier transform because it was observed at lower magnetic field than that taken for Fourier analyses.

were reduced by effects relating to the field modulation technique (see for example Shoenberg 1984). Furthermore, the cyclotron masses of carriers that produce high frequency oscillations are usually large and the amplitudes of the dHvA oscillations are decreasing almost exponentially with the cyclotron mass (see Chapter III). Therefore, quantitative comparison of the dHvA amplitudes can only be made with oscillations of similar frequencies.

Figure V.4 shows the Fourier transform of dHvA data obtained with a sample (#4B) that was cooled between room temperature and 77 K in about one hour. The spectrum is complex with several fundamental frequencies present. The spectra obtained with samples cooled slowly (about 24 hours) between room temperature and 77 K were much simpler and a typical Fourer transform of the data (sample D21) is shown in Figure V.4. The dominant dHvA oscillation of slowly-cooled samples has the frequency $f_1 = 422 \pm 2$ T, its second harmonic is observed at 845 ± 2 T. In the high frequency range an oscillation of frequency $f_2 = 1190 \pm 5$ T is observed. Sometimes a combination of $f_1 + f_2 = 1610$ T was also observed. The carrier effective masses corresponding to f_1 and f_2 are $m_{c1} = 0.146 \pm 0.002\ m_0$ and $m_{c2} = 0.267 \pm 0.003\ m_0$, respectively. In addition, a strong oscillation of frequency of 13 T was observed below a magnetic field of 1 T with all slowly cooled samples. These oscillations were not

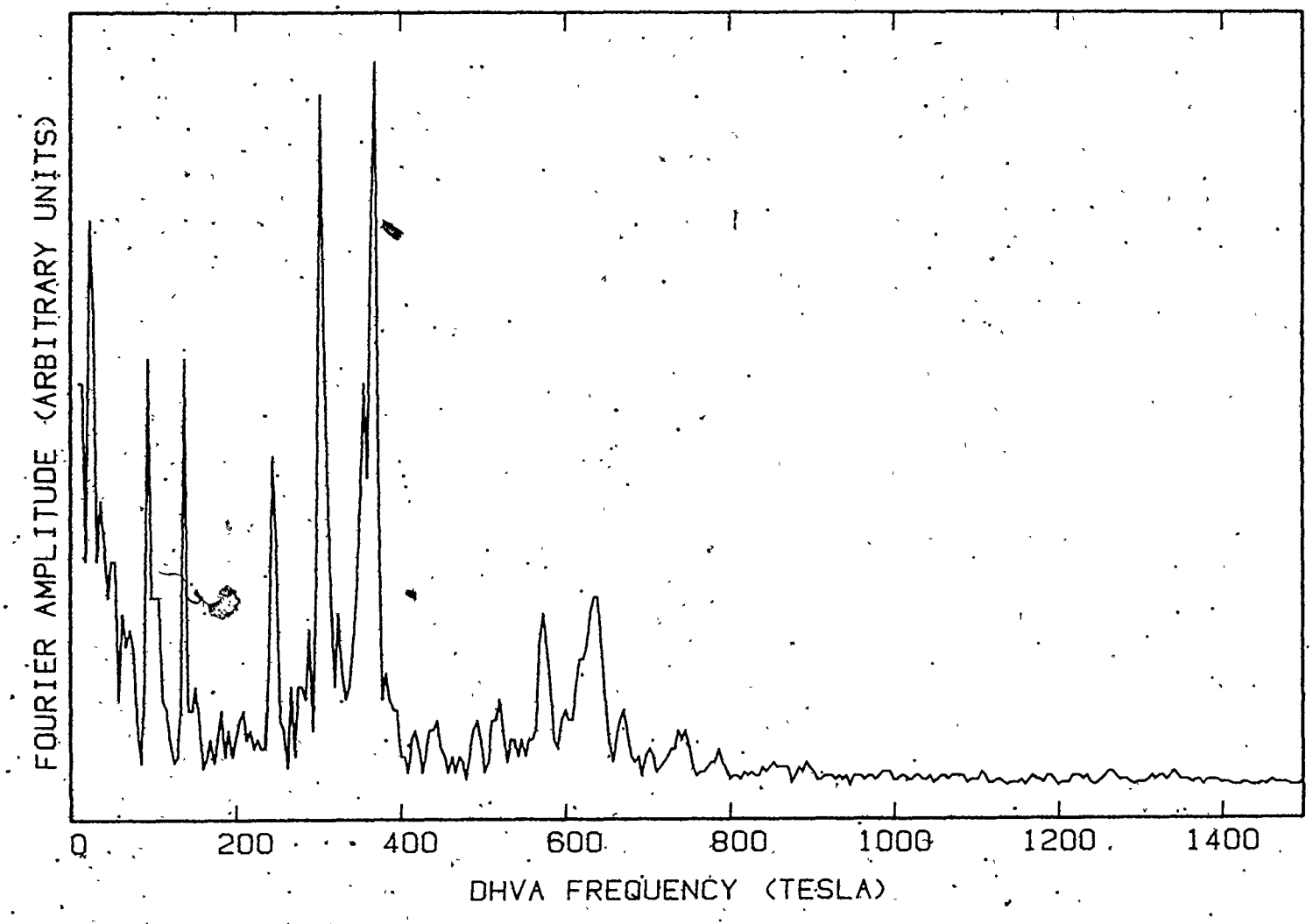

Figure V.4. A typical dHvA spectrum of a fast-cooled sample of stage-2 $SbCl_5$ compound (sample 4B).

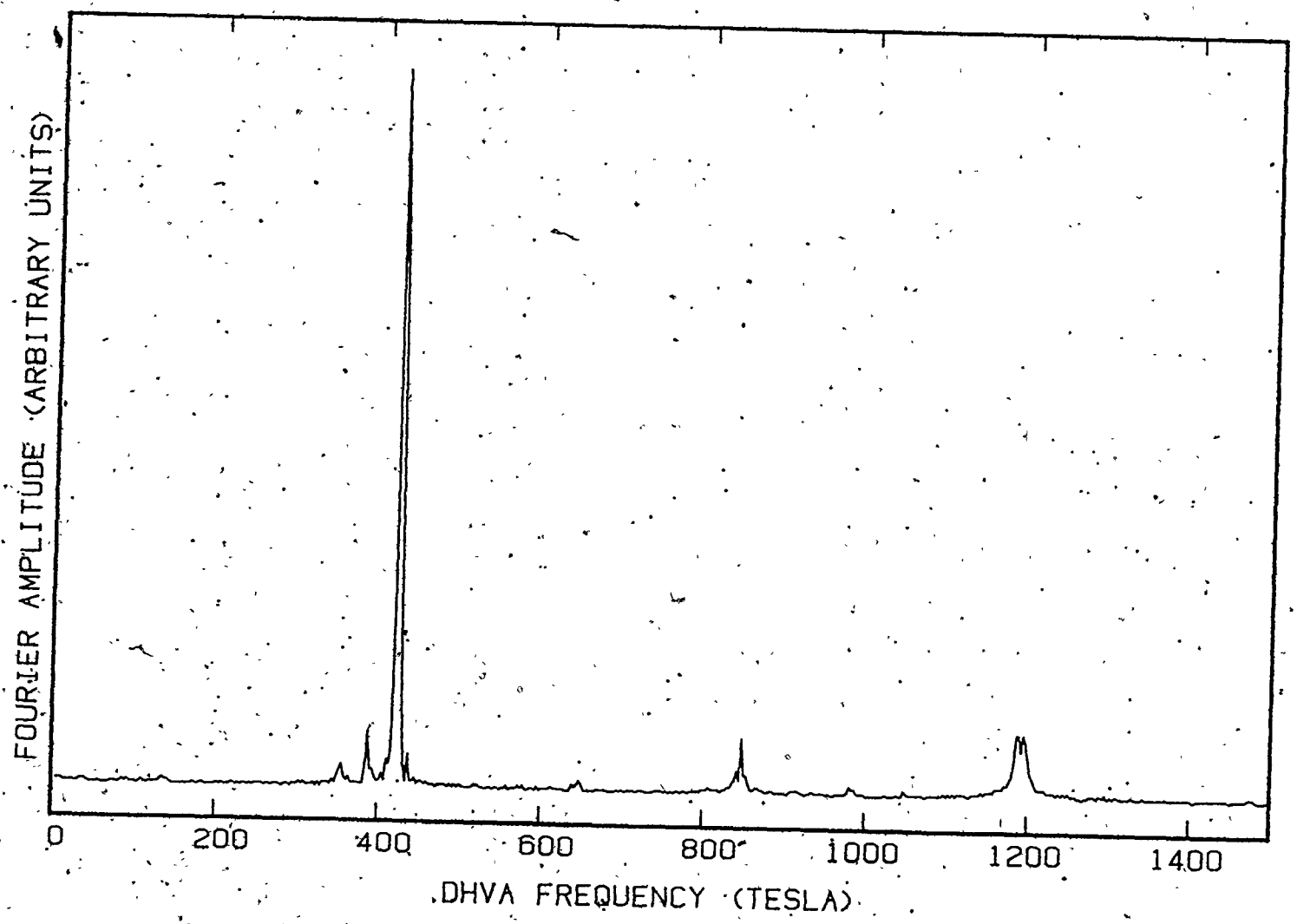

Figure V.5. A typical dHvA spectrum of a slowly-cooled sample (D21) of stage-2 $SbCl_5$ compound.

observed with samples cooled quickly. There are also some of the frequencies that were observed with fast-cooled samples but their amplitudes are much smaller than that of f_1. One sample was cycled a few times between room temperature and 77 K. The first time it was cooled slowly (24 h), then fast (1h) and then slowly again. The dHvA spectra were taken after each cool-down and no change of the spectrum on thermal cycling was observed. This indicates that the first cool-down is important in determining the low-temperature electronic structure of the compound. However, the spectrum obtained with a sample which was cooled down slowly, warmed to room temperature and then quenched rapidly (within a few minutes) to 4.2 K (#30) had frequencies characteristic of both fast and slowly-cooled samples of comparable amplitudes. In this case, there is a memory of the first cool-down and an effect of the later rapid cooling.

The dependence of the relative amplitudes of the oscillations on the cooling rate indicates that they have different origins and should be analyzed separately. Although, some frequencies were observed with all samples they are classified as characteristic of slow or fast cooling depending on the change of their relative amplitudes with the cooling rate. The frequencies characteristic of slowly-cooled samples are f_1, f_2 and the 13 T oscillation

observed at low magnetic fields. The remaining frequencies are attributed to samples cooled fast. The fundamental frequencies, f_1 and f_2, are identified with the basic graphitic bands v_1 and v_2, respectively. The comparison with theory supports that assignment in the following way. The experimental values of the Fermi surface areas corresponding to f_1 and f_2 are calculated using equation V.5 as A_1 = 0.0403 $Å^{-2}$ and A_2 = 0.1136 $Å^{-2}$. The Fermi energy is adjusted to fit the sum of A_1 + A_2 to the rigid band model of Holzwarth (1980) and the value of -0.88 eV is obtained. The calculated Fermi areas of the bands at E_F = -0.88 eV are A_1 = 0.0396 $Å^{-2}$ and A_2 = 0.1139 $Å^{-2}$ which are in agreement with the experimental data. The cyclotron masses are predicted to be 0.144 m_0 and 0.271 m_0 and these also agree with the measured values of 0.146 m_0 and 0.267 m_0, respectively. The fitted value of the Fermi energy also agrees with the estimation of -0.91 to -0.95 eV obtained from optical reflectance studies (Heinz et al. 1983).

From the values of the dHvA frequencies of the basic graphitic bands the charge transfer (equations V.4 and V.5) is calculated as 0.0204 elementary charge per carbon atom. The origin of the 13 T oscillation is not known.

Quantum oscillations in the stage-2 antimony pentachloride compound have been observed previously. Batallan et al. (1978) reported that the dHvA frequencies

are independent of stage index and explained their results using a free-electron model in which the carriers from the intercalate were localized on graphene layers adjoining the intercalate. Takahashi et al. (1981) found different dHvA frequencies which depended on stage index and explained their data by a rigid band model of Blinowski et al. (1980). They also introduced zone folding to explain some of the observed frequencies (Tanuma et al. 1981). The zone folding was assumed to come from the action of an intercalate superlattice.

The frequencies observed in this work with slowly-cooled samples agree with some of the frequencies observed by Takahashi et al. Other frequencies reported by Takahashi et al. and most of the frequencies observed by Batallan et al. were also observed in this work with samples cooled fast (Table V.2). The experimental data of this work confirms both previous results and indicate that the dependence of the spectrum on cooling rate might account for the discrepancy between them. The interpretation of the results in this work differs substantially from that of both previous works. In this work the spectra of slowly and fast-cooled samples were separated and only the f_1 and f_2 frequencies were interpreted using the rigid band model while Tanuma et al. attempted to fit all of the frequencies observed. They postulated that the (7x7) intercalate

Table V.2. The de Haas-van Alphen frequencies of the stage-2 antimony pentachloride compound. The values of frequencies are in Tesla. The assignment of frequencies to slow and fast-cooled samples of this work is based on the change of the relative amplitudes of the frequencies with cooling rate.

Batallan et al. 1978	Takahashi et al. 1981	This work		Yoshida and Tanuma 1985
		Slow cooling	Fast cooling	
		13		24
				32
48			58	52
	86		85	
95			94	92
			110	
			123	
			136	
143			148	142
			158	
191				185
	256		250	250
			300	
382			352	
			364	362
			387	374
	398		399	399
	422	422		
	442			
532			580	
			626	
			648	
	847	845		
			1126	
	1190		1190	
	1520		1610	

superlattice splits the Fermi surface of the basic graphitic bands into smaller pieces and assigned four of the observed dHva oscillations (29 T, 86 T, 256 T and 422 T) with the Fermi surface sections obtained from the model. The value of the Fermi energy of -1.12 eV obtained by Tanuma et al. was not in agreement with the values obtained from optical studies of Blinowski et al. (1980), Eklund et al. (1981) and a more elaborate work of Heinz et al. (1983).

The origin of the complex spectra observed with fast-cooled samples is related to an intercalate phase transition observed at around 200 K (Clark et al. 1982). Electrical resistivity shows a kink at the transition temperature and a hysteresis on thermal cycling. During subsequent cycling, the resistivity kink and hysteresis are reduced. It is likely that fast-cooled samples do not reach the equilibrium structure and the complex dHvA spectrum observed in this work is a result of the presence of strained regions of different structure. The effect of cooling rate on the dHvA effect and intercalate structure was studied independently of this work by Yosida and Tanuma (1985). They showed that with samples cooled rapidly through the transition temperature a substantial portion retains the high temperature structure. The amplitudes of dHvA frequencies were found to be correlated with the amount of the high temperature phase that was present within samples.

The frequencies of oscillations studied by Yosida and Tanuma correspond to the ones observed in this work with fast cooled samples (Table V.2).

Further work was done to elucidate two features of the dHvA effect of the stage-2 compound, an unusual dependence of the amplitude of the f_1 oscillation with the magnetic field and a splitting of the f_2 frequency observed in the Fourier transform spectra. Samples used were prepared from single crystal graphite that permitted the extension of the measurements to lower magnetic field. The magnetic field was varied so that the inverse magnetic field 1/B, was proportional to time. The dHvA oscillations were then periodic in real time and were separated by a low-frequency band-pass analog filter. The recorded signals are shown in Figure V.6. Superimposed on a typical monotonic increase of the amplitude of the 422 T oscillation, a beat pattern is observed with nodes at 1.7 and 4.2 T. In the case of the f_2 oscillation, one node is clearly observed at 3.7 T. The other node is masked by the presence of the third harmonic of f_1 whose frequency $3xf_1$ = 1266 T is similar to that of f_2 and could not be filtered out effectively. The third harmonic of f_1 mixes with f_2 and produces a short beat pattern of a period of a few f_2 oscillations. This short beat disappears at around 2.35 T which indicates that this is a node of the long beat pattern. From the positions of

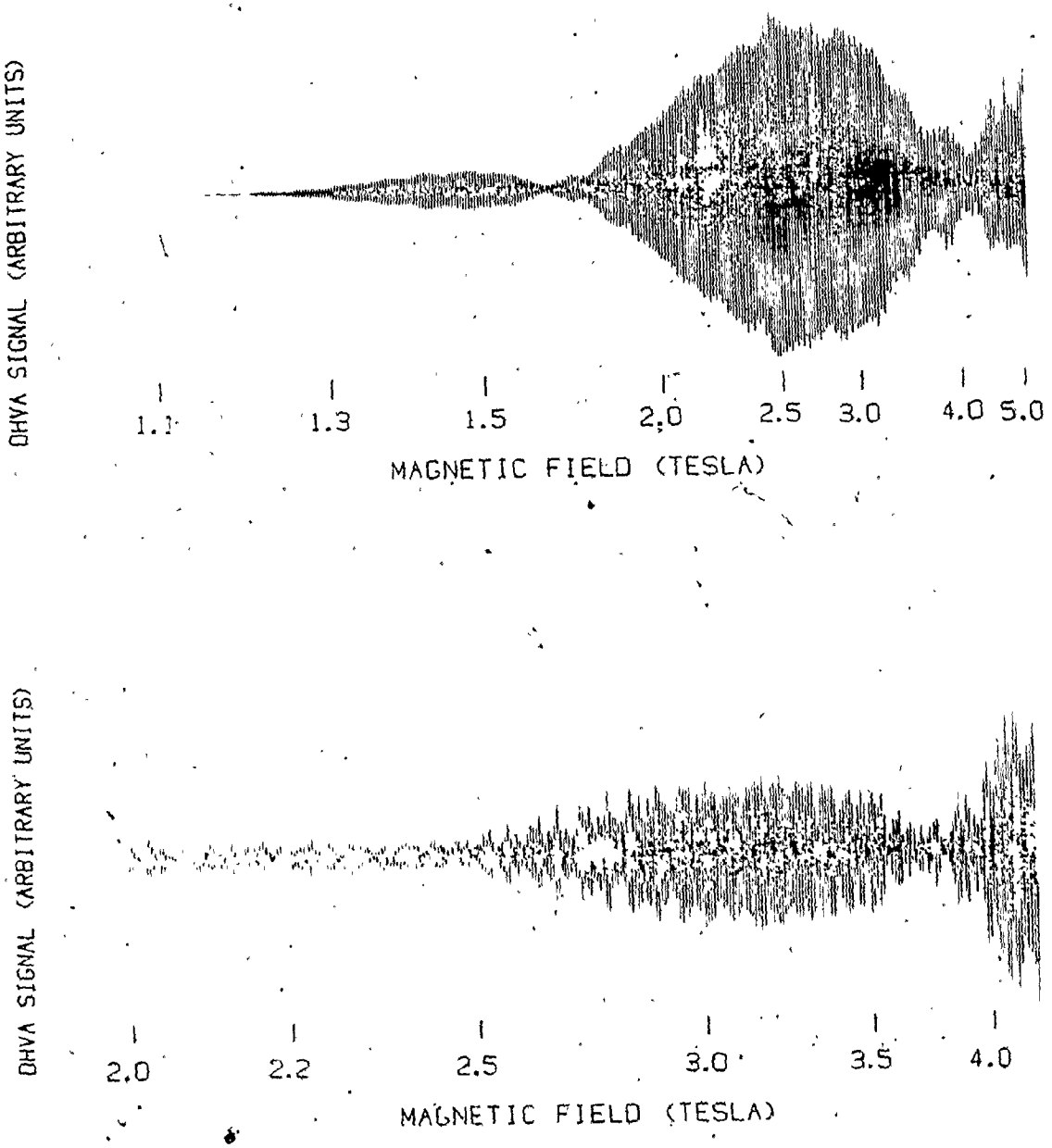

Figure V.6. Recorder traces of the f_1 (top) and f_2 (bottom) oscillations.

the nodes, one calculates differential frequencies of Δf_1 = 3 T and Δf_2 = 6.5 T.

The positions of the nodes did not depend on temperature, modulation field amplitude and frequency. Thus, they are not due to Bessel function zeroes from the modulation technique (Shoenberg 1984). The nodes of the f_1 oscillations were also observed with all slowly-cooled samples (the f_1 oscillation dominates the spectrum and its amplitude can be traced without filtering). This shows that there are two pairs of bands with similar Fermi surface cross-sectional areas and similar cyclotron masses. The existence of four partially filled bands is inconsistent with a simple unit cell of a stage-2 compound composed of two graphene layers and having a graphitic in-plane primitive lattice vectors. It was shown in Chapter II that such a structure gives two partially occupied bands only and this prediction is dependent on the symmetry of the crystal and charge transfer mechanism and is independent of approximations used in the particular band structure calculations. Thus, there has to be symmetry breakdown to double the number of bands. It is very unlikely that an in-plane intercalate superlattice gives doubling of both basic graphitic bands because the Fermi areas of the two bands differ by almost a factor of three. Furthermore, the band parameters were found to be in good agreement with

theoretical predictions. On the other hand, if the c-axis unit vector is twice the distance between two intercalate layers then the states localized on two sides of an intercalate layer are not equivalent (breakdown of the c-axis translational symmetry) and form two bands. The in-plane parameters of the two bands remain unchanged and the energy separation between them is determined by the interaction between atoms separated by an intercalate layer. This interaction is much smaller than the other interatomic interactions and results in the large anisotropy of the conductivity of the compound (Morelli and Uher 1983). The anisotropy of conductivity is three orders of magnitude higher than that of pristine graphite and, therefore, the interaction is expected to be also three orders of magnitude smaller than the interlayer interaction in pristine graphite. Since the difference of the energies of the basic graphitic bands is due to graphitic interlayer interaction, one expects that the splitting of dHvA frequencies of the bands due to the c-axis interaction should be three orders of magnitude smaller that the difference between frequencies f_1 and f_2. This gives the value of the splitting to be of the order of 1 to 10 Tesla which agrees with the measured values of 3 and 6.5 Tesla. Thus, the c-axis superstructure can account for the splitting observed.

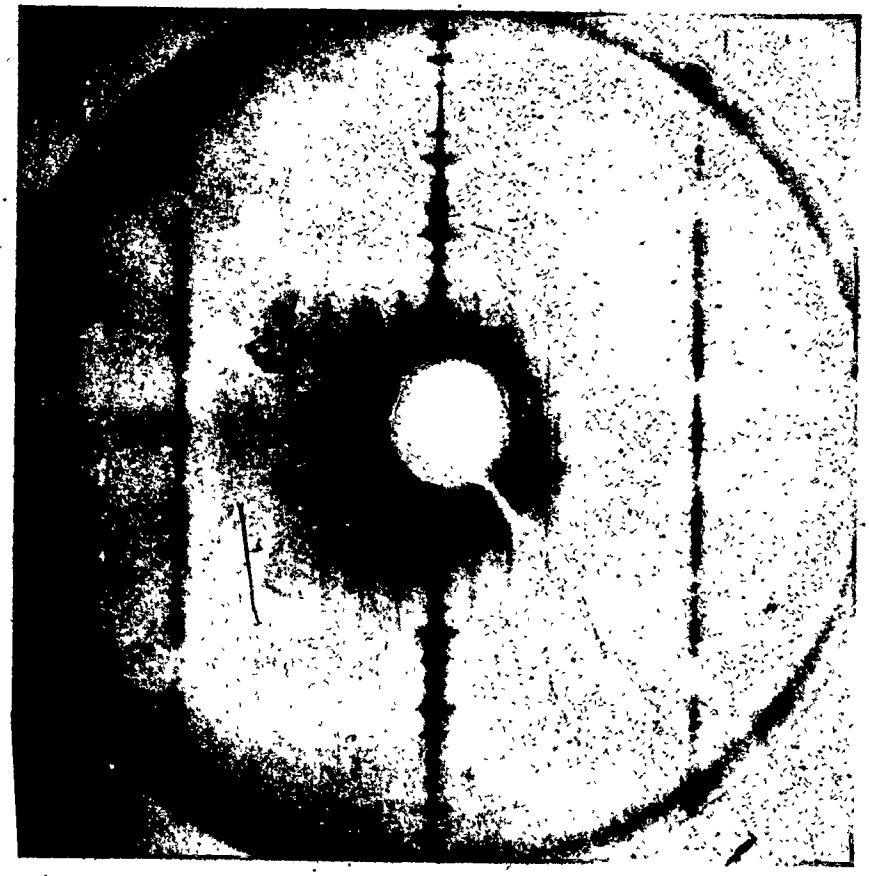

Figure V.7. Precession photograph of the (h0l) plane of stage-2 $SbCl_5$ compound. Three vertical arrays of points correspond to (101), (001) and (10$\bar{1}$) refections, respectively, where the in-plane indices refer to graphite sublattice.

In order to support this hypothesis the c-axis structure of the compound was re-examined. A small piece of single crystal graphite was intercalated and a precession photograph of the diffraction pattern of the (h0l) plane was taken (Figure V.7). From the spacing of the (00l) reflections the c-axis repeat distance of 12.7 Å is obtained which is in agreement with the accepted value of I_c of 12.72 Å. The spacing of (10l) reflections correspond to 25.4 Å twice the value from (00l) reflections. This indicates that, indeed, there is a doubling of the c-axis lattice vector. This doubling was also observed recently by Homma and Clarke (1985).

The observation of the doubling of the c-axis lattice constant explains the observed band splitting and permits one to determine the interaction between states separated by an intercalate layer. Since the value of the interaction is small it can be added as a small perturbation to the two-dimensional Hamiltonian.

We start from a two-dimensional wave function $\psi(k_{xy},z)$ describing an electron state of energy $E(k_{xy})$ localized within a subcell consisting of two graphene layers and extended in the basal plane. The total wave function for the three-dimensional crystal is a sum of Bloch combinations of the function localized on even and odd subcells

$$\psi(k_{xy},k_z,z) = \sum_l \exp(k_z Z_l)\ \psi(k_{xy},z-Z_l) + \\ + \lambda \sum_m \exp(k_z Z_m)\ \psi(k_{xy},z-Z_m) \qquad (V.6)$$

where Z_l and Z_m denote positions along the c-axis of even and odd subcells, respectively. Denoting the interaction between the function localized on neighboring subcells by δ, one obtains the submatrix of the Hamiltonian containing interaction between states of the same energy localized on different subcells in the form

$$H' = \begin{pmatrix} E(k_{xy}) & -2\delta\cos(k_z I_c) \\ -2\delta\cos(k_z I_c) & E(k_{xy}) \end{pmatrix} \qquad (V.7)$$

This gives two energy solutions

$$E = E(k_{xy}) \pm 2\delta\cos(k_z I_c) \qquad (V.8)$$

which correspond to two bands separated at $k_z = 0$ by 4δ.

Using this simple model, one can estimate the values of the parameters δ from the dHvA data. The difference between the Fermi areas of the two bands ΔA, is proportional to the splitting of the dHvA frequencies Δf (equation V.5). Now, $\Delta E = \Delta A \left(\frac{\partial A}{\partial E}\right)^{-1}$ and the derivative $\frac{\partial A}{\partial E}$ is proportional to the cyclotron mass

$$\frac{\partial A}{\partial E} = \frac{2\pi}{\hbar^2} m_c \qquad (V.9)$$

The value of the interaction is then

$$\delta = \frac{\hbar^2}{8\pi} \frac{\Delta A}{m_c} \qquad (V.10)$$

Substituting the experimental values of ΔA into (V.10) and using the measured cyclotron masses, one obtains the values of $\delta_1 = 0.6$ meV and $\delta_2 = 0.7$ meV for the interactions

between the two-dimensional bands v_1 and v_2, respectively.

The interaction between states of neighboring subcells of different energy introduces correction to the band energies of the order of δ^2/E_{nm} where E_{nm} is the difference of unperturbed band energies. This correction is three orders of magnitude smaller than the correction due to interaction between the degenerate states and can be totally neglected.

The splitting of the f_1 oscillation has been observed under high pressure (Iye et al. 1982) and explained qualitatively by the existence of a few extremal cross-sectional areas of the Fermi surface for various values of k_z. With increasing pressure the interatomic distances decrease that increases the interactions between them and leads to the increase of the splitting. This confirms the interpretation presented above but in this work, the splitting of both bands was observed and measured at ambient pressure and analyzed quantitatively to obtain value of interaction between states localized on layers separated by an intercalate layer. This is a first experimental estimation of the interaction of any graphite intercalation compound.

V.3. Stage-1 SbF_6^- graphite.

The measurements of the dHvA effect of SbF_6^- intercalated graphite were performed on samples prepared by the three methods described in Chapter IV. Although, in all cases the same ion is responsible for the charge transfer, the data show differences in the electronic structure arising from the presence of other species co-intercalated with the ion. The de Haas-van Alphen frequencies of several SbF_6^- samples are listed in Table V.3.

A typical dHvA spectrum of a sample prepared in nitromethane solution at room temperature is shown in Figure V.8. The spectrum consists of a low frequency oscillation f_1 = 46.5 Tesla and a strong oscillation of frequency f_2 = 524 Tesla. There are other oscillations at higher frequencies. Their number and amplitudes varied from sample to sample (see Table V.3). With samples prepared at 60°C the f_1 oscillation was not observed and there were fewer irreproducible high frequency oscillations than with samples prepared at room temperature samples.

A different spectrum was obtained with samples prepared in SO_2 solution (Figure V.9). There are three peaks in the Fourier transform at about 600 Tesla. The relative amplitudes and frequencies varied from sample to sample. For example, the frequencies of the peaks in Figure V.10 were 583, 602 and 608 Tesla, while another sample (M5)

Table V.2. De Haas-van Alphen frequencies of several stage-1 SbF_6^- samples.

Sample number	Method of preparation	Frequency (Tesla)	Relative amplitude
F9	Nitromethane solution at 20°C	47	16
		524	100
		1047	8
		1380	14
		1408	11
		1568	8
		1905	6
F12	Nitromethane solution at 20°C	47	16
		525	100
		1048	3
		1382	6
		1408	3
		1421	2
		1572	3
		1599	3
		1898	2
J28	Nitromethane solution at 60°C	520	100
		1031	3
		1362	3
		1633	11
M5	Liquid SO_2 solution	553	47
		574	100
		673	13
		1464	2
		1806	2
M27	Liquid SO_2 solution	583	100
		602	14
		608	24
		1488	3
		1506	2
A11	Reaction with solid 70°C	1600	100
A17	Reaction with solid 65°C	567	15
		1627	100
MA14	Reaction with solid 50°C	543	25
		566	100

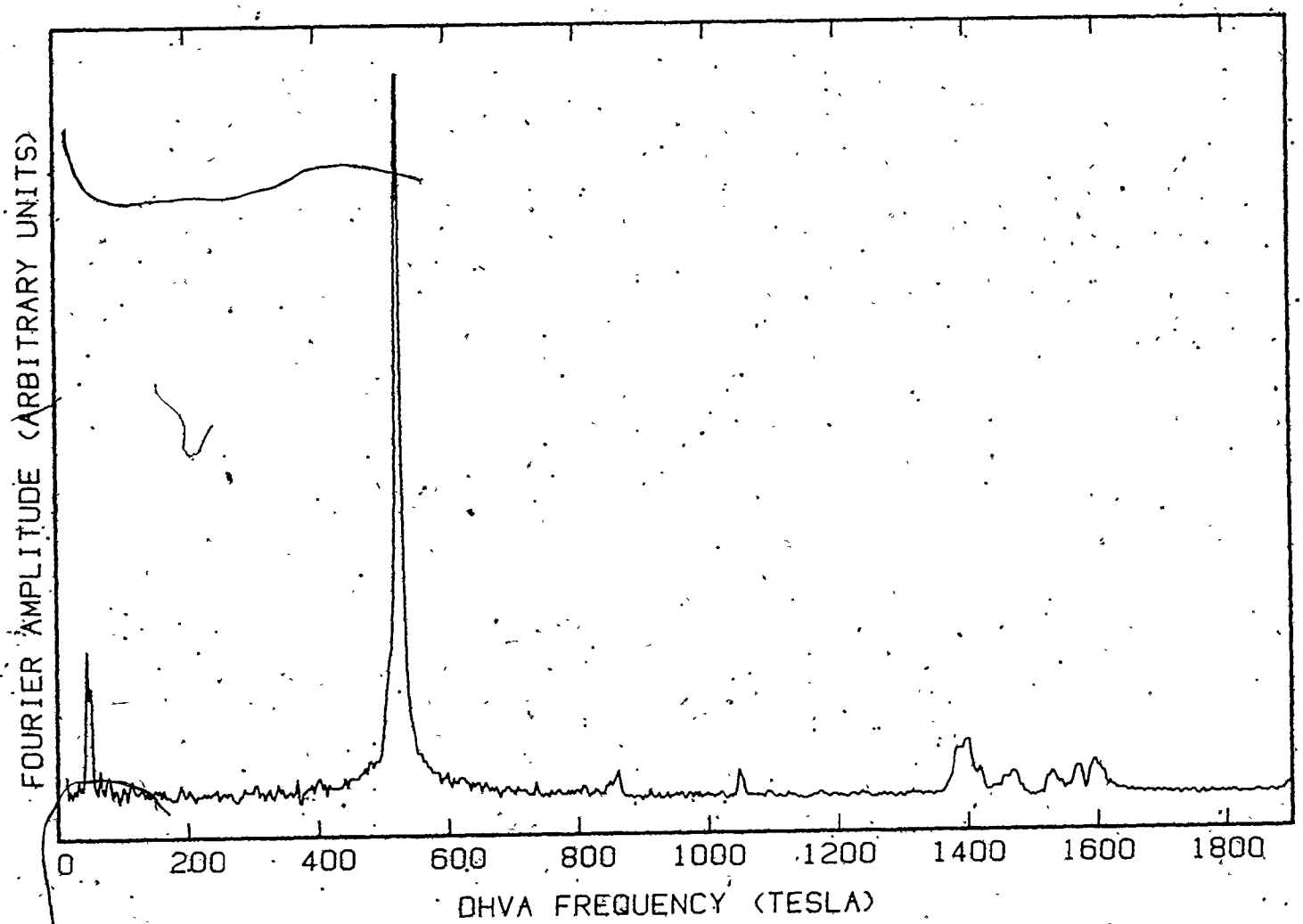

Figure V.8. A typical dHvA spectrum of a stage-1 SbF_6^- sample prepared in nitromethane solution at room temperature (sample F12).

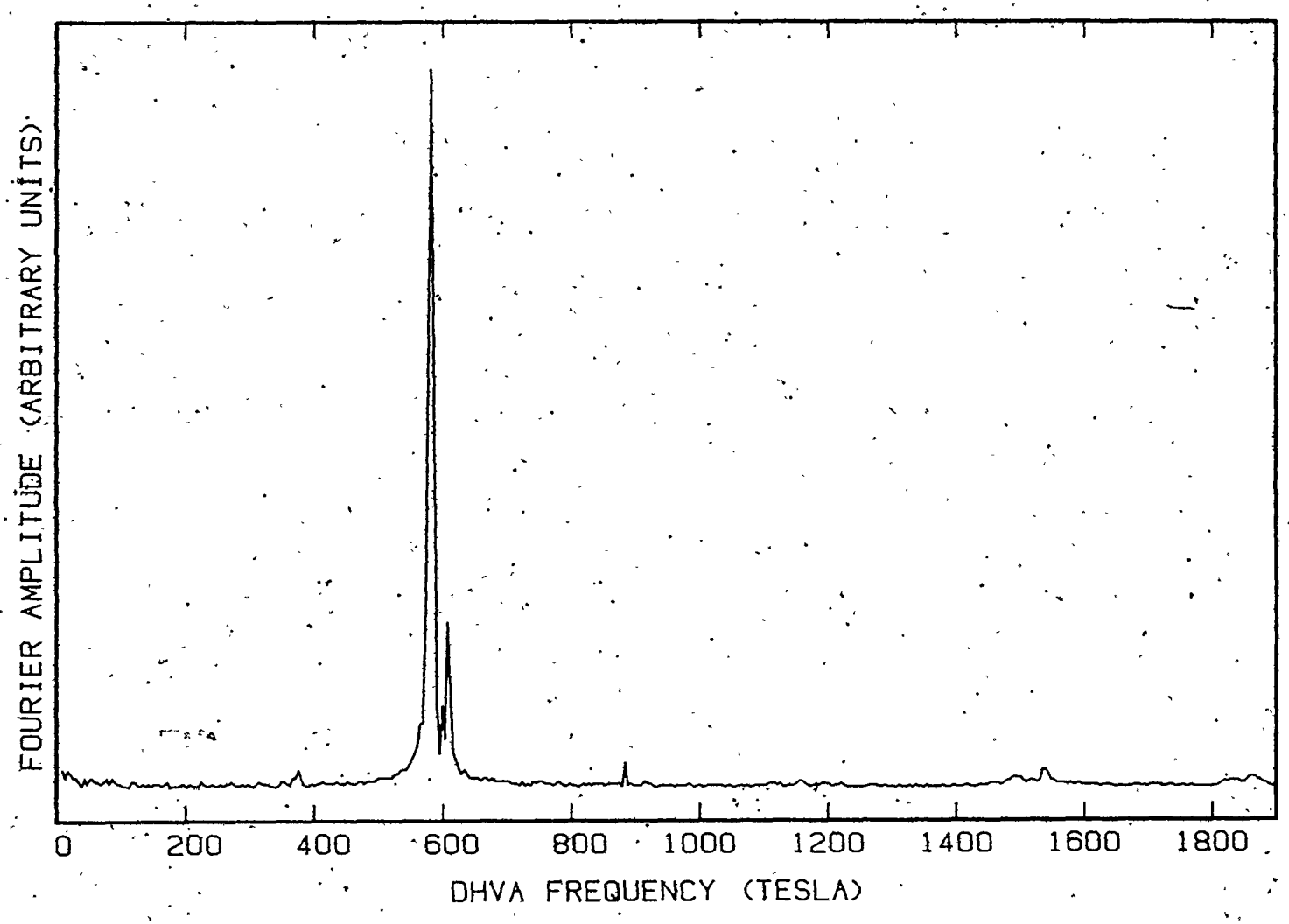

Figure V.9. A spectrum of a sample prepared in liquid SO_2 solution (sample M27).

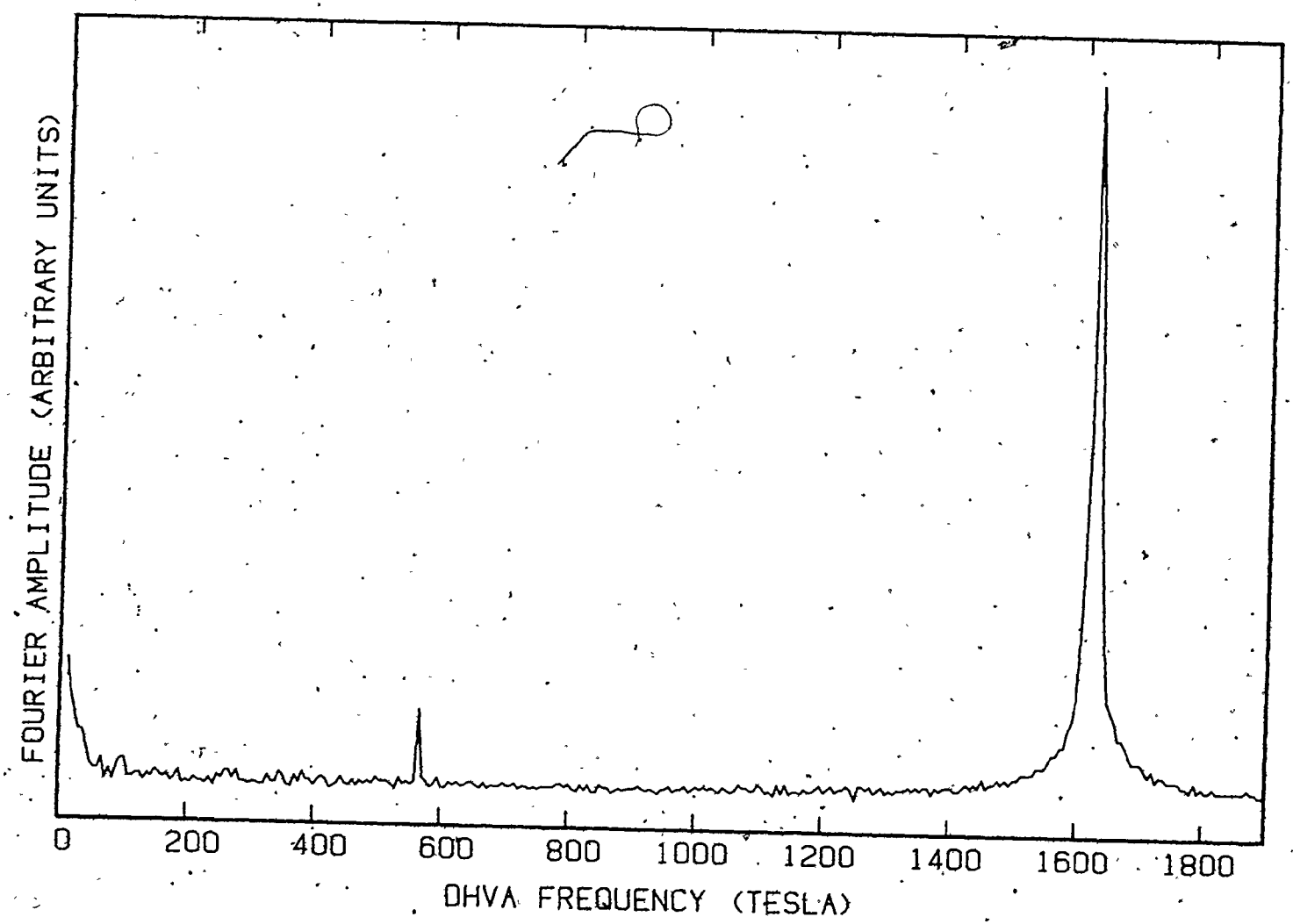

Figure V.10. De Haas-van Alphen spectrum of a sample prepared by direct reaction of solid NO_2SbF_6 with graphite at 65°C (A17).

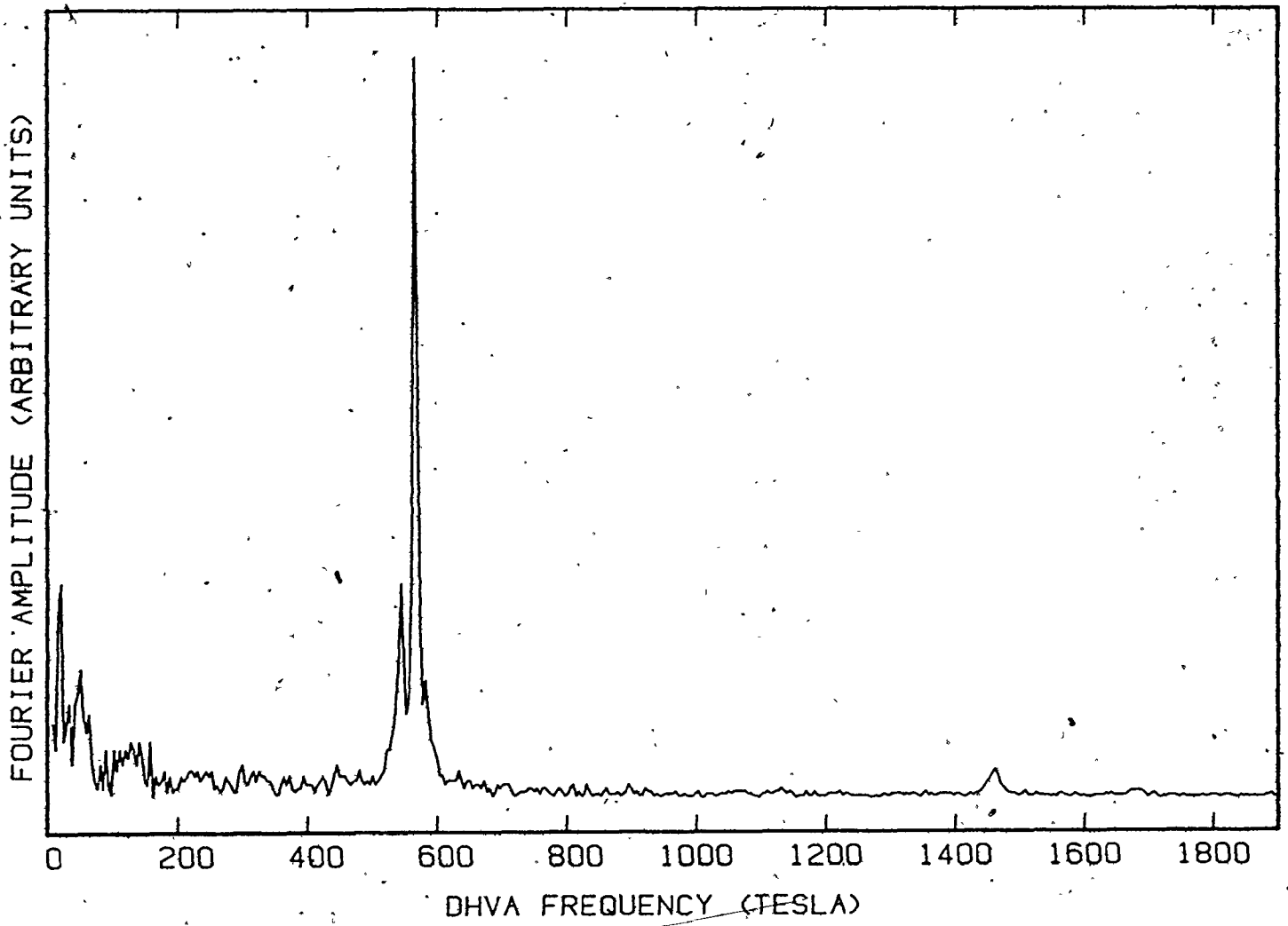

Figure V.11. A spectrum of a sample (MA14) obtained in a reaction of solid salt at 50°C.

had frequencies 553, 574 and 673 Tesla.

The simplest dHvA spectra were obtained in samples prepared by reacting graphite with solid NO_2SbF_6 salt. In two samples (A11) a single frequency was observed at 1600 Tesla and in a third one (A17) the dominant frequency had a similar value of 1627 Tesla (Figure V.10). A second frequency with a value of 56.7 Tesla was also observed in the third sample. These samples were prepared at temperatures above 65 C for three days. Different spectra were obtained from samples (MA14) which were made at a lower temperature for longer times (Figure V.11). Two oscillations of frequencies 543 and 567 Tesla dominated the spectrum.

The chemical composition of the stage-1 SbF_6^- compound synthesized in nitromethane solution was determined by Billaud et al. (1980b) as $C_{23}SbF_6(CH_3NO_2)_{1.7}$. The Mössbauer studies (Boolchand et al. 1983) of the stage 1 SbF_6^- compound showed that antimony is in 5^+ state. The isomer shift and quadrupole coupling constant suggest that the molecule that is intercalated is the SbF_6^- ion. This indicates that the charge transfer is 1 elementary charge per 23 carbon atoms. Electrochemical reaction of $LiSbF_6$ (Jobert et al. 1981) gave 1 charge per 24 carbon atom.

Knowledge of the charge transfer permits one to estimate the range of frequencies expected for oscillations of basic graphitic bands. From equations (V.4) and (V.5) one

obtains a dHvA frequency of 1719 or 1647 Tesla corresponding to the charge transfer of 1/23 and 1/24 electron per carbon atom, respectively. This is close to that observed with samples prepared by reaction of graphite with solid nitryl hexafluoroantimonate. The observed 1627 Tesla frequency corresponds to one elementary charge per 24.3 carbon atoms and is therefore identified with the basic graphitic band. Theoretical calculations give the value for the Fermi energy as $E_F = -1.28$ eV and for the carriers effective mass as 0.331 m_0 for the Fermi surface size corresponding to the 1627 Tesla frequency. The measured effective mass value of 0.321 m_0 compares very well with the theoretical prediction. This further supports identification of this frequency with the basic graphitic band.

The agreement between the number of carriers obtained from the dHvA effect with the amount of the charge transfer found from stoichiometry proves that the anions remain fully ionized within the compound and all the charge on the graphene layers is delocalized.

The samples prepared with solid NO_2SbF_6 at temperatures lower than 60°C showed no signs of the 1627 Tesla oscillation. Instead two frequencies in the range of 550 Tesla were observed. This suggests that for a lower reaction temperature the intercalate forms an ordered superlattice that splits the Fermi surface into smaller pieces.

The presence of a superlattice would explain the low values of frequencies observed in samples intercalated in nitromethane and SO_2 solutions. The absence of an intercalant superlattice at room temperature (Billaud et al. 1980) does not contradict its presence at low temperatures. The resistivity anomalies (Billaud et al. 1982) could result from an intercalant phase transition rather than from nitromethane freezing.

This mechanism, however, does not account for all frequencies in the dHvA spectrum. Variation in the number of frequencies from sample to sample and some irreproducibility suggest that the samples prepared in the solutions are not homogeneous. During the first reaction by-products dissolve in the solution and inhibit subsequent reactions (see Chapter IV) and one might expect that they also affect the first reaction.

With samples prepared in SO_2 solution, none of the frequencies were the same in different samples. This suggests that the charge transfer varies from sample to sample.

V.4. Stage-2 BF_4^- intercalated graphite.

The dHvA spectrum of the BF_4^- is simple. It does not depend on the cooling rate of the samples and consists of five oscillations with frequencies of 523 ± 1, 857 ± 2, 1044 ± 2, 1377 ± 2 and 1895 ± 4 Tesla (Figure V.12). There are two fundamental oscillations of frequencies f_1 = 523 and f_2 = 1377 T. The other oscillations correspond to $f_2 - f_1$, 2 x f_1 and $f_1 + f_2$. The cyclotron masses corresponding to f_1 and f_2 are 0.162 ± 0.001 m_0 and 0.28 ± 0.01 m_0, respectively.

The interpretation of the dHvA data of the compound is straightforward. The fundamental frequencies observed are identified with basic graphitic bands. The identification of the bands can be checked by comparing the charge transfer with the weight uptake. Substituting the Fermi surface areas corresponding to the f_1 and f_2 frequencies into equation (V.4), one obtains charge transfer of one elementary charge per 41.5 carbon atoms. This gives one BF_4^- ion per 41.5 carbon atoms. It is likely that two neutral NO_2BF_4 molecules are cointercalated with each ion as is the case of the reaction of thermally decomposed nitryl tetrafluoroborate with graphite (Billaud et al 1983). Thus, the compound formula is $C_{41.5}BF_4(NO_2BF_4)_2$. The calculated weight uptake is 70.7 % which is in agreement with the measured value of 68 ± 3 %. The charge transfer and intercalate concentration

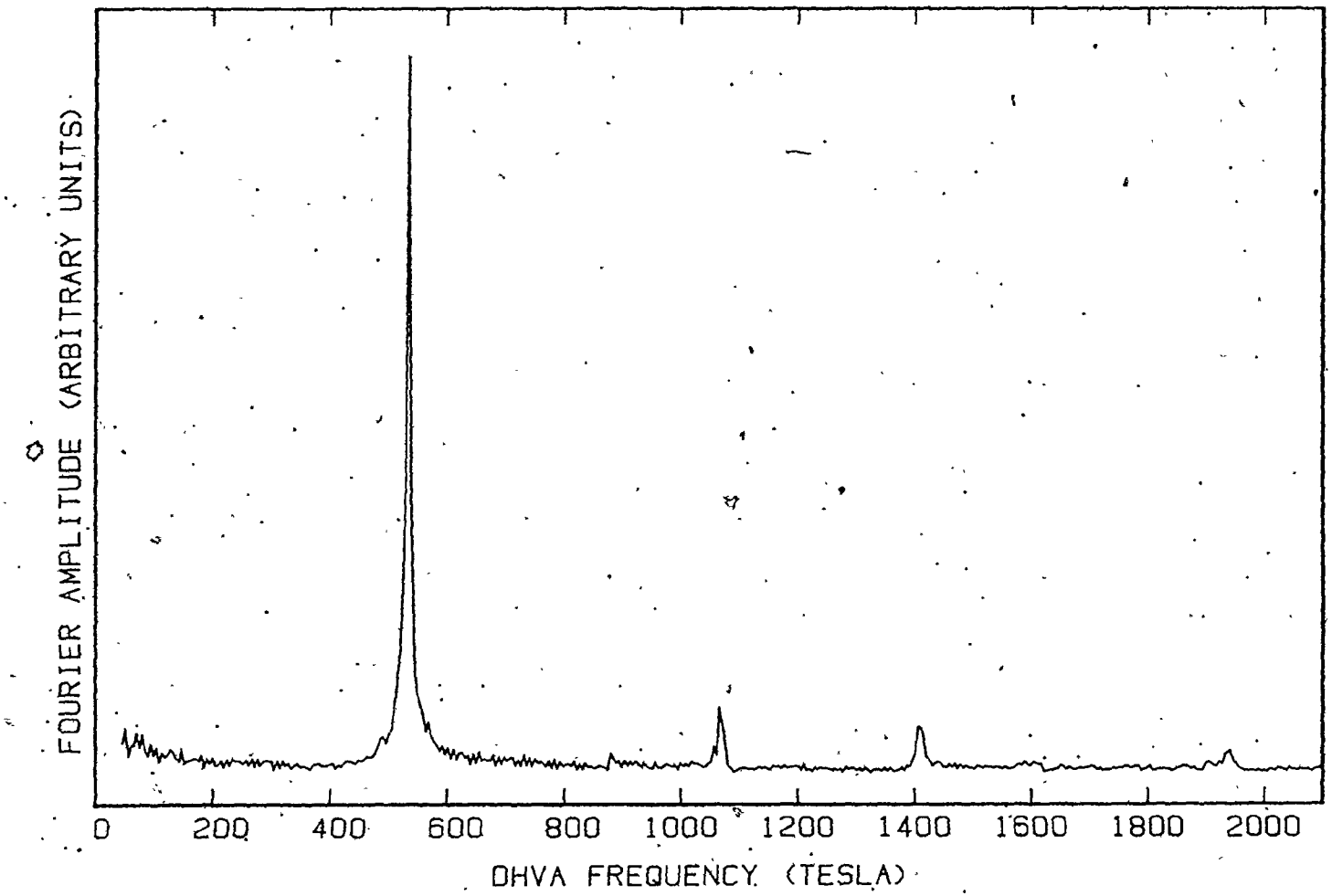

Figure V.12. Fourier transform of the dHvA signal of stage-2 BF_4^- intercalated compound.

in this work are higher than those obtained by methods reported previously (Billaud et al. 1980b, Billaud and Chenite 1983).

The comparison with theory further supports the identification of the bands. The Fermi energy is adjusted to fit the sum of areas corresponding to f_1 and f_2 frequencies and the value of -0.96 eV is obtained. For that value of the Fermi energy theory predicts that the Fermi areas of the two bands correspond to frequencies of 520 and 1392 Tesla which are within 1 % of the experimentally observed values of f_1 and f_2, respectively. The cyclotron masses are predicted to be 0.16 m_0 and 0.30 m_0 for the two bands. The first value matches exactly the experimental one for the f_1 frequency, the second prediction is slightly larger than the observed mass of 0.28 m_0.

CHAPTER VI

BAND STRUCTURE OF GRAPHITE INTERCALATION COMPOUNDS

Graphite intercalation compounds are highly anisotropic and often treated as two-dimensional materials. In this chapter the anisotropy of band parameters and dimensionality of the compounds are discussed. Following this, theoretical models of electronic structure are examined. The anisotropy of the conductivity is also discussed and explained by a band conduction mechanism.

VI.1 Dimensionality of the band structure of acceptor GIC.

The fundamental assumption of rigid band models of the electronic structure of graphite intercalation compounds is that the structure is two-dimensional, that is the interaction between carbon atoms separated by an intercalate layer is zero. This assumption is justified by the large anisotropy of the conductivity, a typical order of magnitude being 10^5. In this work, an estimate was obtained of the interaction between bands separated by an intercalate layer, the one that is responsible for the anisotropy of the electronic properties. In the stage-2 $SbCl_5$ compound, the values of the interactions between valence bands are 0.6 and 0.7 meV. These values are four orders of magnitude smaller

than the largest in-plane interaction parameter γ_0 = 3.2 eV and three orders of magnitude smaller than the value of γ_1 = 0.4 eV for the interaction between carbon atoms of different layers. The resultant width of the band due to c-axis dispersion is also four orders of magnitude smaller than the total width of the bands. However, these numbers are somewhat misleading because the electronic properties are dependent on the band parameters near the Fermi surface only and the Fermi surface size is a small fraction of the in-plane zone size and extends to the zone boundaries in the k_z direction. The anisotropy of the Fermi surface of the compounds is much smaller, the relative difference of the Fermi surface cross-sectional area at the zone boundary and at k_z = 0 is less than 1 %, the actual values for the bands in stage 2 $SbCl_5$ are 0.7 and 0.5 % for bands v_1 and v_2, respectively. The average in-plane Fermi vectors are proportional to the square root of the areas and the relative differences are half the relative differences of respective areas. This means that the approximation that the Fermi surface is independent of k_z is accurate to better than 1 % in graphite antimony pentachloride stage 2. There is no information about the c-axis band parameters of any other acceptor compound. However, one expects that the interactions are of the same order of magnitude as in the $SbCl_5$ compound. Thus, the Fermi surface is approximated well

by two-dimensional models. However, it does not imply that the carriers are localized on one or two graphene layers. In fact, it will be shown later that the carriers can move freely across layers giving rise to metallic conductivity along the c-axis.

VI.2. Rigid band models.

Having established the two-dimensionality of the band structure, one can now check whether the theoretical band parameters are in agreement with experimental data. The experimentally observed parameters are Fermi surface areas and cyclotron masses. The Fermi surface areas A, are directly proportional to the corresponding dHvA oscillations f

$$f = \frac{2\pi e}{\hbar} A \qquad (VI.1)$$

The cyclotron masses are obtained from the temperature dependence of dHvA amplitudes (see Chapter III). The procedure used in this work is as follows: from the theoretical models the reciprocal space areas encircled by constant energy contours are calculated for various energies. The area dependence on energy is differentiated to obtain cyclotron mass according to the definition

$$m_c = \frac{\hbar^2}{2\pi} \frac{\partial A}{\partial E} \qquad (VI.2)$$

where A is area and E is energy. There is a single graphitic band in a stage-1 compound. The value of the Fermi energy is adjusted to fit the Fermi surface area and then

the cyclotron mass corresponding to that area is determined. In a stage-2 compound, one has two bands. The Fermi energy is adjusted to match the sum of the Fermi areas of the two bands.

The dHvA oscillations of the basic graphitic bands were observed in $SbCl_5$ stage 1 and 2, SbF_6^- stage 1 and BF_4^- stage 2 compounds. The measured band parameters are given in Table VI.1.

Table VI.1 Summary of the experimental band parameters.

Compound	Frequency (Tesla)	Fermi area ($Å^{-2}$)	Cyclotron mass (m_0)
$SbCl_5$ stage 1	1212	0.1157	0.271
SbF_6^- stage 1	1627	0.1553	0.321
$SbCl_5$ stage 2	422	0.0403	0.146
	1190	0.1136	0.267
BF_4^- stage 2	523	0.0499	0.162
	1377	0.1315	0.28

The first model discussed here was proposed by Blinowski et al (1980) as was presented in Chapter II. For a stage-1 compound the model predicts that the energy is linear with momentum

$$E = -\frac{\sqrt{3}}{2}\gamma_0 a|k| \qquad \text{(VI.3)}$$

The dispersion is isotropic and the Fermi energy for an acceptor compound is related to the Fermi surface area by

$$E = -\frac{\sqrt{3}}{2}\gamma_0 a (A/\pi)^{\frac{1}{2}} \qquad \text{(VI.4)}$$

The cyclotron mass is given by

$$m_c = \frac{\hbar^2}{2\pi\sqrt{3}\gamma_0 a}\frac{4\pi}{\sqrt{\pi}}\sqrt{A} \qquad \text{(VI.5)}$$

The nearest neighbor interaction parameter γ_0 is taken to be 2.4 eV in the model rather than 3.2 eV accepted for graphite.

Table VI.2. Comparison of experimental data of stage-1 compounds to the model of Blinowski et al.

	Measured		Calculated	
Compound	Fermi area ($Å^{-2}$)	Cyclotron mass (m_0)	Fermi energy (eV)	Cyclotron mass (m_0)
$SbCl_5$	0.1157	0.271	-0.98	0.285
SbF_6^-	0.1553	0.321	-1.14	0.331

The validity of the model of the electronic structure of stage-1 intercalation compounds can be checked by comparing the cyclotron mass dependence on the Fermi cross-sectional area (Table VI.2). The calculated cyclotron mass of the stage-1 $SbCl_5$ compound of 0.285 m_0 is 5 % larger than the observed one of 0.271 m_0. In the case of stage-1 SbF_6^- compound, the calculated value of 0.331 m_0 is only 3 % larger than the observed value of 0.321 m_0. The agreement between theory and experiment is fair but the discrepancy is

larger than the experimental error. If one takes the value of 3.2 eV for γ_0 the discrepancy between observed and theoretical masses is greater; the calculated masses are 0.213 m_0 and 0.241 m_0 for $SbCl_5$ and SbF_6^-, respectively. One can also compare the value of the Fermi energy fitted to the dHvA data of the stage-1 $SbCl_5$ compound with the value obtained from optical reflectance measurements (Heinz et al. 1983). In this work, the Fermi energy is found to be -0.98 eV below the top of the valence band. The work of Heinz et al. placed the Fermi energy at -1.1 to -1.2 eV.

In a stage 2 compound, there are two valence bands whose energies are given by

$$E_1 = -\frac{1}{2}[(\gamma_1^2 + 3\gamma_0^2 a^2 |k|^2)^{\frac{1}{2}} + \gamma_1]$$
$$E_2 = -\frac{1}{2}[(\gamma_1^2 + 3\gamma_0^2 a^2 |k|^2)^{\frac{1}{2}} - \gamma_1] \qquad \text{(VI.6)}$$

The Fermi areas of the bands are given by

$$A_1 = 4\pi(3\gamma_0^2 a^2)^{-1}(E^2 + E\gamma_1)$$
$$A_2 = 4\pi(3\gamma_0^2 a^2)^{-1}(E^2 - E\gamma_1) \qquad \text{(VI.7)}$$

where γ_1 is equal to 0.377 eV. Using this formula, we can relate the Fermi energy to the sum of Fermi surface areas

$$E_F = \left(\frac{3}{8\pi}\right)^{\frac{1}{2}} \gamma_0 a (A_1 + A_2)^{\frac{1}{2}} \qquad \text{(VI.8)}$$

The cyclotron masses are given by

$$m_{c1} = \frac{\hbar^2}{2\pi}\left(\frac{4\pi}{3\gamma_0^2 a^2}\right)(-2E_F - \gamma_1)$$
$$m_{c2} = \frac{\hbar^2}{2\pi}\frac{4\pi}{3\gamma_0^2 a^2}(-2E_F + \gamma_1) \qquad \text{(IV.9)}$$

The theoretical prediction and experimental data are shown in Table VI.3. The value of Fermi energy of -0.80 eV fits both areas of the stage-2 $SbCl_5$ compound. The cyclotron masses are predicted by the model to be 0.178 m_0 and 0.288 m_0 for bands v_1 and v_2, respectively. These predictions are larger than the experimental values of 0.146 m_0 and 0.267 m_0. In the case of the BF_4^- compound, the comparison yields similar results. The value of Fermi energy of -0.87 eV fits well the Fermi surface areas of both bands. The fitted values of cyclotron masses are larger than experimentally observed ones.

Table VI.3. Comparison of experimental and calculated band parameters of stage-2 compounds. Blinowski et al. model.

Compound	Measured		Calculated		
	Fermi area ($Å^{-2}$)	Cyclotron mass (m_0)	Fermi energy eV	Fermi area ($Å^{-2}$)	Cyclotron mass (m_0)
$SbCl_5$	0.0403	0.146	-0.80	0.0394	0.176
	0.1136	0.267		0.1144	0.289
BF_4^-	0.0499	0.162	-0.87	0.0515	0.199
	0.1315	0.28		0.1304	0.31

The agreement between theory and experiment is fair, the theoretical predictions are within 10 % of the experimental values. One can use the model of Blinowski et

al. to make qualitative predictions of the electronic properties of the acceptor compounds. Nevertheless, the discrepancy observed is larger than experimental error.

Analyzing the data of stage-1 compounds, one can assume that the value of the nearest neighbor interaction in graphite intercalation compounds is different from that in pristine graphite. However, if one assumes any other value of γ_0 than 2.4 eV the model fails to fit Fermi surface areas of the two valence bands in stage-2 compounds unless a proportional change of the γ_1 parameter is also assumed. Before jumping to that conclusion one should analyze the electronic structure of the intercalation compounds more carefully.

The model of Blinowski et al. is a first order expansion around the point U of the Brillouin zone. The Hamiltonian matrix elements are linear in momentum. Therefore, it is a good approximation if the Fermi surface is much smaller than the Brillouin zone size. However, the Fermi surface of the compounds studied has a large size; a typical order of magnitude of the Fermi vector k_F is 0.2 $Å^{-1}$ which is more than 10 % of the magnitude of k_U. It is therefore unreasonable to expect that a single or double parameter expansion can accurately describe the Fermi surface properties of the compounds.

The model aimed at describing quantitatively the electronic structure of graphite intercalation compounds was proposed by Holzwarth (1980). The model was presented earlier in this work. It assumes that the interactions between carbon atoms are the same as in graphite and four in-plane interaction and four interplanar interaction parameters are included. The interplanar interactions are, of course, appropriate for stages 2 and higher.

The procedure used to compare the experimental data to theory is analogous to the one used with the Blinowski *et al.* model. Because the model of Holzwarth is more complex, the analytic solutions could not be obtained and, instead, numerical calculations were performed.

Table VI.4. Comparison of experimental data to the theory of Holzwarth.

	Measured		Calculated		
Compound	Fermi area ($Å^{-2}$)	Cyclotron mass (m_0)	Fermi energy (eV)	Fermi area ($Å^{-2}$)	Cyclotron mass (m_0)
$SbCl_5$ stage 1	0.1157	0.271	-1.12		0.274
SbF_6^- stage 1	0.1553	0.321	-1.28		0.331
$SbCl_5$ stage 2	0.0403 0.1136	0.146 0.267	-0.88	0.0396 0.1139	0.144 0.271
BF_4^- stage 2	0.0499 0.1315	0.162 0.28	-0.96	0.0496 0.1329	0.161 0.30

For stage-1 compounds the Fermi energy was adjusted to fit the area of the band calculated from the dHvA frequency. The cyclotron mass was then calculated and compared to the measured value. For stage-2 compounds the Fermi energy was adjusted to the sum of the areas of the two bands. The areas and cyclotron masses of each band were then calculated. The results are shown in Table VI.4. The calculated cyclotron masse of the stage-1 $SbCl_5$ compound is within 1 % of the measured one. In the case of the stage-1 SbF_6^- compound the calculated mass is 3 % larger than the measured one. For stage 2 compounds, the values calculated from theory are within 1 % of experimental parameters. This agreement is very good after we have rounded off the values of the Fermi energy to two decimal places.

The values of Fermi energy obtained from fitting the dHvA data to theory are compared to the results of optical reflectance studies of $SbCl_5$ intercalated compounds. In this work the fitted value of the Fermi energy of the stage-1 compound is -1.12 eV and in the stage-2 compound the fitted value is -0.88 eV (Table VI.4). These values are compared to the data of Heinz et al. who give values of -1.1 to -1.2 eV for the stage 1 and -0.91 to -0.95 eV for the stage-2 compound. The agreement is very good for stage 1 and good for stage 2. One has to note, however, that the dHvA data are obtained at very low temperatures, below 4.2 K, whereas

the optical work was done at room temperature. One can not exclude the possibility that the charge transfer changes with temperature especially in the case of stage-2 $SbCl_5$ where a phase transition is known to occur at around 200 K.

The cyclotron mass used in the above consideration is the band mass obtained directly from band structure calculations according to equation (VI.5). In metals and semimetals, there is an interaction of moving electrons with phonons that results in an increase of energy needed to accelerate an electron by an amount necessary to create a cloud of phonons that follow it. This leads to an increase of the effective mass due to the electron-phonon interaction (see for example Grimvall 1981) and the measured mass is larger than the band mass by a factor of $1 + \lambda$ where λ is the electron-phonon mass enhancement parameter. This parameter is of the order of 0.5 in simple metals and has to be taken into account in any consideration dealing with effective masses of carriers. The value of the λ parameter is temperature dependent and at temperatures much lower than the Debye temperature it approaches the zero temperature limit given by (Grimvall 1981a)

$$\lambda(k) = \frac{1}{4\pi^3} \sum_{\mu} \int \frac{dS_{k'}}{|\nabla_k E|} \frac{|g(k-k';\mu)|^2}{\hbar\omega(k-k';\mu)} \qquad \text{(VI.10)}$$

where ω is the phonon frequency for the phonon vector of $k-k'$, $g(k-k';\mu)$ is the electron-phonon coupling function, the summation is done over all phonon branches and integration

is carried out over the Fermi surface. The integral contains $|\nabla_k E|^{-1}$ multiplied by a non-negative function. Therefore, the value of the integral increases if the density of states at the Fermi energy increases. In fact, with isotropic bands the λ parameter is proportional to the density of states according to the formula

$$\lambda(k) = 2N(E_F) \sum_{\mu} \int \frac{d\Omega_{k'}}{4\pi} \frac{|g(k-k';\mu)|^2}{\hbar\omega(k-k';\mu)} \qquad \text{(VI.11)}$$

In graphite intercalation compounds, the density of states at the Fermi energy is only a fraction of a typical density of states of a metal. The effect of the electron-phonon interaction is then expected to be much smaller. One should, however, make an estimate of an order of magnitude of the effect. The use of equation (VI.11) is not suitable in this case because the coupling function $g(k,k';\mu)$ is unknown. An alternate route is to estimate the carrier scattering time from electrical resistivity measurements. The scattering rate due to phonons at high temperatures ($k_B T \gg \hbar\omega_D$) is related to the value of the λ parameter in the zero temperature limit by a simple relation (Grimvall 1981b)

$$1/\tau = 2\pi\lambda k_B T/\hbar \qquad \text{(VI.12)}$$

The electrical conductivity is related to the square of the electron velocity at the Fermi surface by

$$\sigma_i = \frac{e^2\tau}{4\pi^3} \int \frac{dS_k}{|\nabla_k E|} v_i^2 \qquad \text{(VI.13)}$$

The electron velocity can be calculated from the band structure model. The conductivity is obtained experimentally

and, hence, one can estimate the scattering time. For estimation, we choose the SbF_6^- compound which has the largest Fermi surface and the highest density of states and one expects that the electron-phonon mass enhancement parameter is the largest in this compound. The resistivity of the compound at room temperature is 4×10^{-6} Ωcm (Billaud et al. 1980). Using this value and the band structure parameters in the simplified Blinowski model, one obtains a scattering time of 2×10^{-13} s. Assuming that the scattering at room temperature is phonon-dominated and using equation (VI.12) one obtains the value of $\lambda = 0.02$ which is of the order of the experimental uncertainty and can be neglected.

The agreement of the measured band parameters with theoretical predictions confirms the validity of the rigid band model of the electronic structure of acceptor intercalation compounds. The intercalates used in this work are highly oxidizing and produce compounds with high charge transfer. This is particularly true for the ionic compounds (SbF_6^- and BF_4^-) where oxidation of carbon is done by the nitryl ion (NO_2^+). The charge transfer of the SbF_6^- is close to the ionic limit of one charge per 24 carbon atom (Jobert et al. 1981). In the BF_4^- compound, the carbon charge state of $C_{41,5}^+$ is larger than for most stage-2 compounds (Markiewicz et al. 1983). In all compounds studied here, the rigid band model was found to be valid to describe the

electronic structure and no influence of charging of bands on the interaction parameters were observed.

VI.3. C-axis conductivity.

The electrical conductivity of acceptor intercalation compounds is very anisotropic. The basal plane conductivity is comparable to the conductivity of a metal. The c-axis conductivity is typically five orders of magnitude smaller. The low values of the conductivity along the c-axis is a matter of controversy and various mechanisms have been suggested to explain it (Khanna et al. 1978, Sugihara 1984) The temperature dependence of the c-axis conductivity of stage 1 and 2 $SbCl_5$ compounds shows a typical free-carrier behavior that is a linear increase of the resistivity with temperature (Morelli and Uher 1983). Similar dependence was observed with other acceptor compounds of graphite (Ubbelohde 1972).

In this work an estimate of the c-axis dispersion parameters in stage 2 $SbCl_5$ compound has been obtained. One can, therefore, verify the band conduction mechanism for the c-axis conductivity quantitatively.

The conductivity tensor element is related to the square of the electronic velocity of carriers at the Fermi surface according to the formula

$$\sigma_i = \frac{e^2}{4\pi^3} \int \frac{dS_k}{|\nabla_k E|} \tau v_i^2 \qquad \text{(VI.14)}$$

To estimate an order of magnitude of the conductivity anisotropy, one can use the simplified model of Blinowski et al. for the in-plane dispersion and add simple tight-binding energy dependence along the k_z direction. The total energy is then

$$E = -\frac{1}{2}[(\gamma_1^2 + 3a^2\gamma_0^2|k|^2)^{\frac{1}{2}} \pm \gamma_1] \pm 2\delta\cos(k_z I_c) \quad \text{(VI.15)}$$

Furthermore, because δ is much smaller than γ's the significant contribution to the gradient $\nabla_k E$ comes from the in-plane dispersion. The basal plane conductivity is

$$\sigma_x = \frac{e^2 I}{4\pi^3} \frac{2\pi^2}{\hbar^2 I_c} \left(\frac{\partial E}{\partial k}\right)_{k_F} \quad \text{(VI.16)}$$

and the c-axis conductivity is

$$\sigma_z = \frac{e^2 I}{4\pi^3} \frac{8\pi^2}{\hbar^2} I_c \delta^2 k_F \left(\frac{\partial E}{\partial k}\right)^{-1} \quad \text{(VI.17)}$$

At room temperature, the scattering is dominated by phonons and the scattering time is isotropic and the same for all bands. The anisotropy of the conductivity depends only on band parameters. Substituting the experimental values of the interaction parameters and the Fermi momenta for the stage-2 $SbCl_5$ compound and adding the contributions of both valence bands, one obtains the anisotropy of the conductivity as $\sigma_x/\sigma_z = 9 \times 10^4$. Measurements of basal plane conductivity gave values around $2 \times 10^7\ \Omega^{-1}m^{-1}$ (McRae et al. 1978). The c-axis conductivity was measured by Morelli and Uher (1983) and, at room temperature, a value of $1 \times 10^2\ \Omega^{-1}m^{-1}$ was obtained. Dividing these two numbers one obtains a conductivity ratio of 2×10^5 which agrees within an order

of magnitude with the calculated ratio. This agreement shows that the band conduction mechanism can account for the large anisotropy of the conductivity of stage-2 $SbCl_5$ compound.

CHAPTER VII

CONCLUSIONS

The purpose of this work was to study the electronic properties of acceptor-type graphite intercalation compounds. The work involved sample preparation, characterization, measurements of de Haas-van Alphen effect and theoretical calculations of the band structure.

Sample preparation techniques were perfected and new methods of preparation were developed to obtain pure and homogeneous samples needed for the dHvA study. The reaction of graphite with liquid $SbCl_5$ was carried out to produce stage 1 and 2 intercalation compounds. The pure stage-1 $SbCl_5$ compound obtained by this technique was stable for several months in air. Decomposition of the compound, reported in the literature, was found to be accelerated by the presence of small regions of stage-2 material within samples. The stage-2 $SbCl_5$ compound was obtained by reacting graphite with liquid $SbCl_5$ at about 100°C. The samples were pure and homogeneous. This shows that there is no need for a temperature gradient used in preparations reported previously.

Ionic compounds of graphite were obtained by reaction with nitryl salts. The intercalated ions were SbF_6^-

and BF_4^-. The reaction of nitryl hexafluoroantimonate with graphite was carried out in solution of the salt in dry nitromethane, liquid sulphur dioxide and by reaction with solid salt. Samples obtained in solutions decomposed after they were left in a dry atmosphere. The samples obtained by reaction with solid nitryl hexafluoroantimonate were stable in a dry atmosphere and under vacuum. The BF_4^- compound was synthesized by reacting graphite with solid nitryl tetrafluoroborate. The compound had higher intercalate concentration and higher charge transfer than those obtained by methods reported previously.

Measurements of the de Haas-van Alphen effect were performed on stage-1 $SbCl_5$ intercalated graphite for the first time. The fundamental dHvA frequency was interpreted in terms of the basic graphitic band. The measured cyclotron mass agreed with the theoretical prediction for the value of the frequency observed. Additional dHvA frequencies that were observed were interpreted as resulting from aging of samples that changed composition while preserving staging.

The de Haas-van Alphen spectrum of stage-2 $SbCl_5$ compound were found to depend on the rate of cooling between room temperature and liquid nitrogen temperature. The influence of the signal on cooling rate is one of the factors that can account for discrepancies between previously reported results of Batallan et al. and Takahashi

et al. The dHvA spectrum of slowly cooled samples consisted of two fundamental oscillations which were identified with basic graphitic bands. Both dHvA frequencies and both cyclotron masses agree with the predictions of the rigid band model with the Fermi energy as the only adjustable parameter.

Beat patterns of the fundamental frequencies of the stage-2 $SbCl_5$ compound were identified with splitting of the basic graphitic bands due to doubling of the lattice constant along the c-axis. The doubling of the lattice constant was observed in x-ray diffraction measurements. From the beat frequency, interaction between states localized on layers separated by an intercalate layer was estimated for the first time. Values of interactions of 0.6 meV and 0.7 meV for the two bands are four order of magnitude smaller than the values of in-plane interactions between carbon atoms.

The de Haas-van Alphen measurements on SbF_6^- compound showed qualitatively that the electronic structure depended on the method of preparation. Differences in electronic structure are attributed to differences in the structure and ordering of intercalate layers. The dHvA spectra of samples prepared in solutions showed the presence of inhomogeneities of carbon charge state and/or intercalate structure. The spectrum of the compound prepared by reaction

of graphite with solid salt had one dHvA frequency of 1627 Tesla. The cross-sectional area of the Fermi surface with this frequency is in agreement with the charge transfer expected from stoichiometry. This indicates that all the charge on graphene layers is delocalized. The measured cyclotron mass is in agreement with the one calculated from the rigid band model.

The dHvA spectrum of the stage-2 BF_4^- compound consisted of two fundamental frequencies. The frequencies and cyclotron masses are in agreement with the predictions of the rigid band model.

The rigid band models of the electronic structure of graphite intercalation compounds consider that the structure is two dimensional by assuming that the interaction between states localized on graphene layers separated by an intercalate layer is zero. The value of interaction was measured in this work and is less than 1meV. This shows that there is a small, finite interaction and the dependence of the Fermi surface cross-sectional area on the momentum component perpendicular to the layers is less than 1 % in the stage-2 $SbCl_5$ compound. From the measured anisotropy of the Fermi surface, an anisotropy of the conductivity was estimated. The calculated value of 9×10^4 is of the same order of magnitude as the measured anisotropy.

The predictions of the rigid band models of the

electronic structure of GIC proposed by Holzwarth (1980) were found to be in agreement with experimentally measured frequencies and cyclotron masses with the value of the Fermi energy adjusted to the charge transfer of each compound studied. The model assumes that the interactions between carbon atoms are the same in intercalation compounds as in pristine graphite. The good agreement between theoretical predictions and the experimental data shows that this assumption is valid in the case of the compound studied in this work. The compounds studied here, especially the ionic ones, have high charge transfer. It is likely that this conclusion can be interpolated to most of the acceptor compounds which have lower charge transfer.

The model of Blinowski et al. was found to be less accurate, the discrepancies between the model predictions and experimental data were up to 20 %. This is a result of simplifications of the model which includes only nearest neighbor interactions.

REFERENCES

Batallan, F., Bok, J., Rosenman, I. and Melin, 1978. Phys. Rev. Letters 41, 330.

Billaud, D. and Chenite, A. 1983. Mat. Res. Bull. 18, 1001.

Billaud, D., Flanders, P.J., Pron, A. and Fischer, J.E. 1982. Mat. Sci. Eng. 54, 31.

Billaud, D., Pron, A., and Vogel, F.L. 1980a. Synth. Met. 2, 177.

Billaud, D., Pron, A., Vogel, F.L. and Herold, A. 1980b. Mat. Res. Bull. 15, 1627.

Blinowski, J. and Rigaux, C. 1980. J. Physique 41, 667.

Blinowski, J., Nguyen, H.H., Rigaux, C., Vieren, J.P., LeToullec, R., Furdin, G., Herold, A. and Melin, J. 1980. J. Physique 41, 47.

Boolchand, P., Bresser, W., McDaniel, D., Sisson, K., Yeh, V. and Eklund, P.C. 1981. Solid State Commun. 40, 1049.

Boolchand, P., Bresser, W., McDaniel, D., Eklund, P.C., Billaud, D. and Fischer, J.E. 1983. Mat. Res. Soc. Symp. Proc. Vol. 20 Intercalated Graphite, p389.

Clarke, R., Elzinga, M., Gray, J.N., Homma, H., Morelli, D.T., Winokur, M.J. and Uher, C. 1982. Phys. Rev. B26, 5250.

Croft, R.C. 1956. Austral. J. Chem. 9. 184.

Dresselhaus, M.S. and Dresselhaus, G. 1980. Adv. Phys. 30, 139.

Dresselhaus, M.S., Dresselhaus, G. and Fischer, J.E. 1977 Phys. Rev. B15, 3180.

Eklund, P.C., Smith, D.S. and Murthy, V.R.K. 1981. Synth. Met. 3, 111.

Fischer, J.E. 1977. Mat. Sci. Eng. 31, 211.

Foley, G.M.T., Zeller, C., Falardeau, E.R. and Vogel, F.L. 1977. Solid State Commun. 24, 371.

Friedt, J.M., Poinsot, R. and Soderholm, L. 1984. Solid State Commun. 49, 223.

Grimvall, G. 1981. The electron-phonon interaction in metals, (North-Holland), New York.

1981a. ibid., p108.

1981b. ibid., p251.

Harrison, W.A. 1966. Pseudopotentials in the Theory of Metals, (Benjamin), New York.

Heinz, R.E., Doll, G., Charron, P. and Eklund, P.C. 1983. Mat. Res. Soc. Symp. Proc. Vol. 20 Intercalated Graphite, p87.

Herinckx, C., Perret, R. and Ruland, W. 1972. Carbon 10, 711.

Holzwarth, N.A.W. 1980. Phys. Rev. B21, 3665.

Homma, H. and Clarke, R. 1985. Phys. Rev. B31, 5865.

Iye, Y., Takahashi, O., Tanuma, S., Tsuji, K. and Minomura, S. 1982. J. Phys. Soc. Japan 51, 475.

Jobert, A., Touzain, Ph. and Bonnetain, L. 1981. Carbon 19, 193.

Johnson, L.G. and Dresselhaus, G. 1973. Phys. Rev. B7, 2275.

Jones, W., Korgul, P., Schlogl, R. and Thomas, J.M. 1983. J. Chem. Soc., Chem. Commun. p468.

Khanna, S.K., Falardeau, E.R., Heeger, A.J. and Fischer, J.E. 1978. Solid State Commun. 25, 1059.

Lifshitz, I.M. and Kosevich, A.M. 1956. Sov. Phys. JETP 2, 636.

McClure, J.W. 1957. Phys. Rev. 108, 612.

McDonnnell, F.R.M., Pink, R.C. and Ubbelohde, A.R. 1951. J. Chem. Soc. Part 1, 191.

McRae, E., Fusellier, H., Melin, J., Mereche, J.F. and Herold, A. 1978. Proc. 5th London Int. Carbon Conf.

Markiewicz, R.S., Lopatin, C. and Zahopoulos, C. 1983. Mat. Sci. Soc. Symp. Proc. Vol. 20 Intercalated Graphite, 135.

Melin, J., and Herold, A. 1969. C.R. Acad. Sc. Paris 269, 877.

Morelli, D.T. and Uher, C. 1983. Phys. Rev. B27, 2477.

Murthy, V.R.K., Smith, D.S. and Eklund, P.C. 1980. Mat. Sci. Eng: 45, 77.

Nixon, D.E. and Parry, G.S. 1969. J. Phys. C2, 1732.

Onsager, L. 1952. Phil. Mag. 43, 1006.

Roth, G., Salamanca-Riba, L., Kortan, A.R., Dresselhaus, G. and Birgeneau, R.J. 1984. Extended Abstracts Graphite Intercalation Compounds, Proceedings of Symposium I 1984 Fall Meeting of the Material Research Society, Nov 28-30, Boston, USA, p158.

Shoenberg, D. 1984. Magnetic Oscillations in Metals, (University Press), Cambridge.

Slonczewski, J.C. and Weiss, P.R. 1958. Phys. Rev. **109**, 272.

Sugihara, K. 1984. Phys. Rev. **B29**, 5872.

Takahashi, O., Iye, Y. and Tanuma, S. 1981. Solid State Commun. 37, 863.

Tanuma, S., Takahashi, O. and Iye, Y. 1981. in Physics of Intercalation Compounds, ed. by L. Pietronero and E. Tosatti, (Springer-Verlag) Berlin, p90.

Timp, G., Dresselhaus, M.S., Salamanca-Riba, L., Ebril, A., Hobbs, L.W., Dresselhaus, G., Eklund, P.C. and Iye, Y. 1982. Phys. Rev. **B26**, 2323.

Ubbelohde, A.R. 1972. Proc. R. Soc. **A327**, 289.

Wallace, P.R. 1947. Phys. Rev. **71**, 622.

Yosida, Y. and Tanuma, S. 1985. J. Phys. Soc. Japan **54**, 701; ibid., p707.

Zaleski, H., Ummat, P.K and Datars, W.R. 1984. J. Phys. **C17**, 3167.

Zaleski, H., Ummat, P.K and Datars, W.R. 1985. Solid State Commun. **55**, 401.

Zaleski, H., Ummat, P.K and Datars, W.R. 1985. Synth. Met. (in press).